

Real-time Inhabited Virtual Worlds and Interaction – interactive virtual worlds module

Nadia Magnenat-Thalmann, George Papagiannakis, Arjan Egges, Etienne Lyard

MIRALab, University of Geneva, Geneva, Switzerland

1. Introduction

Virtual Worlds [MK94] and their concept of cyber-real space interplay invoke such interactive digital narratives that promote new patterns of understanding. However, the "narrative" and "interactive" part, which refers to a set of events happening during a certain period of time and providing aesthetic, dramaturgical and emotional elements, objects and attitudes ([NM00], [TYK01]) is still an early topic of research. Mixing such aesthetic ambiances with interactive virtual character augmentations [CMM*03] and adding dramatic tension has developed very recently these narrative patterns into an exciting new edutainment medium [LHM03]. With the interplay of a modern real-time framework for integrated interactive virtual character simulation, we can enhance the experience with full virtual character simulations.

1.1 Overview

During real-time operation and having already prepared the VR content for the virtual simulation, our interactive virtual worlds allow the user to be immersed in them and witness storytelling experiences enacted by realistic virtual humans. Thus in Section 2 of this work we review the modeling processes of building such interactive virtual worlds. In Section 3 we present such a framework which is mandatory in order to handle the exponential complexity of virtual character drama that traditional rendering-centric VR systems cannot anymore handle. In Section 4 we describe our MR new illumination model for virtual characters. Finally in section 5 we present the detailed technologies for advanced real-time virtual human simulation, such as personality, emotion, facial, body, hair and clothes simulations.

Our two case studies in the VR site of ancient Aspendos as well as on the MR (Mixed Reality) site of ancient Pompeii together with the discussion and conclusions are discussed in section 6.

2. Modeling virtual worlds for real time (RT) interactive applications

The deployment of virtual reconstruction methodologies and techniques, aimed at the achievement of photorealistic results for an interactive 3D real time experience in a VR inhabited worlds, have been applied to the virtual restitution of the historical site of Aspendos. The necessary methodological and technical solutions required to realize the visualisation of the Roman theatre of Aspendos along with the inclusion of 3D fully animated Real Time virtual humans re-enacting an ancient Roman play, have been implemented in a real-time VR-AR Framework. Furthermore, specific modelling, illumination and real time rendering strategies, along with the design choices that were operated regarding both the preparation of the textured 3D scene with the animated virtual actors, and concerning the optimizations aimed at the creation of a viable model suited for the needs of a real time interactive visualization, have been carefully considered. For the realization of the 3D model of the Aspendos site, polygonal modelling techniques were generally preferred. Critical parts of the model, such as the Cavea, due to its extremely complex geometrical features, were given special attention to keep an acceptable trade-off between visual accuracy and the performance of the real time simulation. In order to model the Aspendos site virtual environment, accurate topographic data was provided in the form of a 2D elevation map of the area featuring elevation lines every 1 meter. After the repositioning of these splines in a 3D space, it was possible to build a high polygon 3D mesh (80.000 polygons) from which a greyscale elevation map has been extracted to procedurally generate a diffuse textures using distribution parameters such as relative position of the polygons, their orientation and slope.

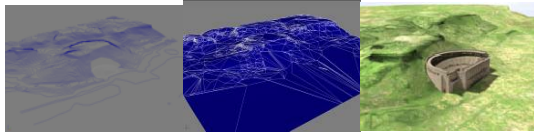


Figure 1: 2D Elevation map of the Aspendos site (left) low polygon optimized mesh of the terrain (center), textured 3D model of the environment with 3D textured model of the modern theatre (right)

To further increase the visual impact of the restituted environment, the addition of trees and vegetation has been included with the implementation of billboard techniques. Such billboards, representing a total of more than 30 different types of trees, have been prepared using as starting point real images of trees and bushes that have been edited to isolate their shape from their original background, and to add an alpha channel to allow their visualization with transparency effects.



Figure 2: Samples from the billboard collection representing the vegetation (left) and rendering of the final model of the environment of the theatre of Aspendos (right)

In order to create the texture tiles to be mapped on the 3D geometry of the restituted theatre, the creation of a library of the main identified diffuse material textures present on the site has been made using as a base the on-site taken high resolution digital photographs: 150 different color corrected textures that can be tiled seamlessly on the objects of the 3D scene have therefore been prepared and assigned to the model's surfaces.



Figure 3: Samples from the texture gallery (left), 3D scene building with and without textures (center and right)

To further improve the overall final visual impact of the 3D interactive real time simulation of the Aspendos site, the addition of diffuse and hard shadows cast by the sun plays a central role. At an earlier stage of the virtual restitution a full texture baking approach of a pre-computed radiosity solution has been used. This approach however implies the creation of one texture per object: the bigger is the object, the higher the resolution of the generated texture has to be in order to avoid visual discontinuities: therefore the risk to overload the video memory, either with excessively high resolution textures or by too many generated

textures, is addressed. To overcome these restrictions the adoption of a light-map and diffuse-map real time multi-texturing approach has been adopted due to the fact that the diffuse textures can be tiled, and therefore their resolution becomes independent from the size of the object upon which they are mapped. Secondly the light maps can be downsized to very low resolutions without compromising the overall visual impact of the simulation, thus eliminating the video memory overload issue. In order to visually simulate a more convincing virtual illumination of the scene, the use of High Dynamic Range Image Based Lighting has also been implemented to create such lightmaps, as shown in the following figure.

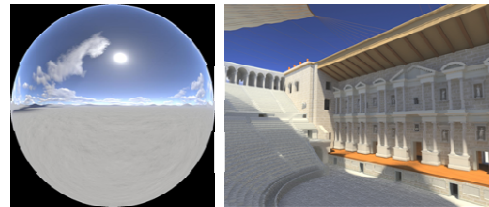


Figure 4: 3D final textured model of the theatre of Aspendos Illuminated with the final light probe

However, even though a first illuminated model of the site featuring HDR IBL has been produced during earlier tests using as source for the illumination photographic light probes, the Aspendos virtual model had to be simulated under specific lighting conditions at specific dates and hours of the day. Thus, the use of virtually generated light probes, allowing an arbitrary positioning of the direct sunlight, by means of parameters such as location, date and time, has been implemented. In order to produce suitable virtual light probes, two approaches were used: the combination of several LDR panoramic images rendered at different exposures, and the direct computation of a synthetic HDR image. Having achieved acceptable results with either method, a virtual light probe featuring the lighting conditions at the site of Aspendos, as chosen by the ERATO consortium, at the 9th of June 2004, 15.00 pm, under an unclouded sky, has been produced and used to compute a global illumination solution (result shown in figure 7, left) for the texture baking process and the creation of the lightmaps to be used for the real time simulation.

The final computed illumination solution has then successfully been used to generate all the lightmaps that subsequently have been assigned to the self-illumination channel of their corresponding surfaces in order to modulate the luminosity of the tiled material textures for the real time simulation. Thus, the previous 3D model based on a full texture baking approach of the lighting simulation has been replaced by the new model employing a lightmap based approach. Such approach allows, in fact, the dissociation of the lighting information from the material textures, and consequently allows for an overall better visual quality of the real time rendered surfaces and a reduction of the total weight of all the textures loaded into memory to perform the simulation. In order to optimize the performance of the real time application, all the lightmaps have been also

down-sampled to a size of 256x256 pixels and have been blurred to remove possible compression artifacts due to their small size in comparison to the spatial extension of their assigned surfaces: the final visual quality achieved, in the form of screenshots taken while running the real time interactive simulation, is illustrated in the following figure.



Figure 5: Real time simulation without lighting information (left), Previous 3D real time full texture baked model (center), screenshots from the final 3D real time simulation of the new model using light-maps (right)

3. Platform choice for inhabited virtual worlds

3.1 MR-Life system design

Our MR (Mixed Reality) system is based on the VHD++ [PPM*03], component-based framework engine which allows quick prototyping of VR-AR applications featuring integrated real-time virtual character simulation technologies, depicted in Figure 6. The framework has borrowed extensive know-how from previous platforms such as presented by [SBT*99]. The key innovation is focused in the area of component-based framework that allows the plug-and-play of different heterogeneous human simulation technologies such as: Real-time character rendering in AR (supporting real-virtual occlusions), real-time camera tracking, facial simulation and speech, body animation with skinning, 3D sound, cloth simulation and behavioral scripting of actions.

The main design principle was to maximize the flexibility while keeping excellent real-time performance. The different components may be grouped into the two following main categories:

1. System kernel components responsible for the interactive real-time simulation initialization and execution.
2. Interaction components driving external VR devices and providing various GUIs allowing for interactive scenario authoring, triggering and control.

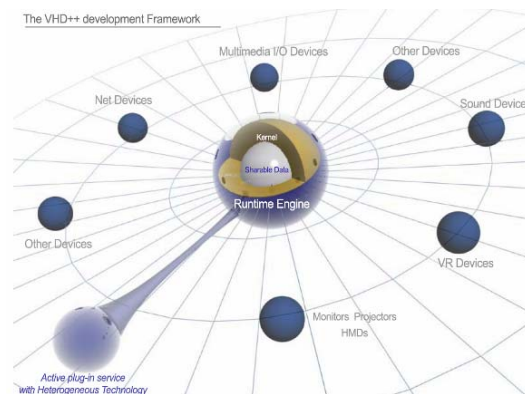
Finally the content to be created and used by the system was specified, which may be classified into the two following main categories: a) Static and b) Dynamic content building blocks such as models of the 3D scenes, virtual humans, objects, animations, behaviors, speech, sounds, python scripts, etc.

3.2. MR Framework operation for character simulation

The software architecture is composed of multiple software components called services, as their responsibilities are clearly defined. They have to take care of rendering of 3D

simulation scenes and sound, processing inputs from the external VR devices, animation of the 3D models and in particular complex animation of virtual human models including skeleton animation and respective skin and cloth deformation. They are also responsible for maintenance of the consistent simulation and interactive scenario state that can be modified with python scripts at run-time. To keep good performance, the system utilized four threads. One thread is used to manage the updates of all the services that we need to compute, such as human animation, cloth simulation or voice (sound) management. A second thread is used for the 3D renderer, who obtains information from the current scenegraph about the objects that must be drawn as well as the image received from the camera. It will change the model view matrix accordingly to the value provide by the tracker. The third thread has the responsibility of capturing and tracking images. The last thread is the python interpreter, which allows us to create scripts for manipulating our application at the system level, such as generating behaviors for the human actions (key-frame animation, voice, navigation).

The MR system presented in Figure 6 features immersive real-time interactive simulation supplied with proper information in course of the simulation. That is why content components are much diversified and thus their development is extremely laborious process involving long and complex data processing pipelines, multiple recording technologies, various design tools and custom made software. The various 3D models to be included in the virtual environments like virtual human or auxiliary objects have to be created manually by 3D designers. The creation of virtual humans require to record motion captured data for realistic skeletal animations as well as a database of real gestures for facial animations. Sound environments, including voice acting, need to be recorded in advance based on the story-board. For each particular scenario, dedicated system configuration data specifying system operational parameters, parameters of the physical environment and parameters of the VR devices used have to be defined as well as scripts defining atomic behaviors of simulation elements, in particular virtual humans. These scripts can modify any data in use by the current simulation in real-time. This allows us to continue running the simulation whilst some modifications are performed.



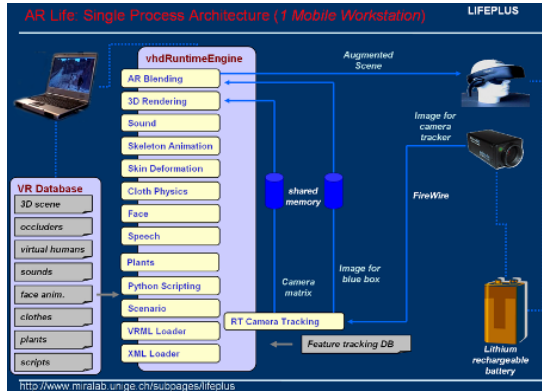


Figure 6: VHD++ AR Framework Overview

4. Real-time illumination models for interactive virtual inhabitants

Virtual Characters have already been synthesized with real actors in common non-real-time mixed reality worlds, as illustrated successfully by a number of cinematographic storytelling examples. These examples involve virtual creatures such as ‘Gollum’ in the “Lord of the Rings™” and ‘King Kong™’ both created by Weta Digital™, the virtual character ‘Jar-Jar Binks’ in “Star Wars I: The Phantom Menace™” created by Industrial Light and Magic™, ‘Stuart’ in “Stuart Little™” created by Sony ImageWorks™ and the virtual ‘Marilyn Monroe’ as appearing in the research film “Marilyn by the lake” by MIRALab, University of Geneva. All these ‘compositing’ examples involve non-real-time (offline) pre-rendered simulations and mostly are rendered and post-processed frame by frame in an ad-hoc manner by specialized digital artists or compositors as they are termed in the industrial domain of special effects (SFX). The active SFX sector with applications in film, television and entertainment industry has exemplified such compositing effects in a constantly growing list of projects. Our main basic research efforts are confined in adding believable and realistically dynamic globally illuminated virtual humans for both the real-time VR [PLF*01] and AR [PSO*05], [PFT05] continuum.

This objective is two-fold, as it demands a) the complete set of technologies for VH simulation [PPM*03] as well as b) an illumination model that is flexible, easy to control and efficient to compute in relation to the other VH simulation technologies [MCS*04]. The main contribution of this effort is to propose a new MR [PSO*05] physically correct illumination model based on Precomputed Radiance Transfer [SKS02], [KLS05] for deformable virtual humans employing ‘real light’ captured as light probes [PFT05]. This would allow for believable MR illumination registration between real and virtual augmentations and exposure matching between the real light as perceived by the real AR camera and the virtual exposure of the acquired, simulated Area Light of the augmented scene. To the best knowledge of the author such an analytical illumination model has not yet appeared in the literature. The following figure illus-

trates and example of our approach with comparison to previous attempts.



Figure 7: Our real-time All-frequency illumination model (middle, right column) as opposed to standard Phong (left column)

In order to enhance the consistency of illumination of the real scene and the virtual characters, we have chosen to extend the Precomputed Radiance Transfer (PRT) illumination model, in order that is applicable to the multi-segmented, deformable and animatable hierarchies that our animation (MIRAnim) system is controlling. The main issue that we resolved was to allow for the multiple segments that the virtual skeleton consists of (due to different joints, segments, cloth, hair meshes) to respond to a high dynamic range area light that can be captured from the real scene, similar to the method described in [PFT05]. Thus starting from the Rendering Equation approximation in diffuse PRT Methods [SKS02], [KLS05]:

$$L_0(x) = \frac{K_d}{\pi} \int_U L_s(l) T^{DSM} dU$$

Where

$$T^{DSM} = V(x, l) \cdot \max(n \cdot l, 0)$$

we define a new visibility function $V(x, l)$ which checks visibility of the current vertex position against not only the current geometric mesh that resides but against a Proxy mesh M' :

$$M' = \sum_{i=0}^n S_i$$

Where S_i are all the Mesh Segments of the skeleton hierarchy of the virtual character. However, not all segments are desired to be able to cast or receive self-shadowing and other GI effects. Thus the construction of the proxy mesh M' is based according to the ‘type’ of the mesh segment, tagged as Receiver or Occluder during the artist mesh preparation loop:

Receiver can receive but cannot cast self shadowing to other objects of the Proxy Mesh
Occluder can cast but cannot receive self shadowing from other objects of the Proxy Mesh



Figure 8: Image without (a, b) and with (c, d) Receiver-Occluder set processing for our dPRT method

This is a disjoint set, i.e. an element cannot participate in both groups. If a 'Receiver' segment is found, it is excluded from the Proxy Mesh, thus being transparent to ray casting hits. If an 'Occluder' segment is found, then this segment is excluded from further dPRT processing and calculation proceeds to next segment. However, this segment is part of the Proxy Mesh and candidate for ray-casting hits by other segments. Figure 8 illustrates the VH result of DSM with and without the Receiver-Occluder specifications. The main artifacts appear between the Skull and Hair segments which is a typical case of VH arrangement, as separate meshes due to separate creation processes and materials involved. However, with the application of our Receiver-Occluder set of elements, this artifact is avoided, as shown in Figure 8.

We employ a Voxel Ray Tracer and Uniform Grid acceleration structure for offline ray-tracing for PRT self-shadowing tests. This uniform grid is being initialized in a first pass with this Proxy Mesh while tested in a second pass, similarly as before with rays originating from every vertex of every segment in the skeleton hierarchy. The main difference is that in the simple Diffuse Shadowed Transfer from Sloan et al. [SKS02], the ray tracer was initialized with containing only the parent mesh of the current vertex x for which rays arriving from directions l where tested.

This simple and efficient scheme of our Proxy mesh, results in our Diffuse Shadowed Merged Transfer that allowed us for correct global illumination effects such as self-shadowing and successful application of diffuse PRT methods for multi-mesh virtual humans.

As shown in the following figure, in the case of multi-segmented, multi-material skeleton hierarchies, even with our Diffuse Shadowed Merged Transfer, incorrect self-

shadowing is performed due to the proximity of the different mesh segments.



Figure 9: Tensor Distance Ray-Hit Relaxation Criteria for DSM Transfer and dPRT. Images shown with (a) and without (b) tensor distance threshold applied.

It is usually manifested as wrong dark coloring in the vertices in the boundary edges of different skeleton segments, as these segments are modeled adjacent in the skin bind pose, but as they are separate segments, still maintain a distance between them, not visible to the eye but large enough for ray casting. Thus one relaxation criteria that we have been applying with positive results is the checking for the tensor distance between the ray origin and the ray-triangle intersection point, against a value ϵ corresponding to the minimum distance between the different mesh segments.

E.g. for the H-Anim [H06] structure this corresponds to $1.71 \cdot 10^{-4}$ m. Hence all false hit-point candidates returned by the ray tracer below this ϵ value correspond to hits between the segment boundaries and thus ignored. Another issue for the shadow feeler visibility rays is that polygons adjacent to the current vertex ray origin are going to be coplanar to many rays originating from that vertex. Thus any ray tested against a polygon that included the ray origin will at best return a hit at that vertex origin. This also leads to incorrect shadowing so it is important that we exclude the polygons that contain our ray origin, from the M' Proxy Mesh. Thus in the construction of M0 we create full Face, Edge, Vertex information adjacency in order to account for this special case. This second criteria has been already known to the ray-tracing community and similar approaches have been discussed. Since the final shading information is stored per vertex in the H-Anim virtual human hierarchy, it is independent of the underlying animation approach. Therefore our virtual human animation system is easily integrated within our MR framework to animate the skeleton of the virtual humans with shading according to the blending schedule that is defined in Section 5. The tutorial slides provide further analytic representation of the discussed algorithms and extensions to realize the above illumination model for virtual humans in interactive virtual and augmented worlds.

5. Simulating realistic virtual humans for real-time applications

5.1 Virtual Human Animation

There exist many techniques for animating virtual characters. Two very commonly used techniques are:

Key-framing: an animation is constructed from a set of key-frames (manually designed by an animator or generated automatically) by using interpolation techniques. Although this method results in very flexible animations, the realism of the animations is low, unless a lot of time is invested.

Pre-recorded animations: an animation is recorded using a motion capture/tracking system such as Vicon or MotionStar. The animation realism is high, but the resulting animation is usually not very flexible.

A method like Principal Component Analysis (PCA) can determine dependencies between variables in a data set. The result of PCA is a matrix (constructed of a set of eigenvectors) that converts a set of partially dependent variables into another set of variables that have a maximum independency. The PC variables are ordered corresponding to their occurrence in the dataset. Low PC indices indicate a high occurrence in the dataset; higher PC indices indicate a lower occurrence in the dataset. As such, PCA is also used to reduce the dimension of a set of variables, by removing the higher PC indices from the variable set. We will use the results of the PCA later on for synthesizing the dependent joint motions. For our analysis, we perform the PCA on a subset of H-Anim joints. In order to do that, we need to convert each frame of the animation sequences in the data set into an N-dimensional vector. For representing rotations, we use the exponential map representation [EMM04, Gra98]. In this representation, a rotation can be represented by a 3-dimensional vector r , as a rotation with angle $|r|$ around axis r .

The exponential map representation of a rotation is very useful for motion interpolation [PR97], because it allows to perform linear operations on rotations. In our case the linearity of the exponential map representation is crucial since the PCA only works in the linear domain. Any rotation matrix can be written in the exponential map representation, and any exponential map representation (modulo 2π) is a rotation. Grassia [Gra98] provides an extensive overview of the advantages and disadvantages of various representations of rotations, including the exponential map.

Using the exponential map representation for a joint rotation, a posture consisting of m joint rotations and a global root translation. In our case, one posture/key-frame is represented by 25 joint rotations and one root joint translation, resulting in a vector of dimension 78. We have applied a PCA on a large set of motion captured postures, resulting in a PC space of equal dimension.

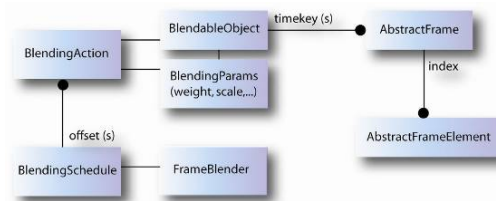


Figure 10: Overview of the blending engine data structure

We will now present our animation engine, called MIRAnim. The main architecture of the animation engine is a multi-track approach, where several animation streams need to be blended into a final animation. The goal of our animation engine is to provide for a generic structure that allows for the implementation of different blending strategies. This is especially important, since our animations use different representations, depending on the application. Additionally, in the final system, we will need to perform blending operations on both body and face animations, which are two completely different animation formats that require different blending strategies. A large set of blending tools, for example time warping, splitting, fading, and so on are available. The advantage of using this generic approach is that once a blending tool has been defined, it can be used for any type of animation, regardless of its structure. In order to be able to use these blending tools, only an interface needs to be provided between the data structure used for blending, and the original animation structure. An overview of the blending engine is provided in Figure 10.

The basic structure used in the blending engine is the so-called BlendableObject interface. A blendable object is the representation of an animation that can be blended with other animations. The main functionality of a blendable object is that it returns a frame, given a timekey. A frame in the blending engine is called an AbstractFrame. An abstract frame consists of a number of elements, called AbstractFrameElement objects. Each of these elements is a list of floating point values. For example, in the case of body animations, an AbstractFrameElement could be a list of 4 floating points, representing a quaternion rotation, or a list of 3 floating points, representing a 3D translation. An abstract frame could then consist of a combination of abstract frame elements that are either translations or rotations. In the case of facial animation, the abstract frame element could be a list of 1 floating point, representing a FAP value in the MPEG-4 standard.

In addition to the basic data structures and tools used for blending animations, the blending engine also provides for a few extensions that allow to further parameterize the animation and blending process. For example, modifiers can be defined which act as a wrapper around blendable objects. Examples of such modifiers are time stretching, flipping, or looping of animations. Again, custom modifiers can be defined for different animation types. To give an example in the case of body animations: a modifier is available that performs a global transformation on the whole animation. Any sequence of modifiers can be used,

since modifiers are again blendable objects.

The final step in obtaining a mix of different blendable objects requires a structure that allows for activating and deactivating different animations according to some blending parameters. This structure is called a BlendingSchedule. Each blending action is associated with a timekey, which defines the time that the blending action should start.

The animation service is built around the blending engine, and it contains specific implementations for controlling both face and body animation. The service can blend several different types of motions, including real-time idle motions and key-frame animations. For each virtual human in the scene, an XML file contains the actions that are available to the human, as well as the parameters for blending these different animations. Internally, a `vhdAnimationProperty` is defined for each virtual human, that contains a blending schedule, and some options, such as a choice whether or not facial and/or body animation should be played or if the translation/orientation of the virtual human was defined on the global (world) coordinate system or local coordinate system. The service also includes an integrated player, that plays and blends scheduled animations in a separate thread for all the humans in the scene.

In the next section, we will discuss the interaction component that controls the animation engine.

5.2 Interaction

As a higher level control mechanism on top of the animation service, we have developed the interaction service. This service mainly handles the spoken interaction between a user and any virtual human in the scene. The core of the interaction service is a dialogue manager [EKM04], that responds to the user according to a predefined script. In order to provide for a more natural interaction, we have integrated the Microsoft Speech SDK (SAPI5.1) into our MR framework, so that Automatic Speech Recognition (ASR) as well as Text-to-Speech (TTS) is available.

From the response text generated by the dialogue manager, the facial speech animation is created automatically [EKM04] using the timing information obtained from the TTS system. Additionally, the responses generated by the dialogue manager contain XML tags, which define specific face and body gestures that should be displayed in synchrony with the speech animation. An example of such a tagged response is given as follows:

```
<begin_gesture id="g1" anim="shake_head"/>
```

```
Unfortunately, I have <begin_gesture id="g2"  
anim="raise_eyebrows"/>no idea <end_gesture  
id="g2"/> what you are talking about.
```

```
<end_gesture id="g1"/>
```

Within each gesture tag, an animation ID is provided.

When the gesture animation is created, these animations are loaded from a database of gestures. Next to the animation itself, the gesture database also contains information related to the scope of each animation (which part of the body it should play on) and the weights of the joints. Each animation is stretched so that it is in synchrony with the speech, and it is blended with the other running animations by the animation service. Because the same service is used for both scripted and interactive animation, it is possible to first play a script as shown in the previous section, and then dynamically switch to animation controlled by the interaction service. Since the animation playing itself is continuously handled by the animation service, the character animation is not disrupted when this switch is made (see Figure 15).

5.3 Body Animation and Motion Retargeting

The general principle for animating a virtual 3D character - whatever it looks like - is as follows. First of all the character is given an underlying skeleton with a hierarchical structure (Figure 1) which is the object that will drive the animation later on. Because of its hierarchical formulation (i.e. each limb is placed with respect to the limb onto the new dimension of the skeleton on which it is being applied, and the character will which it is attached), all the joints rotations and segments offsets must be computed, along with one unique root transformation used for placing the skeleton in the workspace. This approach can be seen as placing the character at its correct location in the 3D space and then adapt its pose for the current frame. It has many benefits such as the possibility to easily edit the skeleton pose in order to make it match a desired configuration by simply rotating the joints (because of the hierarchical formulation, rotating the shoulder joint will make the entire arm follow the shoulder), or the fact that a given animation can be applied on various skeletons without having to recompute the rotation of all the joints. The drawbacks - quite tightly linked to the benefits - are mainly that because there exist no explicit relationship between an animation and the sizes of a skeleton, a motion can be directly applied on only one skeleton and one must modify - or retarget - the motion before applying it on another skeleton. This problem can be illustrated as follow: 2 characters with different sizes and shapes (for instance one tall and one small), while walking, will not cover the same distance if they perform the exact same number of steps. But because the global location of a skeleton is recorded once and for all when the animation is created, the global location of the root joint of the animation will not match have its feet sliding on the ground, if not penetrating it or floating in the air.

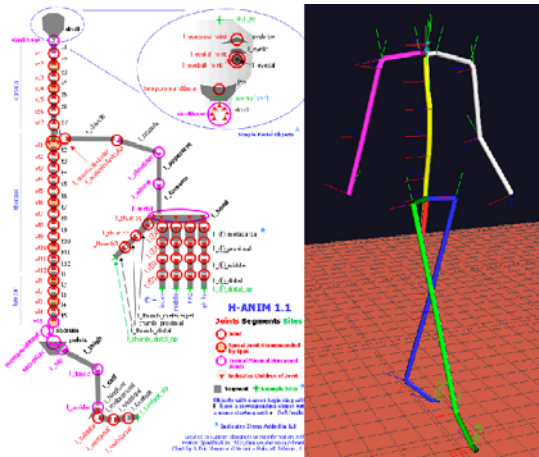


Figure 11: The H-Anim skeletal hierarchy (left) and an instance of it drawn in a 3D workspace (right)

Once the underlying skeleton is animated, the character is given a virtual skin: this is the skinning phase of the animation (Figure 2). A virtual skin is a 3D mesh attached to the skeleton in such a way that it follows the skeleton animation. The attachment process consists of defining a relationship between each vertex of the skin and a subset of bones from the skeleton so that the skin follows the motion of the skeleton in a sound and realistic manner. Even if the skinning attachment is done very carefully by skilled animators, it can also yield to various unpleasant visual artifacts which are usually corrected afterwards by hand. Basically, the same adaptation issues that were found for the skeleton will have their skin equivalent. For instance, if the skeleton animation was created with a slim morphology in mind, applying it to a fat character will make the body penetrate itself because the actual diameter of each limb is now much larger but the animation wasn't adapted accordingly.



Figure 12: The skinning process. The skeleton used for driving the animation and the resulting skin shape were superimposed. The colors of the body parts correspond to the primary bone which drives this particular limb.

Finally, once a nice looking skinned character is obtained, additional features are added: cloth, hair and more.

As stated in the previous section, motion retargeting is a tricky process which is highly required when dealing with body animations.

Various methods were proposed in order to perform this task efficiently, and among the literature a few cornerstone attempts will be outlined here. Popovic and Witkin [POP95] proposed to directly manipulate the motion curves (figure 3) in order to tune an already existing motion. They basically tweak the motion curves in the parameter space by applying interpolating functions (cardinal splines) between an existing motion and user-defined key frames.

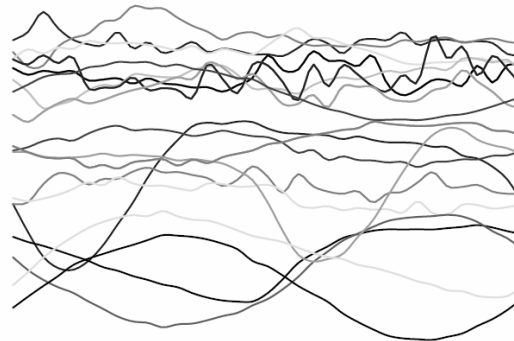


Figure 13: Motion curves extracted from the work from Popovic et Al. [1]

Gleicher [GLEI98] proposed to directly deal with the motion itself rather than its constituting parameters using a spacetime optimization algorithm. His method aims at adapting an existing motion clip so that it matches a new skeleton, and constraints defined by the user (such as foot plant, or grasp...see figure 4). For this, he uses a constrained non-linear solver which enforces the requirements while preserving the original motion. Such solvers are many, and as the original motion doesn't match the constraints, his one goes towards a points which satisfies the constraint while maintaining an objective function as low as possible. In order to distribute the modifications upon the motion over as many frames as possible, the corrections aren't applied directly but rather through splines control points. Later on, Lee and Shin [LEE99] improved this approach by making use of a hybrid inverse IK algorithm and a hierarchy of splines in order to preserve the high frequencies features of the motion.

Tolani et Al. [TOL00] developed a hybrid numerical and analytical IK algorithm which can be applied to a 7 degree of freedom limb. Based on the observation that given a configuration of the elbow and/or wrist, it is possible to restrict the range within which the elbow joint can lie into. When all the possible ranges of possible values for this angle are found, the correct value is then taken using several possible means. For orientation constraints, 2 angle variables are still active after the joints limits simplification and again, an optimization (this time non-linear) must be performed on the two variables in order to find out the correct values for the angles. Choi and Ko [CHO00] proposed a numerical IK method based on inverse rate control

in order to retarget a motion to a new character in real-time. The method uses inverse kinematics and inverse control rate for achieving the compliance with given target positions of end effectors. Unlike regular inverse kinematics, the system doesn't estimate the joints configuration, but rather their velocity which is then integrated over a time step in order to get the real character configuration. Several geometric configuration can be enforced as one primary goal, and a secondary goal is introduced which is match the original motion as much as possible.

Shin et Al. [SHI01] developed a hybrid system focusing on real-time performances in order to drive cartoons characters for TV shows. They implemented first a Kalman Filter in order to stabilize the motion data they acquire from the real-time capture system. Starting from this cleaned up motion they developed a hybrid system for re-targeting the motion in real time to a new character. Their system has 3 separate steps. First a global correction for the root joint is estimated using the intersection between spheres representing a range of motion. Second, a numerical optimization (conjugate gradient) is used in order to estimate the best body (without the limbs) configuration that matches the constraints and remains as close as possible from the original motion. Last, the limbs configuration is adapted using an analytic inverse kinematic method also proposed by them. They proposed an importance based approach in order to choose between re-targeting the motion so that it matches the surrounding environment or stick as much as possible to the original motion. For that, they defined an importance factor for each constraint (i.e. if an end effector must be close to a surrounding object) which is inversely proportional to the distance of the recorded end effector to the considered object.

Kovar et Al. [KOV02] proposed a dedicated –rather simple- method in order to get rid of foot skating (figure 6). The method uses a set of foot plant constraints that are either extracted automatically, or specified by the user. These constraints are then satisfied by smoothly changing the location of the root joint and configuration of the legs.

The root joint adaptation is done by calculating the possible location of the root joint in order to satisfy the constraints using reach spheres. The limbs configuration adaptation is then performed using a variant of the inverse kinematics method proposed by Tolani et Al. Because sometimes the target can cause the limb to jerk in some circumstances, the limb is stretched by a factor of a few percents.

6. Case studies

6.1 Simulating interactive virtual plays in ancient theatres

The ERATO INCO-MED EU Project (<http://www.at.oersted.dtu.dk/~erato/>) aims for the re-enacting of ancient theatrical plays in reconstructed ancient Theatres. Specifically we were involved in the reconstruction of the Hellenistic ancient Aspendos theatre in Minor

Asia, Turkey and the simulation of virtual actors of that historical period, re-enacting parts of ancient plays (Figure 14). Our implemented basic scenegraph OpenGL renderer OpenScenegraph in our VHD++ framework provides both advanced particle system simulation and occlusion and view frustum culling, which have been both successfully integrated and tested in the ERATO platform. The aggressive view frustum culling allows the final scene of 300.000 polygons with 1GB of total textures size, which includes the full 3D model of the theatre, featuring radiosity processed lightmaps applied at material level to simulate global illumination through a multi-texturing approach, and the 3D real time virtual actors illuminated through PRT(precomputed radiance transfer), to be rendered at ~20fps, according to the view frustum and part of the visible scene within the virtual camera frustum.



Figure 14: Screenshots from the final 3D interactive real time simulation featuring our adapted Precomputed Radiance Transfer illumination model for deformable characters and a diffuse map-lightmap approach for static surfaces

Regarding the reconstructed theatre, offline light-mapping rendering methods have been utilized that allowed for viewing the theatre under static area light of the Aspendos virtual Light probe. The main reason for the static lightmap solution was the fact that the reconstructed model exhibited a very high polygonal count with also a high number of required Texture memory, thus making any real-time algorithm not destined for such heavy scenes, difficult to apply. The following figure illustrates a final example with the VHs rendered via the key-fill algorithm for illumination registration in the virtual inhabited world, with the static lit via the same area light, mesh of the theatre of Aspendos.

6.2 Pompeii and the thermopolium of Vetutius Placidus trial

With the help of the Superintendence of Pompeii [ASP05], who provided us with all necessary archaeological and historical information, we have selected the ‘thermopolium’ (tavern) of Vetutius Placidus and we contacted our experiments there. The results are depicted in the fol-

lowing Figure 15 where the technologies employed for simulating and authoring our virtual humans were already described in [PSO*05]. Our latest research efforts provide real-time interaction in such inhabited MR worlds, as depicted in Figure 15. For this AR case study we have extended the system described in [PSO*05] and [PFT05] by allowing for interaction with a virtual human in MR. This aims to allow visitors of ancient Pompeii to be equipped with a mobile AR guide and experience real-time digital narratives of ancient virtual life coming to life within their natural 'real' Pompeian environment. The two crucial components for realizing these AR experiences are a) the feature based camera tracker and b) the MR framework for virtual life simulation and AR registration.

The work presented in this tutorial described the three new components in the previous framework: a) procedural animation, b) interaction and c) MR rendering based on PRT methods. As our original storytelling experience has been intended to revive the life in ancient Pompeii, Italy in an AR simulation manner, a real-size paper maquette of the walls of the Thermopolion of Vetutius Placidus has been recreated in the lab as depicted in Figure 15. The employed hardware platform was based on a P4 3.0 GHz mobile workstation, with a NVIDIA Geforce5600Go graphics card and Unibrain firewire web camera attached on an I-Glasses HMD. The resulting performance was approximately 15fps for 12.000 polygons, depending on the performance of the markerless feature-based camera tracker.

6.3 Conclusions

Nowadays, when laymen visit virtual worlds, generally, they cannot fully grasp the vibrant life that is integrated in these simulated worlds. This is particularly true with ruins such as of ancient sites such as Pompeii and Aspendos, where we would like to interact and understand the behaviors and social patterns of living people from ancient Roman times. With the extensions and algorithms that we propose for virtual human interaction, rendering and simulation coupled under a complete real-time framework for character simulation, we aim to provide new dramaturgical notions for such inhabited virtual worlds. Such notions could extend further research in VR and develop it as an exciting edutainment medium.

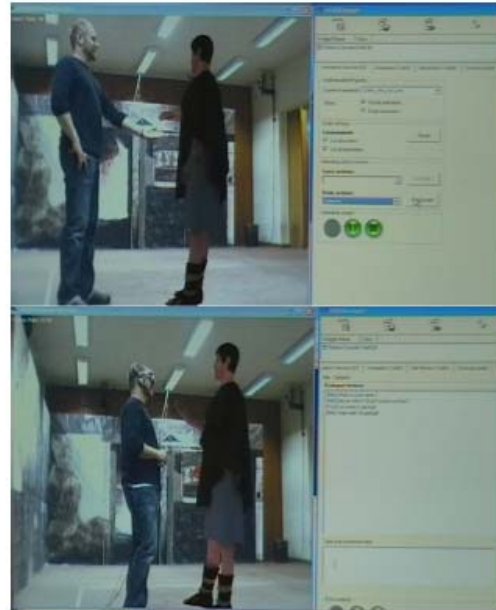


Figure 15: Interaction with a virtual human in an inhabited MR world

7. Acknowledgements

The authors wish to thank Alessandro Foni and Nedjma Cadi for their digital artistic contribution. The work presented has been supported by the EU IST FP6 programme, in frame of the EU IST ENACTIVE (<http://www.enactivenetwork.org/>) project and the EU IST FP5 programme in frame of the EU INCOMED ERATO (<http://www.at.oersted.dtu.dk/~erato/>) project.

References

- [AFO03] Okan Arıkan, David A. Forsyth, and James F. O'Brien. Motion synthesis from annotations. *ACM Transactions on Graphics*, 22(3): 392–401, 2003.
- [ASP05] Archaeological Superintendence of Pompeii, <http://www.pompeisites.org>, accessed at 13/06/05
- [CHO00] K. Choi, H. Ko, Online motion retargeting, *Journal of Visualization and computer animation* 11, 5, 223-235. 2000.
- [CMM*03] Cavazza, M., Martin, O., Charles, F., Mead, S. J., Marichal, X., 2003, "Interacting with Virtual Agents in Mixed Reality Interactive Storytelling", 4th International Workshop on Intelligent Virtual Agents, IVA03, 2003
- [EKM04] A. Egges, S. Kshirsagar, and N. Magnenat-Thalmann. Generic personality and emotion

- simulation for conversational agents. *Computer Animation and Virtual Worlds*, 15(1):1–13, 2004
- [EMM04] A. Egges, T. Molet, and N. Magnenat-Thalmann. Personalised real-time idle motion synthesis. In *Pacific Graphics 2004*, pages 121–130, 2004
- [GLEI98] M. Gleicher, Retargeting motion to new characters, SIGGRAPH 1998
- [Gra98] F. Sebastian Grassia. Practical parameterization of rotations using the exponential map. *Journal of Graphics Tools*, 3(3):29–48, 1998
- [H06] H-ANIM Humanoid Animation Working Group, Specification for a standard humanoid. <http://www.h-anim.org/>, Accessed May 2006.
- [KLS05] Kautz, J., Lehtinen, J., Sloan, P.-P., “Precomputed Radiance Transfer: Theory and Practise”, ACM SIGGRAPH 2005 Course Notes
- [KOV02] L. Kovar, J. Schreiner, M. Gleicher, Footskate cleanup for motion capture editing. SCA 2002.
- [LEE99] J. Lee, S. Shin, A hierarchical approach to interactive motion editing for human-like figures. SIGGRAPH 1999.
- [LHM03] Lindt, I., Herbst, I., Maercker, M., 2003, “Interacting within the Mixed Reality Stage”, Workshop Proceedings AVIR’03 / Magnenat-Thalmann, Nadia [Eds.], 2003
- [MCS*04] Magnenat-Thalmann, N., Cordier, F., Seo, H., Papagiannakis, G., “Modeling of Bodies and Clothes for Virtual Environments”, Proc. of Cyberworlds04, pp. 201 – 208, IEEE Computer Society, 2004
- [MK94] Milgram, P., Kishino, F., 1994, “A Taxonomy of Mixed Reality Visual Displays”, IEICE Trans. Information Systems, vol. E77-D, no. 12, 1994, pp. 1321-1329
- [NM00] Nandi, A., Marichal, X., 2000, “Transfiction”, Virtual Reality International Conference, Laval May 2000
- [PFT05] Papagiannakis, G., Foni, A., Magnenat-Thalmann, N., “Practical Precomputed Radiance Transfer for Mixed Reality”, Proc. of Virtual Systems and Multimedia05, pp. 189-199, VSMM Society, 2005
- [PLF*01] Papagiannakis, G., L’Hoste, G., Foni, A., Magnenat-Thalmann, N., “Real-Time Photo Realistic Simulation of Complex Heritage Edifices”, Proc. of Virtual Systems and Multimedia01, pp. 218-227, VSMM Society, 2001
- [POP95] Z. Popovic, A. Witkin, Motion warping, SIGGRAPH1995
- [PPM*03] Ponder, M., Papagiannakis, G., Molet, T., Magnenat-Thalmann, N., Thalmann, D., “VHD++ Framework: Extendible Game Engine with Reusable Components, for VR/AR R&D featuring Advanced Virtual Character Simulation Technologies”, Proceedings of Computer Graphics International03, pp. 96-104, IEEE Computer Society Press, 2003
- [PR97] F. C. Park and Bahram Ravani. Smooth invariant interpolation of rotations. *ACM Transactions on Graphics*, 16(3):277–295, July 1997
- [PSO*05] Papagiannakis, G., Schertenleib, S., O’Kennedy, B., Poizat, M., Magnenat-Thalmann, N., Stoddart, A., Thalmann, D., 2005, “Mixing Virtual and Real scenes in the site of ancient Pompeii”, *Computer Animation and Virtual Worlds*, p 11-24, Volume 16, Issue 1, Wiley Publishers, February 2005
- [SBT*99] Sannier, G., Balcisoy, S., Magnenat-Thalmann, N., Thalmann, D., 1999 “VHD: A System for Directing Real-Time Virtual Actors”, *The Visual Computer*, Springer, Vol.15, No 7/8, pp.320-329, 1999
- [SHI01] H. Shin, J. Lee, S. Shin, M. Gleicher, Computer puppetry: an importance-based approach. *ACM Transactions on Graphics* 20, 2, 67-94. 2001.
- [SKS02] Sloan, P.P., Kautz, J., Snyder, J., “Precomputed Radiance Transfer for Real-Time Rendering in Dynamic, Low-Frequency Lighting Environments”, Proc. of ACM SIGGRAPH02, pp. 527-536, ACM Press, 2002
- [TOL00] D. Tolani, A. Goswami, N.I. Badler. Real-time inverse kinematics techniques for anthropomorphic limbs. *Graphical models*, 62:353-388, 2000.
- [TYK01] Tamura, H., Yamamoto, H., Katayama, A., “Mixed reality: Future dreams seen at the border between real and virtual worlds”, *Computer Graphics and Applications*, vol.21, no.6, pp.64-70. 2001

Real-time Inhabited Virtual Worlds and Interaction - haptic module

Antonio Frisoli and Massimo Bergamasco and Emanuele Ruffaldi

¹PERCRO, Scuola Superiore Sant'Anna

1. Interacting in virtual worlds with haptic devices

1.1. Introduction to haptic interfaces

The rendering to the human operator of the sensation of physical interaction with a virtual environment (e.g. forces generated either by the weight or by the collision with simulated objects) or with a remote environment (e.g. in teleoperation systems) can be achieved by utilizing appropriate interfaces capable of generating adequate sensory stimuli. Such interfaces, called Haptic Interfaces (HIs), are force feedback devices that can exert a controlled force on the operator's limb like if he would be in touch with a real object.

Force feedback is mainly based on the stimulation of human proprioceptive and kinaesthetic sensorial system, providing information respectively on the body posture, movements and applied tensions.

The Arm and Hand Exoskeleton [Ber96] represents one of the first attempts to transfer the experience in teleoperation master design to the field of haptics. In the first half of the 1990s, the demand of simpler haptic interfaces stimulated the development of new desktop haptic interfaces. In reason of their low cost, today they are with no doubt the most prevalent kind of force feedback interfaces in use.

Generally the user can grasp a handle or a stylus, through which the interaction force generated in the Virtual Environment are exchanged with the user. The contact forces are applied to the endpoint of the stylus, which represents the contact point available for interaction with the virtual environment, and can simulate hand-held tools, such as pens, scalpel, endoscopic surgery tools.

When a mechanism is devised for being used as an Haptic Interface [HCLR94], the dynamic performance of the mechanical structure is an important aspect [Yos90].

2. Haptic Devices at PERCRO

At PERCRO there is a consolidated tradition in designing and building haptic interfaces with different and specific characteristics. In particular in the following two basic systems are described, a desktop single contact point and a two-contact points haptic device.

2.1. The Haptic Master 3DOF device

The Haptic Master is 3 DOF device based on a innovative parallel kinematics which allows only translational motion of the coupler. The coupler is a fully parallel translating platform realized by connecting a base and a moving platform (coupler) via three independent legs. Each leg is characterized by an open serial kinematics composed of 2 links and presents 5 DOF: the two universal joints at the ends and an actuated revolute joint at the elbow provide the pure translation of the coupler.

The third joint of each leg is actuated by a permanent magnet DC motor, through a steel cable transmission system, which introduces some elasticity into the actuation system and determines the dynamic properties of the device. The transmission system acts both as a speed reducer and a mean for localizing the motor far apart from the actuated joint, close to the base, so that moving masses are reduced and consequently reflected inertia at the end-effector too. Ball bearings are used to reduce friction and improve the force-feedback fidelity.

A six component force sensor, ATI Industrial Automation Nano17, is mounted on the coupler below an interface pen-like tool which can be manipulated by the user. The force sensor has a force range of 50 N along x,y axes, i.e. in a plane parallel to the base, and of 70 N along the z axis, aligned with the vertical direction, with a resolution of 0.05 N. High resolution optical encoders are mounted on motor shafts and are used for measuring the current interface position. Since the coupler orientation and position are kine-

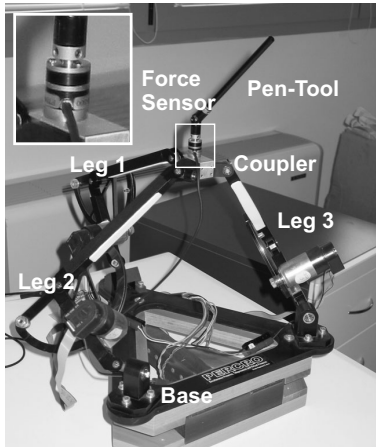


Figure 1: The Haptic Master (a)

matically decoupled, the direct kinematics algorithm of the mechanism is simple and can be computed in real-time.

The control hardware is constituted by a single board computer with PentiumIII 866MHz processor, running a RTAI Linux real-time operative system. A ServoToGo data acquisition board is used for reading force and position signals from the haptic device and commanding the motor signals.

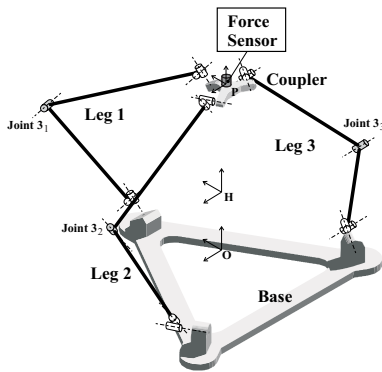


Figure 2: Schematic representation of the Haptic Master mechanism

The maximum peak force that the system can exert at the center of the workspace is 18 N, the stiffness at the end effector ranges from 8 N/mm in the worst condition up to 56 N/mm in the middle of the workspace. The operational workspace is a cylinder with diameter 200mm and height 200 mm and the lowest dynamic mode of the system is located around 55 Hz.

2.2. The GRAB system: a two contact points haptic device

Manipulation by means of standard commercial haptic devices [RHD99], commonly permanently connected to the finger through a thimble, presents some drawbacks for the implementation of effective multipoint systems, such as lack of collocation of thimbles due to the mechanical interference during manipulative procedures, restriction of the common workspace, calibration of the relative position of devices when several ones are used for each contact point.

The haptic interface herein presented was designed to enhance specifically manipulation capabilities [BACS06]. The following specifications were addressed in the design:

- **contact points:** to allow haptic interaction with two or more contact points;
- **workplace:** to fit within a standard office desktop with minimum encumbrance;
- **workspace:** to cover a large workspace for two hands/fingers cooperative manipulation. The optimization of device encumbrance often reduces the amount of workspace available at the end effector. Even if specific virtual panning and zooming exploration procedures can be set up to explore large environments [CK05], these constraints highly reduce the manipulation capabilities of the device;
- **force range:** to display forces typical of manipulation by hands in unstructured environments;
- **isotropy:** to achieve an isotropic behavior both under kinematic and dynamic conditions. Isotropy display of forces and inertias is more important for multipoint displays, since differences of transparency between different fingers are easily perceived;
- **other performances:** to minimize residual friction, reflected inertia and increase mechanical force bandwidth; all these factors influence the transparency of the device.

2.2.1. System design

The system is composed of two identical robotic arms with equivalent RRP RR kinematics, shown in Figure 3, that provide the force-feedback for the two fingers. The user can operate the device by inserting his fingers in two thimbles placed on the end-effectors of both the arms, so that both single hand (thumb and index) and two hands (right and left indexes of two hands) interaction are possible. A set of rubber thimbles of different sizes allow any finger size to properly fit in the device.

Each arm has 6 degrees of freedom (dofs), of which the first three ones, required to track the position of the fingertip in the space, are actuated, while the last three ones, required to track its orientation, are passive. The first three dofs are kinematically equivalent to the combination of two orthogonal and incident rotational pairs and one prismatic pair, that drives a barrel along a third incident axis. The combination

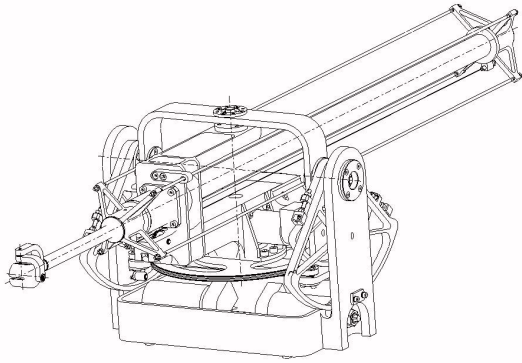


Figure 3: Schematic model of the device

of these three dofs allow to position the end-effector over a large workspace. The last three rotational pairs form a spherical wrist that allow the rotation of a sizable thimble around a common center. Figure 4 shows the kinematics and the geometric notation adopted for the description of the device.

The first two degrees of freedom are actuated by means of a differential transmission composed of two capstans acting on a common driven pulley. The concurrent motion of these capstans produce a barrel rotation (link 3) along the horizontal axis z_0 . The differential (opposite) motion of the capstans produce a barrel rotation along the vertical axis y_0 .

This kind of transmission makes the operation of device symmetric with respect to two possible motions of the barrel (tilting and yawing), achieving a high kinematic isotropy along these directions.

According to this design the maximum continuous force in the worst case condition is $4N$, while the maximum peak force in the same position is $10N$. These forces can be applied in any direction. Typical maximum continuous force value (in the center of the workspace) is $7N$ in all directions.

2.2.2. Workspace

The dimensioning procedure also considered to guarantee a minimal workspace including a box of $300 \times 400 \times 600 \text{mm}$. The reachable workspace is given by the intersection of the two manipulator workspaces, as shown in figure 5. The geometry of the optimized workspace allows to integrate the two devices placed one in front of each other. This arrangement does not affect considerably the common reachable workspace allowing therefore the user to manipulate objects over a large space.

The mechanical interference of the structures is a further limitation occurring during the integration of several devices into the same workspace. In fact manipulation of virtual objects requires the user to freely move and rotate his own hand(s). In this system the degree of interference between the two structures is reduced, and does not occur during

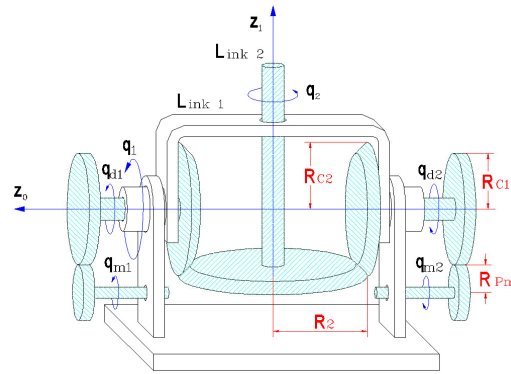
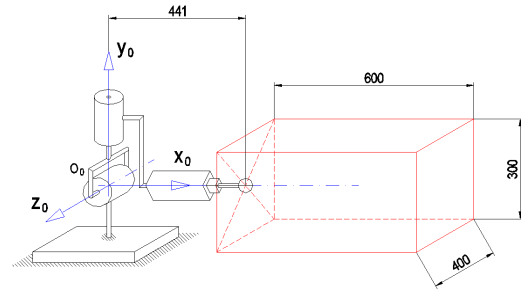


Figure 4: Kinematics of first three DOF and kinematic notation

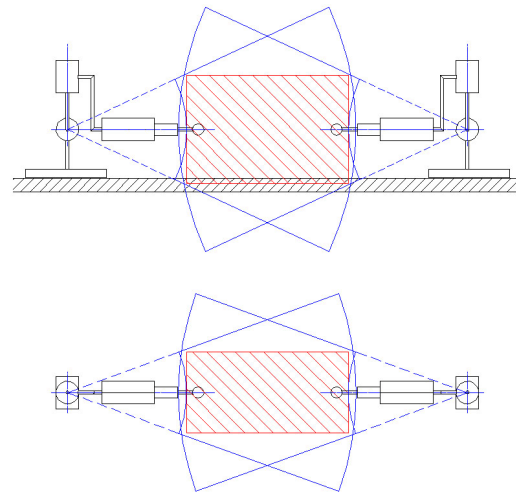


Figure 5: Workspace of two arms

common manipulative procedures either with one hand or two hands.

As far as the reflected mass/inertia is concerned, the use of a differential transmission systems has allowed to make the properties of the mass matrix more regular, reducing consequently the effect of Coriolis and inertia disturbances during

fast motions. Specific design solution of the actuation and the transmission are arranged to fix the transmission cables to the links, reducing the pretensioning of cables and relative friction. No reduction gear was employed in the design, achieving therefore an almost zero backlash system. The actuation was made by low-inertia brushed DC servomotors, with an iron-less construction of the rotor. The kinematic solution allowed to ground the first two motors with larger bulk and thus reducing the amount of moving masses. The third motor, that provides the translational motion of the barrel, acts also as counterbalance of the barrel weight in the worst kinematic position, i.e. when the barrel is completely extended.

2.2.3. Static and dynamic performance

The whole structure was completely made in aluminum with some parts in carbon fiber. All links were designed for maximizing mechanical stiffness. In order to reduce the moving mass of the barrel while preserving torsional stiffness, four additional rods were added along each barrel.

A particular attention was given to the mechanical stiffness of the barrel along the y and z directions. Such stiffness depends on the extension of the barrel and may become critical when it is completely extended. In order to evaluate the compliance along these directions we evaluated the two main contributions:

- a linear contribution c_{lin} due to the transmission system, concentrated at the level of rotational joints 1 and 2. This compliance is constant at level of joints, while the equivalent compliance at the end-effector is proportional to the square of barrel displacement (L);
- a flexional contribution c_{flex} , due to the mechanical rigidity of the barrel axis which bends under the action of a tangential force (in y,z planes) applied at its end-effector. The barrel was considered equivalent to a cantilevered rod and therefore its compliance may be expressed as a cubic relationship between the applied force and the barrel displacement (L).

According to the above consideration the final compliance at the level of the end effector, can be expressed as

$$c_y = c_{lin} + c_{flex} = a_1 L^2 + a_2 L^3 \quad (1)$$

This compliance was experimentally determined by fixing the end-effector of the device to a rigid support and applying a command torques to the motors corresponding to increase forces in the direction F_y . The displacement error was measured using the information provided by the encoders for different values of the barrel displacement. The interpolating cubic curve was found as the best least-square fit with experimental data and is shown in figure 6. Experimental measured stiffness spans in the range from 1.5 to 13.5 N/mm.

The performance of the device along the barrel axis, since

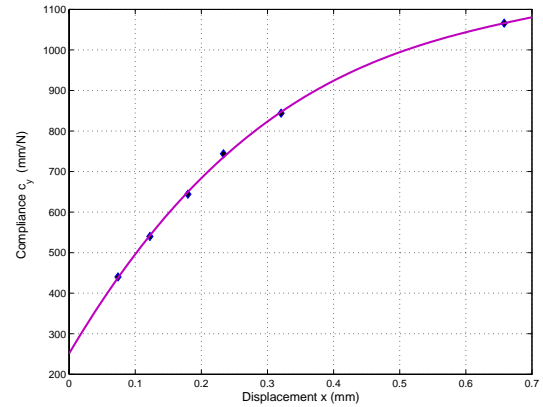


Figure 6: Experimental mechanical compliance along y in the worst case condition

it is almost aligned with the grip direction, can greatly affect the control of grip during simulation. The stiffness of the device along the barrel axis was experimentally assessed, by connecting the end-effector to an ATI nano17 force sensor, and grounding the sensor to a rigid support. The experimental stiffness estimation was found as the least square linear correlation between measured forces and displacements along the barrel axis. A value of $K_x = 23.74 N/mm$ ($R_{sq} = 0.994$) was found.

Also the dynamic performance of the device was experimentally assessed, by measuring the force response of the device along the barrel direction (x axis) in the same conditions as above. The input torque to the motor was a chirp input command. The force response is shown in Figure 7, and confirms that the device can reach a large dynamic bandwidth along the x direction, between 70 and 80 Hz.

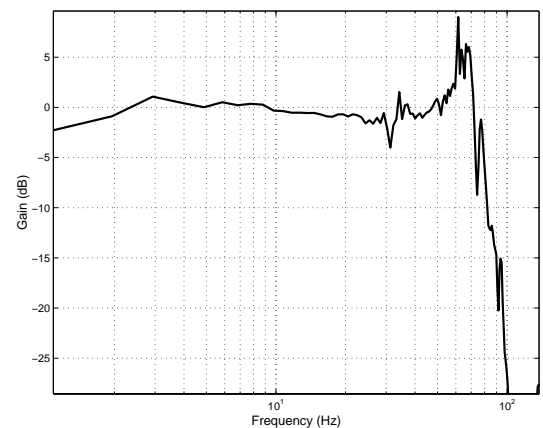


Figure 7: Dynamic force bandwidth of the device along x direction

3. Control schemes for haptic interfaces

The dynamic relation between the contact force and the contact point velocity during a one point physical interaction between two bodies is called impedance. An ideal (in the sense of transparency) haptic device has to reproduce the same mechanical impedance of the virtual object the user is touching. Admittance and impedance control are the two principal classes of controllers used in haptic interfaces [FSA*04]. In the following we will indicate the mechanical impedance of the master haptic device, of user's hand and the desired virtual impedance respectively with Z_M , Z_H and Z_D ; \mathbf{F}_v are the forces voluntarily exerted by the operator.

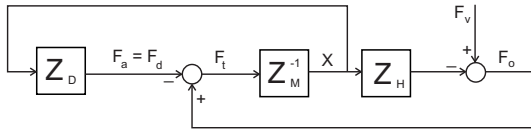


Figure 8: Scheme of an impedance control

In the impedance control the actuator force \mathbf{F}_a is computed on the basis of the position \mathbf{X} of the end-effector through the desired impedance Z_D mathematical relationship:

$$\mathbf{F}_a = Z_D \mathbf{X} \quad (2)$$

This method is the most commonly employed in haptic interface systems [YYMZ95, AH99], since it does not require any additional force sensor and can be particularly effective if the impedance of the device can be considered negligible, as reported in [MS94].

The addition of a feedforward pre-computed torque or the feedback linearization of the dynamics are common techniques which can be used together with the open-loop force control, in order to compensate the dynamics of the device and improve the transparency of the device. However an exact knowledge of the dynamic model of the system is required to achieve an ideal cancellation of undesired effects.

Force sensors can be usefully employed for improving the transparency of the device, guaranteeing a sufficient system stability with a good quality of perceivable force.

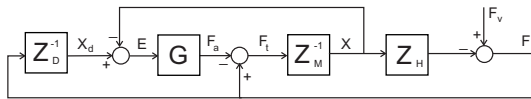


Figure 9: Position-based impedance control

Unlike the admittance control developed for robotic applications [GN94], the approach adopted by Maples e Becker [MB86], known as "Position-based Impedance Control", is

based on the reading of the interaction force at the user's contact point, providing back the desired position at the end effector according to the desired virtual impedance

$$\mathbf{X}_d = Z_D \mathbf{F}_o \quad (3)$$

Such a control scheme is known as "Admittance control with position feedback". An internal control loop G is adopted to regulate the position.

In a third class of controllers a closed-loop internal controller is added to the previous scheme to regulate the interaction forces. Such a method, known as 'Force-based Impedance Control' [Law88], has also been implemented on different devices [BABF92].

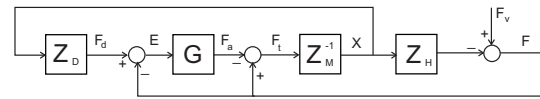


Figure 10: Force based Impedance Control

The presence of the controller G allows to cancel the dynamics of the mechanism, in order to render more transparent the force feedback.

It can be argued that while the impedance control is more suitable for mechanisms with negligible dynamics, the 'Position-based Impedance' and 'Force-based Impedance', by using high gains G , are commonly applied to mechanisms with significant dynamics. For these reasons a 'Force-based Impedance' control law has been adopted for the Haptic Master 3DOF device, which is described in the following.

3.1. Formal definition of passivity

Consider to have two variables that can be associated to the concept "effort" y and "flow" x . Usually flow refers to a generalized vector of velocities and angular velocities, while effort refers to a generalized vector of forces and torques. The inner product of effort and flow is the instantaneous power input to the associated physical system, and can be formalized by introducing a scalar product between x and y

$$\langle x|y \rangle = \int_0^{\infty} (x(t), y(t)) dt \quad (4)$$

where $(x(t), y(t))$ is usual scalar product.

Similarly for discrete systems we can define:

$$\langle x|y \rangle = \sum_i (x(i), y(i)) \quad (5)$$

3.2. Definition of passivity

So a system with input x and output y is *passive* if $\exists \beta$

$$\langle x|y \rangle_T \geq \beta, \forall T \quad (6)$$

where the notation means that the function is zero for $t > T$, while is defined for $t \leq T$.

A system is strictly passive if $\exists \delta, \beta$

$$\langle x|y \rangle_T \geq \delta \|x_T\|^2 + \beta \quad (7)$$

3.3. Equivalent formulation of passivity

Suppose that the function $h(t)$ is associated to its transfer function \hat{h} through the convolution integral,

$$y(t) = \int_0^t h(t-\tau)u(\tau)d\tau = h * u \quad (8)$$

and so in the frequency domain:

$$\hat{y} = \hat{h}\hat{u} \quad (9)$$

If we consider the *Parseval theorem* that states that, given the Fourier transform $\hat{y}(j\omega)$ and $\hat{x}(j\omega)$:

$$\int_0^\infty x(t)y(t)dt = \frac{1}{2\pi} \int_{-\infty}^\infty \hat{y}^*(j\omega)\hat{x}(j\omega)d\omega \quad (10)$$

where the asterisk $*$ denotes the complex conjugate

We have that the passivity of a system with transfer function \hat{h} , and input u_T should satisfy the following equality

$$\begin{aligned} \langle u_T(t)|(h * u_T)(t) \rangle &= \int_0^\infty u_T(t)(h * u_T)(t)dt = \\ &= \frac{1}{2\pi} \int_{-\infty}^\infty \hat{u}_T^*(j\omega)\hat{h}(j\omega)\hat{u}_T(j\omega)d\omega \end{aligned} \quad (11)$$

that can be rewritten as

$$\langle u_T(t)|(h * u_T)(t) \rangle = \frac{1}{2\pi} \int_{-\infty}^\infty \|\hat{u}_T(j\omega)\|^2 \hat{h}(j\omega)d\omega \quad (12)$$

Then since $\hat{h}(j\omega) + \hat{h}(-j\omega) = 2\Re(\hat{h}(j\omega))$, because \hat{h} is a transfer function with real coefficients, in order to be physically realizable, we can equivalently state

$$\langle u_T(t)|(h * u_T)(t) \rangle = \frac{1}{\pi} \int_0^\infty \|\hat{u}_T(j\omega)\|^2 \Re(\hat{h}(j\omega))d\omega \quad (13)$$

or as it is also often found:

$$\langle u_T(t)|(h * u_T)(t) \rangle = \frac{1}{2\pi} \int_{-\infty}^\infty \|\hat{u}_T(j\omega)\|^2 \Re(\hat{h}(j\omega))d\omega \quad (14)$$

From (12) we can see how the passivity implies that we should have that:

$$\forall \omega > 0 \quad \Re(\hat{h}(j\omega)) > 0 \quad (15)$$

or equivalently *the Nyquist polot of h is in the right half-plane.*

For a MIMO system, considering the equivalent $\hat{h}(j\omega) + \hat{h}(-j\omega) = 2\Re(\hat{h}(j\omega))$, we can express the passivity condition by imposing the following condition on the transfer function matrix H :

$$\forall \omega > 0 \quad \hat{H}(j\omega) + \hat{H}^T(-j\omega) > 0 \quad (16)$$

The Virtual Environment was classically modeled as an impedance with damping factor b_e and stiffness k_e :

$$\begin{cases} F_e = -\left(b_e + \frac{k_e}{s}\right)V_e & \text{if } X_e \text{ is penetrated inside the wall} \\ F_e = 0 & \text{during free motion} \end{cases} \quad (17)$$

3.4. Classical approach to passivity

In [BC94] a classical approach for computing the limits of the stability for a class of sampled-data systems is presented.

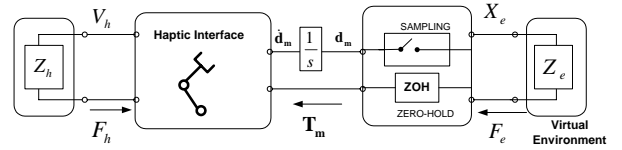


Figure 11: Scheme of the interfacing between a haptic device and the virtual environment

The haptic interface behaves as a rigid body with mass m with some viscous friction b , while the impedance exerted by the human operator is passive.

The operator can be replaced with an impedance Z_h [MIHB85] bounded by the maximum value of:

$$Z_{h,max} = 300 \frac{N \cdot sec}{m} + \frac{1000 N}{s} \frac{N}{m} \quad (18)$$

If as in [BC94] the transfer function of the haptic interface system is reduced to a first-order system, composed of a mass m and a damper b on which both operator and actuator forces are acting (see figure 12), then the transfer function of the operator+HI system, observed at terminals of Z_e is given by:

$$G(s) = \frac{1 - e^{-Ts}}{s^2} \frac{1}{ms + b + Z_h(s)} \quad (19)$$

where the Zero Holder has been classically modeled as

$$ZOH(s) = \frac{1 - e^{-Ts}}{s} \quad (20)$$

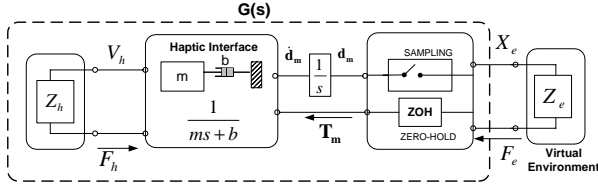


Figure 12: The simplified representation of HI such as in [BC94]

On the basis of (19), [BC94] has found, after a linear fractional transformation, the explicit expression for the Z-transform [BMZ96] of function $G(s)$, given as:

$$\begin{aligned} G^*(j\omega) &= \frac{1}{T} \sum_{k=-\infty}^{k=+\infty} G(s + jk\omega_s) = \\ &= \frac{T}{2} \frac{e^{-j\omega T} - 1}{1 - \cos(\omega T)} \frac{1}{mj\omega + b + Z_h(j\omega)} \quad (21) \\ \omega_s &= \frac{2\pi}{T} \end{aligned}$$

where T is the sampling time. By imposing conditions for closed loop stability by the Small Gain Theorem to (21) for $Z_e = k_e + \frac{b_e}{T}(1 - z^{-1})$ [†], it is found that the following expression should hold [CS94]:

$$b > \frac{k_e T}{2} - b_e \cos(\omega T) \quad (22)$$

At less than half the Nyquist frequency (which may be 500 Hz or greater), the factor $\cos(\omega T)$ is positive, and so we can assume as condition for stability as:

$$\frac{b + b_e}{k_e T} > \frac{1}{2} \quad (23)$$

3.5. Z-Width of the Haptic Display

Figure 13 reports experimental conditions for stability of an Haptic Interface system.

The implementation of the derivative was based on a low-pass filter, with pole at 60 Hz, and was numerically realized with backwards integration.

The upper limit on b which is shown in figure 13, refers to the amplification of noise due to the discrete-time differentiation of a quantized signal. The position sensors were high resolution encoders with 4000 pulses per round, with an angular resolution of 0.0016 rad.

[†] This is the case when euler method is used for the discrete-time numerical integration of dynamic equations

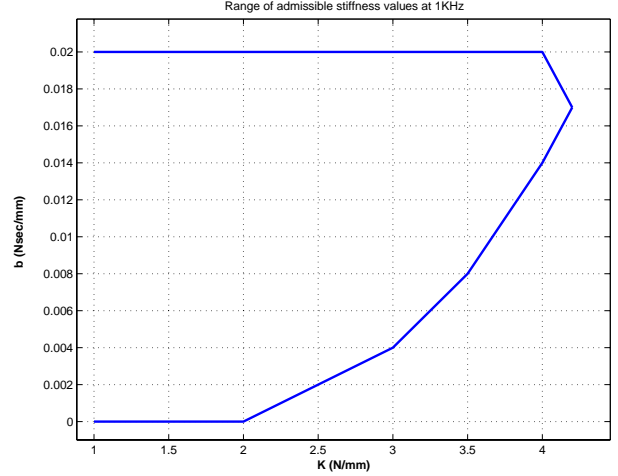


Figure 13: Z-width plots for $f_s = 1\text{KHz}$ and derivative with low-pass filtering

3.6. Impedance based closed-loop force control

When velocity or acceleration sensors are available, the cancellation of inertial terms can be obtained with a feedforward compensation scheme using either a pre-computed torque or inverse linearized dynamic model. In such a case the accuracy of the mathematical model can greatly condition the effectiveness of the implemented control and the computation time is affected by the complexity of the model.

The usage of force sensors, placed at the zone of connection with the operator, allows to achieve an analogous result, but requiring lower computation time. In the case of Haptic Interfaces, the closed loop control must be designed in order to guarantee a full range stability independently of user's behavior.

If we consider a simplified model of the haptic device as given by (??), it is easy to see how a proportional action of the controller will not be sufficient to have a robustly stable feedback control law. At least an integral action is required in order to have a first order dynamics of the controller:

$$\mathbf{F}_a = \left(G + \frac{K_i}{s}\right)(\mathbf{F}_d - \mathbf{F}_o) = C(s)\Delta\mathbf{F} \quad (24)$$

where $C(s)$ indicates the Laplace transfer function of the force controller.

Notwithstanding the accuracy that can be achieved with a PI controller, by adding in feedforward the open-loop value of desired force \mathbf{F}_d , the response of the controller is improved. In this way the closed loop control is used only to cancel modelling errors which cannot be compensated in open loop.

$$\mathbf{F}_a = \mathbf{F}_d + \left(G + \frac{K_i}{s}\right)\Delta\mathbf{F} \quad (25)$$

3.7. Evaluation of transparency

In order to analyze the transparency of the device under a simple force control loop, suppose, for reducing the mass M of system (??) felt by the operator, to adopt the control law $F_a = -GF_o$, where G is the control gain.

So from the dynamics equation of this system we find:

$$M\ddot{\mathbf{x}} = -\mathbf{F}_o(1+G) \rightarrow \ddot{\mathbf{x}} = -\frac{(1+G)}{M}\mathbf{F}_o \quad (26)$$

In this case by acting on the values of gain G it is possible to reduce the value of reflected inertia given up to $\frac{M}{1+G}$. For higher gains G it is possible to reduce the perceived mass up to zero, while for a value of $G = -1$ it is simulated the dynamics of an infinite mass.

When the elasticity of the system is not negligible, assumptions of (26) are no longer valid, but the model represented in Figure 14 should be adopted.

If the same control law is adopted $F_a = -GF_o$, by introducing the notation $\tau = \frac{M_m}{M_l}$, it can be shown that the controlled system admits an analogous representation in terms of physical equivalents, shown in Figure 14, where the new values of M'_m and k' are given by:

$$\begin{cases} M'_m &= \alpha M_m = M_m \frac{\tau-G}{\tau(1+G)} \\ k' &= \beta k = k \left(\frac{\tau-G}{\tau}\right) \end{cases} \quad (27)$$

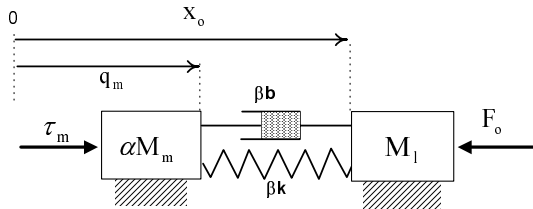


Figure 14: Equivalent system of the two-mass model

Note that now the endpoint mass M_l actuated by the environment is unchanged, and it is an "uncontrollable element".

It is worth to notice that the total reflected mass of the system is unchanged with respect to the case of single rigid body, since:

$$M_{tot} = M'_m + M_l = \frac{M_m + M_l}{1+G} = \frac{M}{1+G} \quad (28)$$

Clearly large negative feedback are not admissible in this case, since $G > \tau$ would result in a negative spring, mass and damper, then implying a violation of the coupled stability

criterion and therefore the potential instability when coupled to a passive environment.

Moreover is easy to show that in the best case of realization of a dynamic compensation with $G = \tau$, we can achieve a perceived mass of M_l , as can be verified by direct substitution into (28).

4. Grasping in Virtual Environments

Grasping is one of the basic haptic modes [DK02] and has key importance in most types of interactions between humans and the world surrounding them. Grasping an object allows us to identify some of its properties (geometry, material, surface textures) [KLCR99], change its physical state (position in space, internal structure) and use it for mediated interaction with other objects. The haptic mode is highly dependent on the application [Ka90, DK02]. The possibility of interacting with more than one point of contact seems to be fundamental for the manipulation of objects in virtual environments: for instance, tasks such as determining temperature or hardness require only one point of contact, while determining shape and size of an object are usually more efficiently conducted with more than one point of contact.

Humans unconsciously use suboptimal [GW84] algorithms for the prehension of objects when performing tasks with their hands. For instance, during a peg-in-hole task, they precisely adjust the relative position and interaction force between the peg and hole. Johansson and Westling conducted a series of experiments, relating tactile information to grip force when performing a lifting task [RJ84]. The ability to adjust grip force appears to be independent of the surface friction characteristics, but further studies from the same authors confirmed that this is not true for the case of objects with different curvature, and propose an active role of rotational friction for the stabilization of the grip [GJJ98]. The nature of contact during slip provides important tactile cues regarding features on the surface as well as the nature of movement of the object, and can explain how humans take advantage of slip sensitivity when perceiving objects.

Even if almost all existing haptic interfaces provide a user interaction based on a single contact point, an increased number of contact points, not only allows to display a more natural haptic interaction [JM03, FBW*04], but also improves the quality of interaction that users can perform in the environment. Multipoint haptics [BFSB04a, BSD04] refer to those devices that can simultaneously interact with the user through more than one contact point. These systems allow the representation of force and torque feedback during the simulation of dexterous manipulation and complex maneuvering of virtual objects and can improve the interaction in several applications, e.g. assembly and disassembly in virtual prototyping [MPT99a, MW03], medical palpation during simulated physical examination of patients [KNK*05] and many other ones. The existing devices at the state-of-the-art have several limitations for the simulation of grasping

with more than one contact point, both in terms of workspace and mechanical interference among fingers. Furthermore, the limited amount of available devices for multifinger manipulation also has slowed down the development of haptic rendering modules for multiple contact points.

Non-direct contact haptic devices [SYYM04], such as encountered haptics, who externally track the position of the human fingers, represents a promising technology for the implementation of haptic devices with multiple contact points. Some preliminary prototypes [CFM*05] have been already developed, but however, the level of technology is still far from reaching the quality for a satisfactory multipoint interaction.

From a psychophysical point of view, the interactions with virtual objects during multipoint manipulation poses several interesting research questions at the level of sensorimotor coordination of movement in humans. This issue is of great interest in the context of virtual environments, where the simulation can be used also for assessing the performance of humans in the execution of a given task [YI03].

There is also an increasing request from applications of a better integration of the physical stimuli during manipulation in virtual environments. In the CREATE [DAM*03] project, children can learn the elements and the geometry of a Greek temple by reassembling it from its ruins. In the advanced visualization system the haptic rendering generates the physical perception of the contact and the ability of manipulating objects in a natural fashion, increasing the user's attention and control during the execution of the task and the realism of the interaction. A snapshot of the application is shown in the left side of Figure 15, while in the right side it is shown the equivalent virtual manipulation analyzed in the present work.

The purpose of this work is to assess the capabilities of haptic systems for grasping and manipulation of virtual objects. A new haptic device for manipulative tasks with two contact points is used, designed to overcome most of the existing technological constraints, such as achievement of the collocation of several contact points, increase of force and common workspace capabilities.

The present work also investigates the relationship between the psycho-physical perception of prehension and the features of the physical model used for the force control of the device. Such a model is based on several parameters, that represent several physical behaviors such as gravity, friction and dynamics. An assessment phase, designed according to experiments already conducted in real environments, highlighted a good matching between the manipulation in virtual environments and reality, providing further indications for the design and the setup of physical manipulative virtual models.

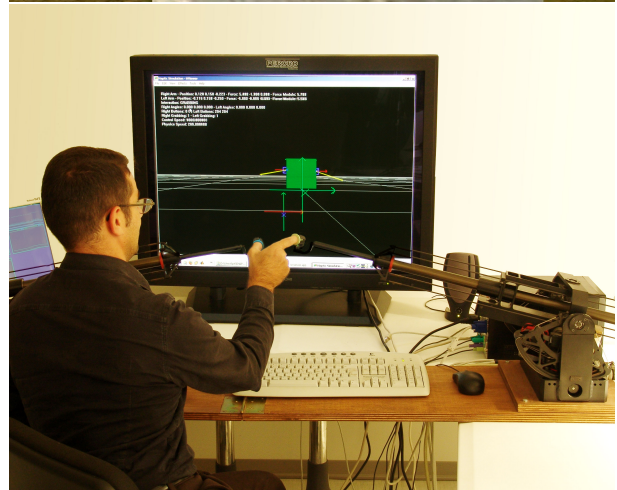
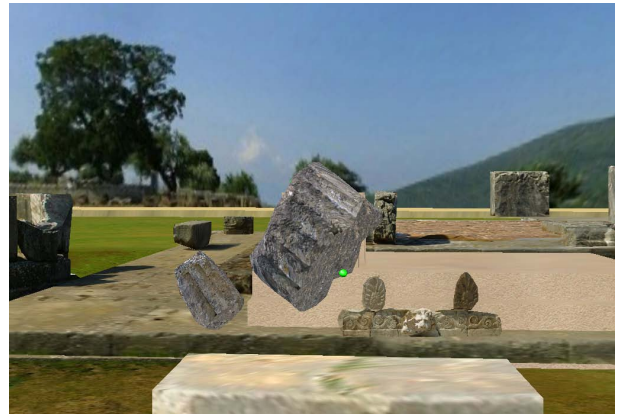


Figure 15: The CREATE application context and the underlying manipulative model

5. Overview of a classical haptic rendering architecture

The VE engine implements a specific architecture for computing the force feedback during the exploration and manipulation of the objects in the virtual environment. This process should provide a stable force feedback according to the forces arising during explorative and manipulative tasks, such as inertia, weight, contact and friction forces.

5.1. General architecture

The complexity of the interaction in manipulative environments requires a multithreaded/multirate architecture. Diagram 16 describes how components are connected and grouped in different computing threads. There are two fundamental state information exchanged by the modules:

- the Device State, representing all the information coming from the device, e.g. the position of the contact points;

- the Object State, characterized by the position and orientation of each object in the virtual space and their properties.

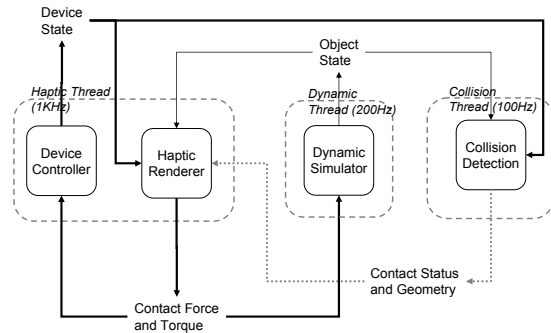


Figure 16: The Haptic Rendering Architecture

Stability of the haptic response requires that the rendering process (Haptic Thread) should be updated at high speed frequency (1KHz typical). The Haptic Renderer receives the Device State as input from the Device Controller and computes the corresponding contact forces as output. The haptic rendering is performed on the basis of the collision information of the haptic contact point with the objects, computed by the Collision thread, running at a much lower rate. The Collision Detection computes the set of primitives that are in a volume around the contact point, then used by the Haptic Renderer to compute the force feedback. The Collision Detection is actually implemented using an external module based on bounding volume hierarchy and running at about 100Hz.

The simulation of the dynamics of the objects is achieved through a Dynamic Simulator, that is carried out through a separate thread running at about 200 Hz, because its computation is potentially intensive, depending on the complexity of the environment and the kinematic constraints between the objects.

In the complete architecture, two geometrical representations are associated to each object: the first one is the haptic geometry used for the collision detection with the haptic contact points and the second one is the physics geometry that can be simpler. This approach allows to achieve a precise haptic interaction, while maintaining a smooth dynamic simulation.

The contact force exerted by the user are applied to the touched object through the Dynamic Simulator, allowing the direct manipulation of the object. It is worthwhile to analyze some stability considerations regarding the manipulation of virtual objects. Whenever an object is grasped in virtual environment by the user's fingers, it is virtually tied to the contact points through a couple of springs representing the vir-

tual stiffness of the environment. In this case, the stability limits of manipulation are determined by the typical resonance frequency of this kind of contact, that can be computed as:

$$\frac{1}{2\pi} \sqrt{\frac{2K_s}{M_v}}$$

where K_s is the object stiffness in the virtual environment and M_v represent the virtual object mass. For the cases considered in the present work, masses ranging from 0.1 ÷ 0.5 Kg and stiffness ranging from 500 ÷ 2000 N/m, the typical resonance frequencies varies between 5 ÷ 45Hz, well beyond the frequency of the dynamic simulation.

5.2. The linear friction model

The force information for controlling the objects is determined through the position of the contact points. The position of each contact point is measured directly by the haptic interface (\mathbf{x}_h) and the relative feedback force (\mathbf{F}) is computed through a constraint-based proxy method with friction, based on [ZS95b, MH04, BDS03]. The haptic rendering algorithm computes the position of an additional point \mathbf{x}_p , called proxy, lying on the object geometry, and on the basis of current \mathbf{x}_h position of the haptic interface and contact geometry (\mathcal{C}) the force is generated through a *direct rendering* method $\mathbf{F} = G(\mathbf{x}_h, \mathbf{x}_p, \mathcal{C})$, using the coupling between the proxy \mathbf{x}_p and the interface position \mathbf{x}_h . The proxy algorithm should take into account the movement of the object, and in particular it is necessary to update the last proxy position with the movement of the object: this is easily achieved by representing the proxy in object coordinates.

The standard proxy algorithm is modified with the linear friction algorithm using the friction cone model [MH04]: the movement of the proxy towards the goal position is prevented by the friction, and perceived by the user as a tangential force. The algorithm works by building a friction cone with the top at the haptic contact point, the base centered at the god point and an aperture depending on the friction coefficient. If the last proxy position is inside the cone the proxy is not moved and the user perceives a tangential force opposite to the moving direction, otherwise the proxy is placed at the boundary of the cone. The evaluation of the position of the proxy respect to the friction cone is equivalent to decomposing the contact force in the normal and tangential components and evaluating if the tangential is greater than the normal force multiplied by the static friction coefficient. The advantage of this algorithm with respect to others are that is only position based and it does not require a velocity estimation for the evaluation of the friction force.

The static friction is extended with the dynamic friction by using a proxy algorithm with two states, slip and not slip. During the not slip state the proxy is not moved if inside the static friction cone otherwise the state is changed to slip and the proxy moved to the border of the dynamic friction

cone; when in slip mode the state is changed to not slip if the proxy is inside the dynamic cone otherwise the state is kept and the proxy moved to the border of the dynamic friction. The figure 17 shows the two friction cones and the transition diagram.

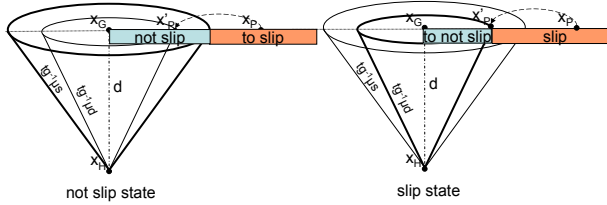


Figure 17: The linear friction cones

The algorithm can be numerically implemented through the following steps, performed while the finger is in contact with the object and the contact is not broken. At a generic k -th time sample:

a: Computation of goal position. The new goal position is computed as $\mathbf{x}_g = \mathbf{x}_s$, where \mathbf{x}_s is the surface point which minimizes the distance between the HI point \mathbf{x}_h and the contact surface. \mathbf{x}_g is assumed as the new goal value for \mathbf{x}_p .

We assume the following definitions:

$$\begin{cases} r = \|\mathbf{x}_g(k) - \mathbf{x}_p(k-1)\| \\ d = \|\mathbf{x}_g(k) - \mathbf{x}_h(k)\| \end{cases} \quad (29)$$

b: Analysis of the friction condition. In static conditions the new position of the proxy can be expressed as:

$$\mathbf{x}_p(k) = \mathbf{x}_p(k-1) \quad \text{if} \quad \frac{|F_t(k)|}{\mu_s |P(k)|} = \frac{r}{\mu_s d} < 1 \quad (30)$$

where $|P| = k_l d$ is the force directed along the contact normal and k_l is the haptic servo-loop gain, equivalent to the linear stiffness, used for calculating the elastic penetration force.

Otherwise, conditions of dynamic friction should be applied and the god-object, sliding over the surface, is moved on the boundary of the dynamic friction cone:

$$\mathbf{x}_p(k) = \mathbf{x}_g(k) + \mathbf{r}' \quad (31)$$

with

$$\mathbf{r}' = \frac{\mathbf{x}_p(k-1) - \mathbf{x}_g(k)}{r} \mu_d d(k) \quad (32)$$

c: Computation of friction force. A new force $\mathbf{F}(k) = k_l(\mathbf{x}_p(k) - \mathbf{x}_g(k))$ is computed using the new value of \mathbf{x}_p .



Figure 18: Example of object grasping

Force $-\mathbf{F}(k)$ is applied to the virtual object, while a force $\mathbf{F}(k)$ is also applied to the user.

d: Computation of the new position of the object. New velocity (\mathbf{v}, ω) and position (\mathbf{x}, θ) are computed for the virtual object.

e: Update of the proxy position. The current value of \mathbf{x}_p is corrected to take into account the displacement of the virtual object:

$$\mathbf{x}_p = \mathbf{x}_p + \mathbf{x}_c \quad (33)$$

The algorithm is repeated from step a.

5.3. The grasping model

The above architecture is easily extensible to multiple contact of points: the Device Controller invokes the haptic rendering for each contact point, and the Collision Detection component performs a collision test for each contact point. From the point of view of the dynamic simulation the two contact points are invisible and they affect the simulation by applying forces on the grasped object.

The grasping of objects in this system is based on the friction and on the dynamic simulation of the objects. The grasping force exerted by the user over the object produces a friction tangential force for each of the contact points that allows to raise and manipulate the object. This model is well integrated in the dynamic simulator because when the object comes in contact with other objects the user receives a force feedback as a change of depth caused by the movement of the object. The figure 18 shows a simple example of object grasping in this system, with the display of the two contact points and the contact forces shown as the yellow vectors.

In the design phase of the grasping there are some parameters that are correlated and should be correctly evaluated

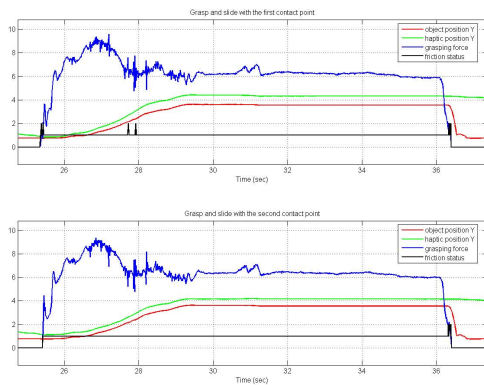


Figure 19: Forces and position during holding and release of a virtual object

for allowing a precise grasp of the object: the static friction coefficient, the mass of the object and the stiffness of the object. In the evaluation part of this paper the effect of these different parameters were analyzed on a group of subjects.

Figure 19 shows the behavior of the system during the grasping of an object, with a diagram for each contact point. Three phases can be identified: the first is the lifting phase when the user starts to grasp the object, the second is the holding phase and finally there is the releasing phase when the object starts to slide. In the diagrams the green and red lines represent the position of the contact point and the object along the Y axis (aligned along the gravity vector). During the lifting and holding phases the two positions have a constant difference that depends on the grasping point on the object, then in the releasing phase they diverge because the object is falling. The black line shows the status of the friction that is zero when there is no contact, one during the non-slip state and two in the slip state: it is clear that during the lifting and holding phases the proxy is in non-slip state because it is firm between the fingers and, when the object is released, initially it changes to slip mode and then the contact is lost. Finally the blue line represents the grasping force that has an increasing and varying behavior during the lifting phase, but it is almost constant during the holding phase.

6. Evaluation of grasping load and slip force in pick and place operations

In order to assess the efficiency of the device and the rendering for pick and place operations, a specific evaluation was performed to compare the available data on human grasping of real objects [GW84, JGB73] with the virtual case. The influence of weight on static grip has been experimentally studied by [GW84], where safety margins for grasping for

prevention of slipping are analyzed. The safety margin is defined as the difference between the grip force and the slip force, that is the minimum grip force required for preventing slipping.

6.1. Subjects and general procedures

Three healthy right-handed men, aged between 27 and 35 yrs, served as subjects for the study. The subjects sat on a height-adjustable chair. In this position the subject might held with his right hand the two thimbles connected to the haptic interfaces, and respectively wear them on the thumb and right index of his hand. A wide visualization screen was placed in front of the screen and a desktop, where during the experiment the subject was invited to place its elbow. A sequence of 27 objects was presented twice to each subject, for a total of 54 runs performed by each subject. All the objects in the randomized sequence were cubes with the same geometry, with pseudorandom changes in the weight m (0.1, 0.2, 0.4 Kg), in the friction coefficient, both static μ_s (0.4, 0.8, 1.2) and dynamic μ_d (0.3, 0.6, 1.1), and in the stiffness k (0.5, 1, 2 N/mm). In each randomized sequence all the possible combinations of weight, friction and stiffness, without repetition, were presented to the subject. The values of μ_d were univocally associated to μ_s . The experiments were conducted with only one grasping condition, with the object hold between index and thumb tip of the same hand. Values for friction coefficients were assumed by [KBF*97] where experimental values of linear friction are reported between index tip and different materials, equal respectively to 0.42, 0.61 and 1.67 for rayon, suede and sandpaper.

6.2. Methods

The experiment consisted of a series of test runs. At the start of the experiment, one object with the shape of a cube was visualized at the center of scene.

Each subject was asked to grasp the object by index and thumb fingers, and to get acquainted with the weight of the object, by lifting it up and letting it falling down by continuously decreasing the gripping force.

After the necessary time to get acquainted with the object, the subject was asked to hold the object stationery in the air for 10 seconds with the minimum grasp force that he considered necessary, with the elbow leaning on the plane. When the subject was holding the object in the fixed position, both grasp F_n and friction F_t forces (respectively normal and tangential to the object surface) and positions of finger tips, object and proxies were recorded for each contact point. Statistical analysis was performed in SPSS 13.0.

6.3. Results

A significant correlation was found between the values of the gripping force F_n and stiffness, weight and friction values, as shown in table 1. The value of grip force F_n was found

to be significantly positively correlated with mass and stiffness, while negatively with friction value. Table 1 reports the correlation coefficients obtained with a Spearman non parametric test and significance level $p < 0.001$.

Table 1: Correlation table (** $p < 0.001$).

| Correlation measure | |
|---------------------|------------------|
| | Grip force F_g |
| Friction μ_s | -0.346** |
| Mass m | 0.391** |
| Stiffness k | 0.333** |

Figure 20 presents several bar plots comparing the grasping force F_g in different conditions according to change in friction (top-bottom) and mass(left-right). Different colors are used for clustered bars representing the effect of stiffness in each test run.

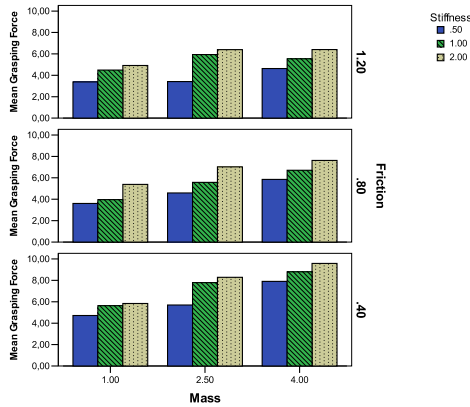


Figure 20: Mean grip force as a function of stiffness, friction and mass values

In figure 21 it is shown the change of grip force F_g vs. weight, with superimposed the error bars with confidence interval of 95%, for 9 different conditions given by different combination of friction (bottom-top) and stiffness (left-right).

6.4. Discussion

From the analysis of the results, it can be seen as greater gripper forces are required for holding heavier weights and stiffer objects, while lower gripper forces are required for higher friction values. This confirms the empirical laws that have been already found in the case of manipulation of real objects with bare fingers. In [GW84] it was found that the relative safety margin, defined as the safety margin in percent of the grip force, was about constant during lifting with increase of weights, was almost constant with change of weight. The calculation of the safety margin in the case of

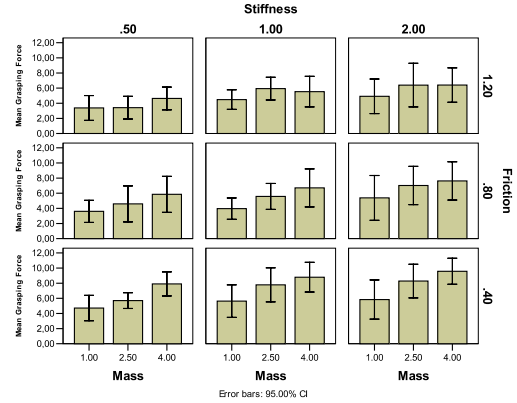


Figure 21: Mean grip force and as a function of stiffness, friction and mass values

virtual manipulation allows to make an interesting comparison. As it is shown in the logarithmical plot in Figure 22 in the case of virtual manipulation, the safety margin tends to be reduced with increasing weight of the lifted mass.

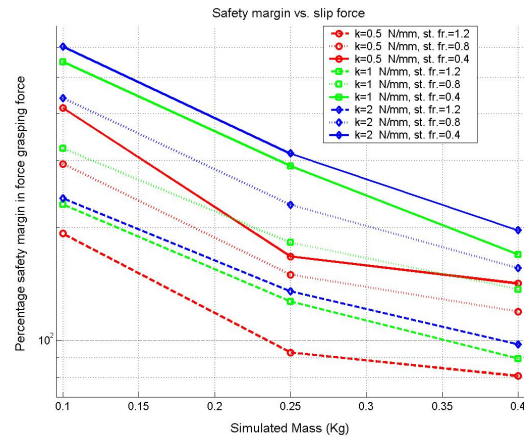


Figure 22: Relative safety margin during grasping vs. manipulated mass for different condition

This can be explained by the larger dispersion of grip forces observed for lower mass values. In fact, due to the absence of local sensation of slip, it was more difficult to discriminate the weight of lighter objects. Moreover lighter objects required a smaller resolution in the control of force (ΔF), that is limited by the position resolution of the device ΔX , according to the law $\Delta F = k\Delta X$, where k is the simulated contact stiffness. This is confirmed by the finding that better safety margins are obtained for lower values of the stiffness, as it is evident from the plot of figure 23, where grip forces are plotted vs. slip forces. While the minimum required grip

force is represented by the diagonal line, experimental data can be clustered in three main groups according to the value of contact stiffness during the simulation.

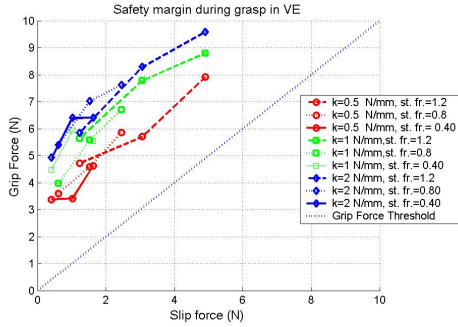


Figure 23: Grip vs. slip force, showing the relative safety margin during grasping of virtual objects

The evaluation of the performance during grasping and weight lifting, has shown that the simulation produces outcomes that are similar to experimental findings on real objects. We are currently testing the behaviour of the system when the contact friction is also implemented. Future activities will consider including evaluation with respect to angular motions and the comparison of additional feedback stimuli (audio and tactile).

7. Point based rendering

7.1. Soft contact and rotational friction

Traditionally, haptic rendering algorithms can be divided into two main categories. Three degrees of freedom algorithms, such as the god-object and the proxy [ZS95a, RKK97] have been extremely popular due to the overwhelming majority of three degrees of freedom devices available on the haptic market and due to their simplicity and computational efficiency. Six degrees of freedom devices [WMT99, OL03] simulate a more general type of contact, the one between two generic objects, but tend to be more computationally costly and harder to use given the still limited availability of satisfactory six degrees of freedom haptic devices.

In [BFSB04b] the authors of this paper proposed a simple extension to the god-object algorithm allowing to simulate a soft-finger contact, i.e. a point-contact with rotational friction constraints. The advantage of this algorithm is that it lets users interact more realistically with a virtual object using two points of contact. In this case, in fact, users are capable of applying form closure to an object, something that

| Surface material | μ_l | μ_r mm | μ_r/μ_l mm |
|------------------|-----------------|------------------|---------------------|
| Rayon | 0.42 ± 0.07 | 3.05 ± 0.57 | 7.39 ± 0.91 |
| Suede | 0.61 ± 0.1 | 3.84 ± 0.74 | 6.37 ± 0.88 |
| Sandpaper | 1.67 ± 0.24 | 10.11 ± 1.50 | 6.20 ± 1.54 |

Table 2: Experimental values of means \pm SD of μ_l , μ_r and their ratio measured at the index fingertip for different materials

they would not be able to do using two point contacts such as the ones simulated by using the god-object and/or proxy algorithms. This extra capability, however, comes at no real additional computational cost, given that collision detection is still point based.

One of the limitations of the algorithm proposed in [BFSB04b] was to consider the effect of rotational friction and linear friction as two completely uncoupled. This is not the case in reality, as proven for instance by Howe and Cutkosky in [HC96]. In order to take into account the mutual effect of linear and rotation friction on each other, in this section we present a soft-finger god-object algorithm based on the concept of limit curve, which was used in [HC96] to study robotic sliding manipulation [BFSB04a, FBR*07].

7.2. Tangential forces and torques during the control of grip

During the manipulation of objects our fingertips are generally subjected to tangential torques about the axis normal to the grasp surface in addition to linear forces tangential to the grasp surface. Experimental researches conducted by [JP98, KBF*97] sensorizing human fingertips during object manipulation have shown as friction tangential forces and torques are linear dependent on the value of the exerted grip force. Our experimental observations [BFSB04b] confirmed how this relationship could be assumed linear in the range of operating forces during human grip. In particular Johansson et al. [KBF*97] reported accurate values of linear and rotational friction coefficients, assuming that the following expressions hold:

$$F_{fr} = \mu_l P \quad (34)$$

$$M_{fr} = \mu_r P \quad (35)$$

More interestingly, from the analysis conducted on different surface materials (rayon, suede, sandpaper), he found that the ratio μ_r/μ_l has a value that is almost independent of the material, as it is reported in table 2. In order to be more general, the relationship between M_{fr} and P can be described also in terms of an analytical function Γ according to the model used to describe the elastic properties of the fingerpad, so that expression (35) becomes $M_{fr} = \Gamma(P)$.

This result can be easily explained by analyzing the

physics underlying the generation of the friction. In fact the resultant linear and friction forces can be found by integrating the pressure and tangential forces distribution over the fingerpad area during the contact.

Let us assume that the fingerpad is modelled as a sphere, the contact area is assumed to be a circle of radius a , and the pressure distribution is assumed to be axial-symmetric. Under the effect of contact force P , a distribution of pressure $p(r)$ is generated over the contact area, such that:

$$P = \int_0^a p(r) 2\pi r dr \quad (36)$$

Under static conditions, friction forces depend on the friction coefficient μ . In such case p produces on a infinitesimal area dA a tangential traction generating a friction moment M given by:

$$M = \int_0^a \mu_l p(r) 2\pi r^2 dr \quad (37)$$

If we assume that the contact is occurring under limit Hertzian conditions, it can be found that:

$$\frac{\mu_r}{\mu_l} = \frac{M}{\mu_l P} = \frac{3\pi}{16} a(P) \quad (38)$$

Under the hypothesis of uniform distribution of pressure we can find instead:

$$\frac{\mu_r}{\mu_l} = \frac{2}{3} a \quad (39)$$

So the ratio of rotational μ_r to linear friction μ_l is a constant parameter depending on the contact geometry (subject's fingerpad), and can be considered almost independent of the material. Its value is proportional to the radius of the contact area of the fingerpad. A numerical algorithm for the realistic simulation of frictional properties should consider this ratio as a constant independent of the task. So in the remaining analysis, we will adopt the values of linear and rotational friction coefficients derived from table 2.

7.3. The extended soft-finger god-object algorithm

In the following we will present two algorithms that can be used to simulate the haptic interaction between a set of human fingertips and a virtual object. The first algorithm proposed is simpler to understand and can be easily added on top of pre-existing state of the art haptic rendering algorithms supporting point-contact interaction. The second algorithm is based on more complex mathematical foundations, making it more difficult and harder to implement on top of pre-existing algorithms, but is capable of simulating the interaction between linear and rotational friction effects

of the human fingertips in a more realistic way. It is important to note that both algorithms are independent of the type of model chosen to simulate rotational friction between a human fingertip and an object. For a review of possible models see [BFSB04b].

7.4. The proxy algorithm with uncoupled friction

A 4 DOF god-object can be used to simulate a soft finger contact. Three of such degrees of freedom describe the position that the point of contact would ideally have when touching a virtual object, as for the standard god-object algorithm with linear friction [BDS03]. A fourth variable is added to describe the relative angular motion between the two soft finger avatars and a virtual object. It is important to note that the two parts of the algorithm are disconnected, i.e. they do not influence each other in any way.

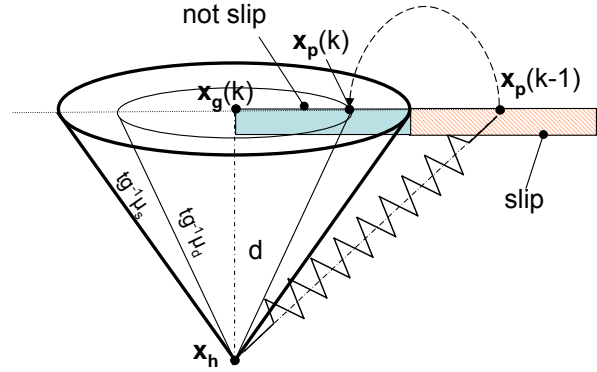


Figure 24: The classical friction cone for simulation of linear friction

When a soft finger avatar comes into contact with a virtual object α_p is set to the current value of the angle describing the rotation of the soft finger avatar α_0 . The position of the haptic interface is described by the position of the HI point \mathbf{x}_h . The following steps are then performed until contact is not broken.

At a generic k -th time sample:

- a: Computation of goal position.** The new goal position for the god-object is computed as $\mathbf{x}_g = \mathbf{x}_s$, where \mathbf{x}_s is the surface point which minimizes the distance between the HI point \mathbf{x}_h and the contact surface. The new angular position of the user's fingers is calculated as $\alpha_g = \alpha_s - \alpha_0$, where α_s is the angular rotation measured by the haptic device. \mathbf{x}_g and α_g are assumed as the new goal values respectively for \mathbf{x}_p and α .

We assume the following definitions:

$$\begin{cases} r = \|\mathbf{x}_g(k) - \mathbf{x}_p(k-1)\| \\ \rho = |\alpha_g(k) - \alpha_p(k-1)| \\ d = \|\mathbf{x}_g(k) - \mathbf{x}_h(k)\| \end{cases} \quad (40)$$

b: Analysis of the friction condition. In static conditions the new position of the god-object can be expressed as:

$$\begin{cases} \mathbf{x}_p(k) = \mathbf{x}_p(k-1) & \text{if } \frac{|F_r(k)|}{\mu_s |P(k)|} = \frac{r}{\mu_s d} < 1 \\ \alpha_p(k) = \alpha_p(k-1) & \text{if } \frac{|M(k)|}{\Gamma(P(k))} = \frac{k_r \rho}{\Gamma(P(k))} < 1 \end{cases} \quad (41)$$

where $|P| = k_l d$ is the force directed along the contact normal and $\Gamma(P)$ depends on the model chosen for the rotational friction and k_l and k_r are the haptic servo-loop gains, equivalent to a linear and rotational stiffness, used for calculating the elastic penetration force and torque.

If a linear approximation is used for the function $\Gamma(P(k)) = \mu_r P(k)$, then the second condition can be rewritten as:

$$\frac{k_r \rho}{k_l \mu_r d} < 1 \quad (42)$$

Otherwise, conditions of dynamic friction should be applied and the god-object, sliding over the surface, is moved on the boundary of the dynamic friction cone:

$$\begin{cases} \mathbf{x}_p(k) = \mathbf{x}_g(k) + \mathbf{r}' \\ \alpha_p(k) = \alpha_g(k) + \rho' \end{cases} \quad (43)$$

with

$$\begin{cases} \mathbf{r}' = \frac{\mathbf{x}_p(k-1) - \mathbf{x}_g(k)}{r} \mu_d d(k) \\ \rho' = \frac{\alpha_p(k-1) - \alpha_g(k)}{\rho} \frac{\Gamma(P(k))}{k_r} \end{cases} \quad (44)$$

In case of a linear approximation for the Γ function, the equivalent condition is reduced to:

$$\rho'(k) = \frac{\alpha_p(k-1) - \alpha_g(k)}{\rho} \frac{k_l}{k_r} \mu_r d(k) \quad (45)$$

c: Computation of friction force and torque. A new torque $M(k) = k_r(\alpha_p(k) - \alpha_g(k))$ and a new force $\mathbf{F}(k) = k_l(\mathbf{x}_p(k) - \mathbf{x}_g(k))$ are computed using the new value of α_p and \mathbf{x}_p . Torque $-M(k)\mathbf{v}_n$ and force $-\mathbf{F}(k)$ are applied to the virtual object (where \mathbf{v}_n represents a unit vector with direction along the contact normal). A force $\mathbf{F}(k)$ and a torque $M(k)\mathbf{v}_n$ are also applied to the user (if the device used is capable of actuating such wrench).

d: Computation of the new position of the object. New velocity (\mathbf{v}, ω) and position (\mathbf{x}, θ) is computed for the virtual object. Angle α_c representing how much the

object has rotated about axis \mathbf{v}_n is computed as

$$\alpha_c = |\omega \cdot \mathbf{v}_n| \Delta T \quad (46)$$

where ΔT is the servo-loop sampling time.

e: Update of god-object position. The current value of α_p and \mathbf{x}_p are corrected to take into account the displacement of the virtual object:

$$\begin{cases} \mathbf{x}_p = \mathbf{x}_p + \mathbf{x}_c \\ \alpha_p = \alpha_p + \alpha_c \end{cases} \quad (47)$$

and then repeat from step a.

7.5. Analysis of joint application of linear and rotational friction

Considering the effects of linear and rotational friction as completely uncoupled is an approximation of what happens in reality. The limit curve method introduced by [HC96] is reviewed in this paper to develop an algorithm which takes into account the interplay of these two separate effects.

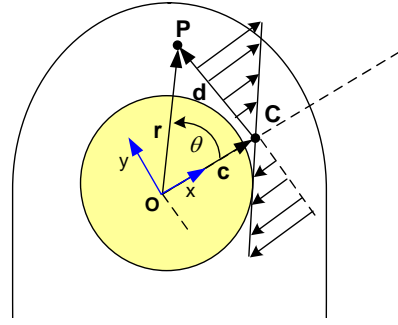


Figure 25: Kinematics of the sliding of the fingerpad over the surface

Refer to Figure 25, where a human fingerpad is represented. When contact with an object arises the distribution of pressure p between fingerpad and object can be assumed to be symmetric. According to the formulation in [HC96], we will refer to a reference system with origin at the center of symmetry of the pressure distribution p and will consider that the sliding of the fingerpad over the surface can be described as the combination of a translation and rotation around the Center of Rotation (COR) C, shown in Figure 25. Another assumption following [HC96] is that the friction is independent of sliding speed, so that the velocity can be represented aligned along the unit vector:

$$\hat{\mathbf{v}}(x, y) = \frac{[-d_y \ d_x]}{\|\mathbf{d}(x, y)\|} \quad (48)$$

The friction force per unit of surface is so given by the following:

$$\left(\frac{|F_t(k)|}{\mu|P(k)|}\right)^2 + \left(\frac{|M(k)|}{\Gamma(P(k))}\right)^2 = \left(\frac{r}{\mu d}\right)^2 + \left(\frac{k_r \rho}{\Gamma(P(k))}\right)^2 < 1 \quad (52)$$

Equivalent p -curves and c -curves can be directly traced in the plane $r - \rho$, proving a direct geometric interpretation, useful for the implementation of the algorithm. Condition (52) is simplified when the Γ function is assumed to be $\mu_r P$:

$$\left(\frac{r}{\mu d}\right)^2 + \left(\frac{k_r \rho}{\mu_r k_l d}\right)^2 < 1 \quad (53)$$

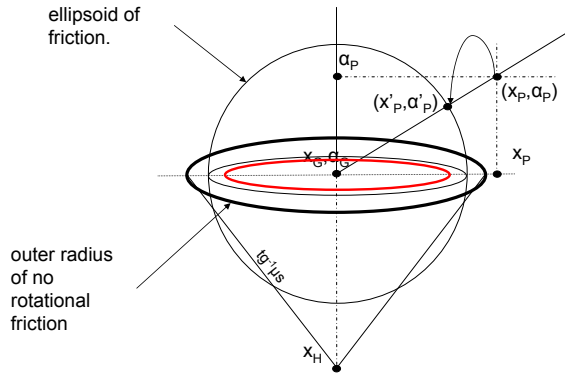


Figure 28: The interpretation of the mixed rotational-linear friction adaptive cone

When condition (53) is not verified, the linear $\mathbf{x}_p(k)$ and rotational $\alpha_p(k)$ proxies should be moved on the corresponding p -curve, by computing suitable increments r' and ρ' that satisfy equation (53). The increments r' and ρ' are found as the intersection in the (r, ρ) plane of the c -curve through $[r, \rho]$ with the corresponding p -curve for the level of normal force P , as shown in Figure 28. This shift corresponds to consider that the characteristics of the instantaneous sliding motion are preserved ($c = \text{const}$), but the reaction forces are changed to satisfy the physics of the system.

7.8. Combination of linear and rotational friction: the proxy algorithm with coupled friction

Given the elements exposed in section 7.5, it is now possible to formulate a god-object algorithm that combines linear and rotational friction effects. At a generic k -th time sample, step \mathbf{b} of previous algorithm is changed to \mathbf{b}' as follows:

b': Analysis of the friction condition. Compute $\varepsilon = x^2 +$

y^2 by:

$$\begin{cases} x = \frac{r}{\mu d} \\ y = \frac{k_r \rho}{\Gamma(P(k))} = \frac{k_r \rho}{\mu_r k_l d} \end{cases} \quad (54)$$

When the god-object is inside the equivalent friction cone, the position of god-object is not changed and so:

$$\begin{cases} \mathbf{x}_p(k) = \mathbf{x}_p(k-1) & \text{if } \varepsilon \leq 1 \\ \alpha_p(k) = \alpha_p(k-1) & \text{if } \varepsilon \leq 1 \end{cases} \quad (55)$$

If $\varepsilon > 1$, the god-object is sliding and the point $[r, \rho]$ is moved to $[r', \rho']$ on the the boundary of the corresponding p -curve, as it is shown in Figure 28. So we have:

$$\begin{cases} \mathbf{x}_p(k) = \mathbf{x}_g(k) + \frac{r'}{r} (\mathbf{x}_p(k-1) - \mathbf{x}_g(k)) \\ \alpha_p(k) = \alpha_g(k) + \frac{\rho'}{\rho} (\alpha_p(k-1) - \alpha_g(k)) \end{cases} \quad (56)$$

8. Six DOF Haptic and volume based rendering

6DOF haptics is needed in all the applications where rotational cues are required for resolution, such as manipulation of complex assemblies or virtual prototyping.

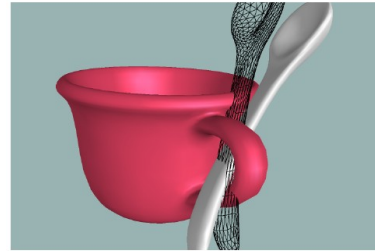
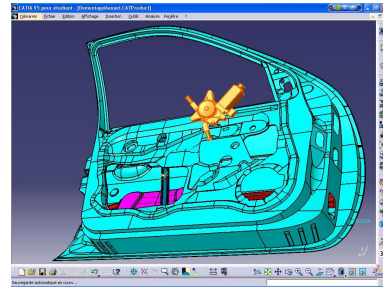


Figure 29: Examples of applications requiring volumetric rendering

Clearly the 6DOF approach introduces some challenges. For instance in common Virtual Prototyping applications it is required to:

- avoid penetration;
- rigid bodies with no shape constrains;
- Complex Collision Detection impacts on the required haptic rate

- Quality of the interaction, that means essentially stability and contact stiffness.

The following diagram in Figure 30 provides a synthetic view of all the aspects involved in 6dof haptic rendering:

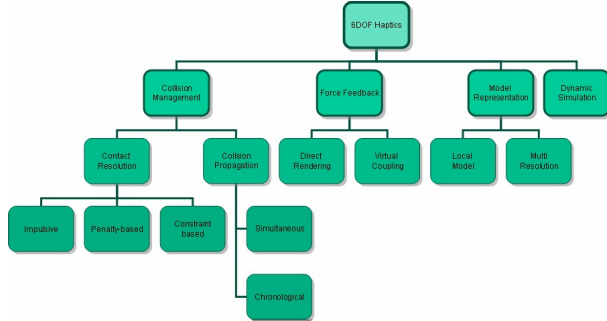


Figure 30: An overview of volumetric rendering

The standard 3DOF proxy is simple and efficient. It is normally modelled just a single point (or a small sphere when soft contact is included), but it is missing a dynamic behavior during contact. This dynamic behavior can be simulated by adopting an event based haptics

For 6DOF we have a complex shape proxy object. We can create a Dynamic Proxy by two main options for the interaction:

- Direct Rendering
- Virtual Coupling

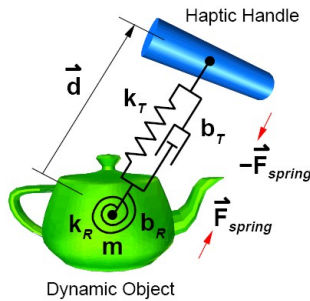


Figure 31: The virtual coupling allows to simplify volumetric rendering interaction

As shown in Figure 31, the Haptic Handle is attached to a Dynamic Object. We need to simulate the Dynamic Object, but how can we choose the correct parameters? This is related to the stability issues discussed in the previous sections of this tutorial. For example suppose to have a small mass m , e.g. 14g. Oscillations in the coupling can be prevented by avoiding imaginary solutions in the equivalent second order dynamic system Given mass and viscosity, the stiffness can

be easily required as the one associated to the critical damping for a second order system by the equation $b_T^2 > 4k_T m$, where the parameters are physically represented in Figure 31.

The virtual coupling in 6dof can be easily implementing, by introducing a single body dynamic simulator with explicit integration

$$\frac{d}{dt} \begin{pmatrix} x(t) \\ q(t) \\ P(t) \\ L(t) \end{pmatrix} = \begin{pmatrix} v(t) \\ \frac{1}{2} \omega(t) q(t) \\ F(t) \\ \tau(t) \end{pmatrix} \quad (57)$$

and we compute the equivalent force to be applied as

$$\vec{F} = k_t (\vec{x}(t) - \vec{x}_h(t)) + b_t (\vec{v}(t) - \vec{v}_h(t)) \quad (58)$$

For a 3 DOF device the rotational component can be omitted.

The penetration depth can be used as a mean for the estimation of the interaction force. Each contact on the two objects is a t-uple (p_0, p_1, n, δ) , optionally with also the velocities (v_0, v_1) . In some cases the contact can be disregarded if the two objects at the contact points are separating, that means that the relative velocity $v_{rel} = \vec{n} \cdot (\vec{v}_1 - \vec{v}_2) \leq 0$.

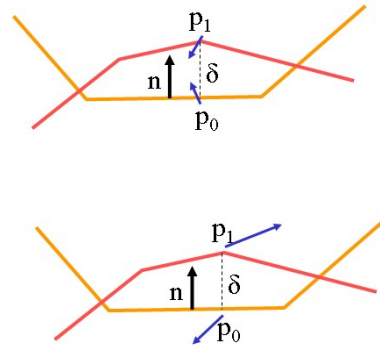


Figure 32: Reference frames for computation of interaction force with penetration depth

Alternatives to the method of penetration depth are constituted by volume and distance estimation, as shown in Figure 33. While the latter can be useful for a soft finger model, the second one is a simplified, but working approach.

When multiple contacts are present between two colliding objects, the issue of contact clustering should be analyzed. Each contact provides a force contribution and the number of contacts can vary from one step to the following:

- Iterative separation velocity selection during collision handling
- Force Contribution Mean
- Contact Clustering

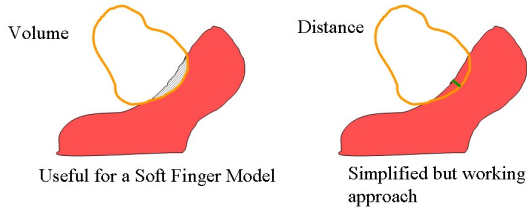


Figure 33: Volume vs. distance volumetric rendering

We can cluster the contact points:

- By a threshold distance δ
- In K groups using K -mean clustering

The cluster equivalent contact point is obtained by averaging the contained contact points properties. Also the collision detection cost impacts on the haptic rate. Possible solutions are represented by:

- Constant-time collision detection
- Local model representation
- Multi-resolution
- Continuous collision detection

Voxel models can be efficiently used to reduce the time required for collision detection. A Voxel representation of an object is a uniform space partitioning of arbitrary object geometry, that apply also to objects from imaging technologies. Every spatial cube can be empty or full. Additionally we can define Surface and Proximity voxels.

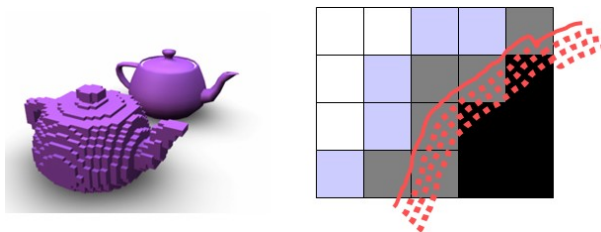


Figure 34: Example of voxel representation of objects

The collision test between a surface and a voxel model can be conducted by testing each surface point of the probing object against the static voxels of the world. Cost is limited by the number of points in the Shell [MPT99b]. The force contribution of each collision can be computed by a Tangent Plane Force Model.

Multiple contacts contributions are averaged to an arbitrary number N . The force is sent to the device through Virtual Coupling. Penetration is avoided by enlarging the surface border around objects. Additional improvements come from time coherency.

9. Application

The planning of reconstructive surgery operations currently requires the creation and manipulation of a physical model with consequent problems in precision and cost. The adoption of computational tools for the simulation and planning of surgical intervention would reduce cost and time and would increase the precision of the resulting surgical plan. Our goal is thus to allow the interactive visualization and haptic manipulation of CT scan data of an individual during preoperative planning of reconstructive facial surgery. In this scenario, the surgeon is able to manipulate the position of bones and bone fragments to identify the ideal post-operative bone placement. Effective simulation of this process requires six-degree-of-freedom (6DOF) force feedback, representing the interaction between bone fragments. This work presents a novel solution to this problem, based on a large-array voxel representation. This work extends a previous work in haptic simulation of bone surgery [MGBS05] and builds upon existing voxel-based haptic rendering algorithms [MPT99b]. The algorithm presented in this work is based on the computation of all collision points between voxel models. [MPT99b] introduces the related voxmap-point-shell algorithm, in which a single moving object is point-sampled and tested against a static voxel model containing all other objects in an environment. The present work extends this approach to allow collisions among any objects in a scene, using sphere trees. Sphere trees are rotationally invariant and have a small test cost and are thus a common technique for hierarchical bounding of volumes. However, for large-array voxel models such as those required to represent CT scans, the cost of the storage of the sphere tree (or, in general, any collision tree) is prohibitive and prevents the applicability of this technique. In this work we have overcome this problem to provide collision computation at haptic rates.

Method One of the typical approaches for the storage of voxel models is the octree, which allows reduced memory storage and a hierarchical representation of the voxel model. In this work we have used the octree as the basis for the construction of an implicit sphere tree for collision detection. An implicit sphere tree is a tree of spheres whose center and radius are computed during the collision test and depend only on the status of the octree at a certain level.

Computing collisions between two moving voxel models requires us to account for differing reference systems. The approach presented in [MPT99b] did not address this problem, because only one object was moving and only a limited number of points of the point shell needed to be transformed to the reference system of the static voxel model. In our implicit sphere tree we are able to compute the collision in world coordinates by transforming the relative positions of all the sphere centers in the lookup table, which corresponds to 256 or less coordinate transformations, and the relative positions of the 8 children in the octree.

The search for collision points between two voxel mod-

els starts with the top-level bounding spheres whose centers are computed in world coordinates and then descends the tree looking for all the collisions between the child spheres corresponding to the child octrees. This may proceed down to the single-voxel level, or may terminate at a certain level depending on the required precision. The descent can be optimized by taking into account only surface voxels, which are voxels with one or more free voxels as neighbors. The following image shows slices from eight levels of a typical octree; nodes drawn in purple contain surface voxels.

During collision computation, we identify all colliding points and apply the resulting force feedback to a virtual object. We use a virtual coupling technique to reduce the noise caused by rapid variation of the number of contacts. The force feedback for each collision is computed by evaluating the penetration of one of the spheres against the surface plane of the other sphere. The surface plane is stored directly inside the voxel model in the form of the distance to the nearest surface point and the normal at that point as shown in the following diagram:

The algorithm discussed in this paper has been implemented in C++ as an extension to the open source CHAI3D library for haptic interaction and tested on a 2GHz Pentium M machine using a PHANToM device (Sensable Technologies, Woburn, MA) for the haptic feedback.

The resulting implementation allows the interactive manipulation of virtual bones at haptic rates with models of 2563 voxels. The haptic rate limit (1kHz) is reached when the number of contacts is over one thousand, a condition that in practice never arises, since this induces a force feedback magnitude greater than a typical maximum device force.

A preliminary test of the algorithm with users shows that it is possible to manipulate complex objects as in Figure 1 with realistic feedback of the collisions.

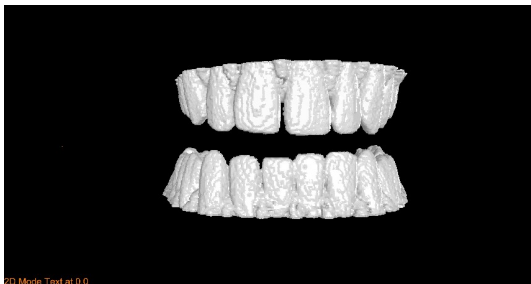


Figure 35: An application of reconstruction from CT scans

9.1. HapticWeb: a new tool for rapid prototyping of web-enabled haptic applications

Haptic Web is a powerful development environment within the XVR framework (see <http://www.vrmedia.it>) for details. This part of the tutorial it will introduce the basic

functionalities of the XVR development environment, with a specific description of the Haptic Web module for interfacing with haptics. See enclosed slides hands-out for further details.

10. Interaction in Virtual Worlds with haptics - Application examples

This module will introduce some application case studies based on the results of previous conducted research projects. The first case-study will present the main research issues for the interaction with digital models of sculptures in a virtual museum (<http://www.pureform.org/>). This case-study reviews techniques for modeling complex real shapes, starting from digital acquisition by laser scanner of real objects and then overviewing the steps needed to achieve their digital representation in VEs [FJBL05, JBF03]. Issues for the effective presentation to users and evaluation of level of involvement in the simulation will be also presented, on the basis of the results of the exhibitions conducted in European museums within the Pure Form project. The second case-study presents an effective methodology for replicating the behavior of primary commands of car in virtual reality by means of haptic interfaces [FCM*05]. In particular simple models for simulating the behavior of a steering wheel and a manual gearshift are reviewed.

10.1. The Pure Form system

Haptic perception represents the most immediate and intimate way of interacting with sculptures and other objects of art. In traditional museums, for reasons of security and preservation, touching sculptures is not allowed to visitors, and their experience falls short of a full appreciation of the artistic value and intrinsic beauty of the collections. Moreover, the appreciation of visual art is often denied entirely to blind and visually impaired visitors. Various examples exist of systems where haptic interfaces are used to interact with art forms. Most of such examples are based on using haptic devices as creative tools [BSC00], and less often haptic devices have been used as tools for better appreciating art pieces [MSS*00]. The Museum of Pure Form [Ber, BF03], through the conjunction of virtual reality (VR) and haptic technologies, aims to explore new paradigms of interaction with sculptural pieces of art. It offers an alternative to haptic perception of artistic forms, by recreating a virtual gallery featuring three-dimensional digitised sculptures from European and worldwide museums with which visitors can interact using their senses of touch and sight. The Museum of Pure Form has had a number of deployments in cultural heritage institutions across Europe. In September 2003 for the first time a multimedia room was opened to the public at Museo dell'Opera del Duomo (OPAE), Pisa (Italy). Formal evaluation of the project took place at University College London in November 2003, where several experiments on the sense of presence were conducted using the Haptic

Interface system in a CAVE-like environment [CNSD93], the ReaCTor. A CAVE-like room (CAVE Automatic Virtual Environment, i.e. a room with the floor and 3-4 walls back-projected with a stereoscopic visualization of a virtual computer-generated scenario, was used for the experiments. The tests were conducted within the ReaCTor at the Department of Computer Science, University College London, where the PURE-FORM exoskeleton haptic display was installed. Visitors could navigate through a virtual museum, select a virtual ancient Egypt artifact from the Petrie Museum or work of art from OPAE and interact with it.



Figure 36: The Pure Form system in the CAVE

The evaluation campaign continued at Galician Centre for Contemporary Arts (CGAC), Santiago de Compostela (Spain), and at the Nationalmuseum (NMS) of Fine Arts, Stockholm (Sweden) during the first three months of 2004. In early 2004 the Pure Form systems were exhibited throughout the month of February at CGAC, where more than 400 users explored the potential of haptic interfaces for engagement with artworks. A simultaneous audio narration with synchronized images provided an explanation of the relevant features of each work, explaining the author's choices and situating the work in its historical period or movement.

The exhibition of Pure Form at NMS was arranged in March and April 2004 in connection with a larger exhibition "False and Genuine" featuring genuine works of art and different kinds of copies, authorized as well as forged. The virtual works of art to be explored haptically were here considered as a special kind of copy. This section will present the results of the evaluations that were conducted at the two museum exhibition sites during 2003-2004. The aim was to evaluate the impact of such systems on the public, the added value compared to traditional displays, and the potential development as a multi-media dissemination tool for museums.



Figure 37: The exhibition in CGAC



Figure 38: One of the sculptures belonging to the virtual collection on display

10.1.1. System description

The Museum of Pure Form system is a complete Virtual Reality system with advanced human-computer interfaces, composed of the following subsystems:

1. the haptic interface system;
2. the database of the 3D models of sculptures;
3. the stereoscopic visualization system;
4. the software module dedicated to the haptic rendering and force generation;
5. the software module dedicated to the graphic rendering.

The need of a more realistic haptic interaction in VE has encouraged the development of devices that make use of multiple points of contact, when the interaction is not tool-based. In the Pure Form system two haptic devices have been specifically devised in order to provide the user forces on two contact points on the hand and were employed during the exhibitions, one exoskeleton device and one desktop device. The anthropomorphic exoskeleton HI can be worn on

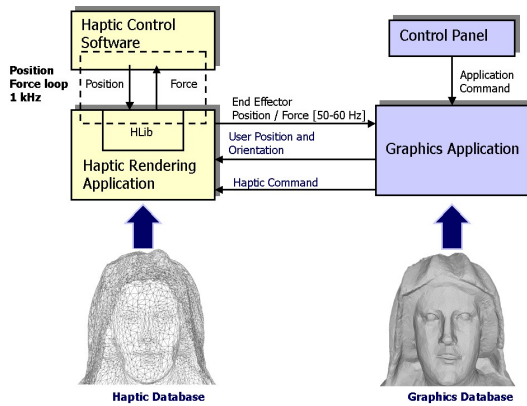


Figure 39: The overall system software architecture

the operator arm and is particularly suitable for installations in full immersive Virtual Reality environments, since it is possible to avoid the optical interferences between the projector beams of lights visualizing the virtual scene and the mechanical parts of the haptic interface. It is composed of two subsystems, the Light-Exos and the Pure-Form Hand-Exoskeleton.



Figure 40: The L-exos in its full configuration

The Light-Exos [FRM*05] is a wearable robotic device that allows the user to experience a direct interaction with a Virtual Reality System. It is both a sensorized and actuated mechanism, thus allowing respectively to track the arm position and to exert forces on it. It is mounted on a mobile support, which leaves the user the freedom of mov-

ing around. The Pure-Form-Hand-Exoskeleton (PFHE) is a portable Haptic Interface designed to exert forces of arbitrary direction and amplitude on the index and thumb fingertips, and is coupled with the Light-Exos. The union of these two sub-systems combines the greater workspace of the arm exoskeleton with the higher performance of the hand exoskeleton.

Seventeen sculptures belonging to different historical periods were digitized through laser scanning and post-processed to produce accurate polygonal meshes. The count of polygons of meshes was then reduced in order to reduce the complexity of the models and improve the performance of both haptic and graphic rendering algorithms.

10.1.2. Motivation of the study and objectives of the evaluation

The aim of the evaluation was to evaluate the PURE-FORM haptic displays used by museum visitors. The results from evaluations at two museums CGAC and NMS are reported, where the PURE-FORM exoskeleton haptic display was used.

The methodology adopted was assessment by self-reporting and numeric assessment through ratings given over numerical scales. The questionnaire was structured into 4 main parts:

- General section
- Overall experience of the system (including haptic one)
- System usability
- User's profile

Typical assessment of usability was performed, according to ISO 9241 definition, as composed of:

- Effectiveness : How well the user achieves the goals they set out to achieve using the system.
- Efficiency: The resources consumed in order to achieve their goals.
- Satisfaction: How the user feels about their use of the system

Questionnaires were used at all museums. The questions were partly common in the different contexts, but they were also partly different depending on local conditions. A statistical analysis was carried out to point out the main aspects of the evaluation. A factor analysis was conducted on data and it will be outlined during the presentation in the tutorial.

10.2. Haptic systems for simulation of primary commands of cars

Virtual prototyping and digital mock-up technologies can reduce the time and costs necessary to develop and construct new products and bridge the disciplinary and distance gaps among collaborators working on the same project. Virtual prototyping is based on the simulation in a realistic

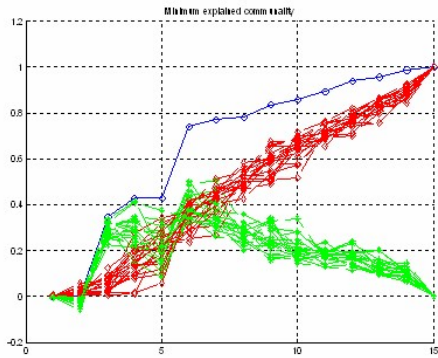


Figure 41: Example of statistical processing for factor analysis of results

three-dimensional virtual environment of the functionality expected from the new product. Before the real construction of the first prototype, it enables designers to evaluate the fulfillment of ergonomics, engineering and design requirements, and the feasibility/adequacy of the product to the foreseen usage. One of the key issues in Virtual Prototyping applications is the capability provided to the operator of interacting in an efficient and sensorially sufficient way with the virtual model of the object. The sense of touch appears to be fundamental to assess the properties of the prototype of a complex system, such as a vehicle. Although CAD systems are becoming widespread, there is still some important information that a CAD program alone cannot supply. The designer cannot see from the CAD how the operator will fit into cab or assess how the controls will feel during operation. During the development of new vehicles the designer must still wait until a mock-up or a prototype is built to find out how the controls feel and whether or not they are easy to use. Vehicle simulators immersed in Virtual Environments where either the contact or the inertial forces are replicated to the operator, have been successfully employed for the evaluation of ergonomics aspects in the cockpit. Vehicle simulators, and in particular aircraft simulators for use in training pilots, are generally equipped with various control devices such as acceleration, brake and clutch pedals, gear change lever and steering wheel, to enhance the realism of the simulation. In most of such simulators, control commands are passive sensorized systems, which measure only the commands executed by the user. In such systems the force behavior is regulated by the mechanics of the control commands, designed to replicate the force response of real commands. The adoption of Haptic Interfaces (HI) within simulator systems can improve the functionalities of the simulator. The mechanical response of HI can be logically programmed and controlled. In such a way in the tests within a simulator, users can evaluate the vehicle under different conditions, with changes in

kinesthetics or haptic parameters. This is particularly useful when ergonomics aspects are taken into consideration.

10.2.1. The physical model of gearshift

Differently from other primary controls, the gearshift force behavior is highly non-linear and unpredictable, since is related to the instaneous collisions that occur in the gearbox [AFS*01]. The gearshift force response was modelled through an analytical approach based on the force contents displayed during the engagement as measured experimentally, and through preliminary assessment of results. The particular force response of a gear-shift can be described as a function of the three different main stages, occurring during the gear engagement: the synchronization, the engagement and the impact against the mechanical stop. Since the gearshift is a multi-body dynamical system, each stage is associated to the interaction of different parts in the gear-box. The modelling of the force response in three stages allows to simplify its analytical description. A typical force response of an automotive gearshift, derived from experimental results, is shown in Figure 3.

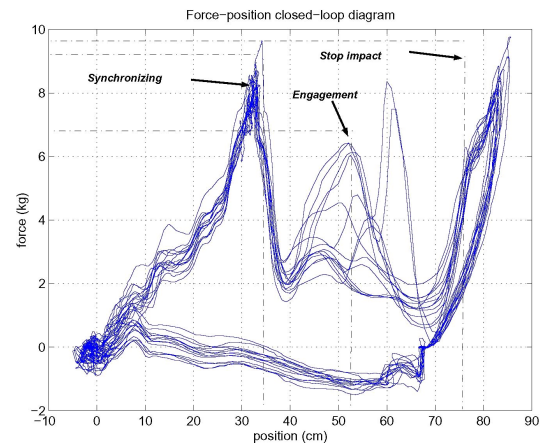


Figure 42: Experimental force response of a gearshift according to the lever position

In the first level of implementation of the simulator, a haptic device with two degrees of freedom, based on a parallel mechanism, allowing the lever to pivot around two independent orthogonal axes, was specifically developed to comply with the following requirements: Workspace: the knob must be able to reach every point on a spherical surface whose extension depends on lever length. In addition lever length must be variable from 110 to 160 mm. Projecting the workspace on a plane parallel to the table the knob trajectory must be included in a rectangle. Force: this HI must exert in engaging direction a force of 100 N and in selection direction a force of 60 N. Thus the haptic interface mechanism can replicate the movement of the gearshift lever on

a spherical surface. Its mechanical implementation is shown in Figure 4



Figure 43: *The haptic interface simulating the gearshift*

An analytical model of the gearshift behavior was synthesized to replicate a correct force-feedback to the operator. The different phases of the gearshift were modeled through a dynamic model with both continuous and discrete states (each discrete state was associated to a gearshift stage). The model of the engagement process takes as input the user forces exerted on the knob and provides as output the knob position and velocity. The model can be divided in two parts:

- A time varying continuous dynamics module which depends on the actual gear stage.
- A discrete state machine which determines the gear stage on the basis of the knob position, the user's force and the previous machine state.

The discrete module receives as inputs the position of the knob and the force exerted by the user. The discrete states of this module represent the different gearshift stages, i.e. the synchronization, the engagement and the end impact. For instance if the user is pushing forward during the synchronization state, a transition is activated to reach the engagement state. Conversely if the force is suddenly reverted, a transition to a free motion state is activated. The conditions under which the transitions can occur are based on position, force and time actual values. So the duration of the synchronization stage is imposed by a time-dependent out-transition from this state. Figure 5 shows an experimental test of the implemented dynamic model during the simulation of pure engagement operations with force feedback. It can be seen how experimental results produce a good fit with simulated ones.



Figure 44: *The simulated force response of a gearshift*

10.2.2. - The fully virtual level of immersivity

The fully immersive development level addressed in the Virtual project has foreseen the integration of an exoskeleton haptic device, replacing the physical primary commands developed in the first level. In this development level, one of the adopted visualisation devices is a CAVE-like visualization system. The rider wears only simple shutter glasses integrated with an Head Tracker, so that he can experience a 3D stereo vision in every direction, but having the possibility to see his own body superimposed to the virtual scenario.



Figure 45: *The fully-virtual integrated simulation of driving*

The force feedback is exerted on the right arm of the rider. An exoskeleton based haptic interface is in connection with the right arm of the rider at the level of the palm, of the forearm and of the upper arm. This haptic can acquire the movement of the rider's arm and to exert controlled forces through predefined contact surfaces with the rider's arm. The following components were integrated at this development level:

- Active pedals: to simulate the physical interaction with the primary commands of feet;
- Two Sensorized gloves: to track the position of the two arms and of the user's hands;
- CAVE+ Shutter Glasses + Head Tracker: the graphics simulation was updated according to the current point of view of the user detected by the head tracker;
- Haptic interface: a force-feedback arm exoskeleton, to simulate both static and dynamic interaction with the primary commands.
- HeadPhones: to reproduce the audio information, according to the dynamic status of the simulation.

From the user point of view the exoskeleton haptic interface is able to make the rider feel the resistant forces of the Steering Wheel and the Gear Shift and/or the interaction force arising during possible collision of the arm with the fittings of the car. The Pedals are still present in the system and the acoustical feedback is a 3D-positional one. The system was adjustable and reconfigurable, since the exoskeleton was mounted over linear slides, allowing its positioning relatively to the driver's seat. An optical tracker was used to detect the absolute position of the first link of the exoskeleton.



Figure 46: The simulation set-up and the driving interface.

10.2.3. Interaction with the driving simulation

The force feedback of the arm exoskeleton was basically employed at two different levels: Static feedback: when the data glove detected an open posture of the hand, the user can perceive by touch the shape of the primary commands that were approximated through the simple geometries shown in the figure below.

Dynamic feedback: when the user closed his hand while in contact with one of the primary commands, the hand was assumed to hold the command and its behavior was associated to the dynamic of the command. Figure 10 shows for instance the virtual kinematic constraint that was recreated

through the exoskeleton where the user was grasping the gearshift handle. On this kinematic constraint, the dynamic response associated to the engagement process was superimposed.

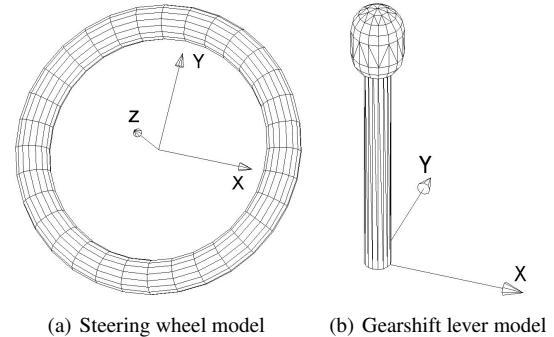


Figure 47: The geometries used for simulating the steering wheel and the gearshift

References

[AFS*01] ANGERILLI M., FRISOLI A., SALSEDO F., MARCHESCHI S., BERGAMASCO M.: Haptic simulation of an automotive manual gearshift. In *Proceedings of IEEE Roman* (2001).

[AH99] ADAMS R., HANNAFORD B.: Stable haptic interaction with virtual environments. *IEEE Transactions on Robotics and Automation* 15, 3 (1999), 465–474.

[BABF92] BERGAMASCO M., ALLOTTA B., BISIO L., FERRETTI L.: An arm exoskeleton system for teleoperation and virtual environments applications. In *IEEE International Conference on Robotics and Automation* (1992), pp. 1449–1454.

[BACS06] BERGAMASCO M., AVIZZANO CA. FRISOLI A. R. E., S. M.: Design and validation of a complete haptic system for manipulative tasks. *Advanced Robotics, Special Issue on Haptic Display: beyond visual and aural interaction* 20, 3 (2006), 367–389.

[BC94] BROWN J., COLGATE J.: Factors affecting the z-width of a haptic display. In *Proc. of the IEEE ICRA conference* (1994).

[BDS03] BARBAGLI F., DEVENGENZO R., SALISBURY K.: Dual-handed virtual grasping. In *2003 IEEE International Conference on Robotics and Automation, ICRA 2003* (Taipei, Taiwan, 2003), vol. 1, pp. 1259–1263.

[Ber] BERGAMASCO M.: Le Musee del Formes Pures. *8th IEEE International Workshop on Robot and Human Interaction, RO-MAN 99*, 27–29.

- [Ber96] BERGAMASCO M.: Force replication to the human operator: the development of arm and hand exoskeletons as haptic interfaces. In *Robotics Research, The Seventh International Symposium* (1996), Giralt G., Hirzinger G., (Eds.), Springer-Verlag, pp. 173–182.
- [BF03] BERGAMASCO F., FRISOLI A.: The museum of pure form. *The 11th International Conference on Advanced Robotics* (2003).
- [BFSB04a] BARBAGLI F., FRISOLI A., SALISBURY K., BERGAMASCO M.: Simulating human fingers: a soft finger proxy model and algorithm. In *Proceedings. 12th International Symposium on Haptic Interfaces for Virtual Environment and Teleoperator Systems* (2004), pp. 9–17.
- [BFSB04b] BARBAGLI F., FRISOLI A., SALISBURY K., BERGAMASCO M.: Simulating human fingers: a soft finger proxy model and algorithm. vol. 1, pp. 9–17.
- [BMZ96] BONIVENTO C., MELCHIORRI C., ZANASI R.: *Sistemi di Controllo Digitale*. Progetto Leonardo, 1996.
- [BSC00] BUTTOLO P., STEWART P., CHEN Y.: Force-Enabled Sculpting of CAD Models. *Proceedings ASME Int. Mech. Eng. Congress and Exposition, Dynamic Systems and Control Div 2* (2000), 1175–1182.
- [BSD04] BARBAGLI F., SALISBURY K., DEVENGENZO R.: Toward virtual manipulation: from one point of contact to four. *Sensor Review* 24, 1 (2004).
- [CFM*05] CINI G., FRISOLI A., MARCHESCHI S., SALSEDO F., BERGAMASCO M.: A novel fingertip haptic device for display of local contact geometry. In *Proceedings of WorldHaptics, First Joint EuroHaptics Conference and IEEE Symposium on Haptic Interfaces for Virtual Environments and Teleoperator Systems* (Pisa, 2005), pp. 602–605.
- [CK05] CONTI F., KHATIB O.: Spanning large workspaces using small haptic devices. In *First Joint Eurohaptics Conference and Symposium on Haptic Interfaces for Virtual Environment and Teleoperator Systems (WHC'05)* (2005).
- [CNSD93] CRUZ-NEIRA C., SANDIN D., DEFANTI T.: Surround-screen projection-based virtual reality: the design and implementation of the CAVE. *Proceedings of the 20th annual conference on Computer graphics and interactive techniques* (1993), 135–142.
- [CS94] COLGATE I., SCHENKEL G.: Passivity of a class of sampled-data systems: Application to haptic interfaces. In *Proc of the American Control Conference* (1994).
- [DAM*03] DETTORI A., AVIZZANO C., MARCHESCHI S., ANGERILLI M., BERGAMASCO M., C.LOSCOS, A.GUERRAZ: Art touch with create haptic interface. In *Proc. of ICAR03, The 11th International Conference on Advanced Robotics* (2003).
- [DK02] DOUGLAS S. A., KIRKPATRICK A. E.: Application based evaluation of haptic interfaces. In *Proceedings of the Tenth Symposium on haptic interfaces for virtual environment and teleoperator systems* (2002).
- [FBR*07] FRISOLI A., BARBAGLI F., RUFFALDI E., SALISBURY K., BERGAMASCO M.: A limit-curve based soft finger god-object algorithm. In *Proceedings. 12th International Symposium on Haptic Interfaces for Virtual Environment and Teleoperator Systems* (2007).
- [FBW*04] FRISOLI A., BARBAGLI F., WU S.-L., RUFFALDI E., BERGAMASCO M.: Comparison of multipoint contact interfaces in haptic perception. In *Workshop on Multipoint Interaction in Robotics and Virtual Reality, ICRA04* (2004).
- [FCM*05] FRISOLI A., CARROZZINO M., MARCHESCHI S., SALSEDO F., M. B.: Haptic systems for simulation of primary commands of cars. In *Proceedings of Virtual Concept* (Biarritz France, 2005), Springer.
- [FJBL05] FRISOLI A., JANSSON G., BERGAMASCO M., LOSCOS C.: Evaluation of the pure-form haptic displays used for exploration of works of art at museums. In *CD Proceedings of WorldHaptics, First Joint EuroHaptics Conference and IEEE Symposium on Haptic Interfaces for Virtual Environments and Teleoperator Systems* (Pisa, 2005).
- [FRM*05] FRISOLI A., ROCCHI F., MARCHESCHI S., DETTORI A., SALSEDO F., BERGAMASCO M.: A new force-feedback arm exoskeleton for haptic interaction in virtual environments. *Haptic Interfaces for Virtual Environment and Teleoperator Systems, 2005. WHC 2005. First Joint Eurohaptics Conference and Symposium on* (2005), 195–201.
- [FSA*04] FRISOLI A., SOTGIU E., AVIZZANO C., CHECCACCI D., BERGAMASCO M.: Force-based impedance control of a haptic master system for teleoperation. *Sensor Review* 24, 1 (2004), 42–50(9).
- [GJJ98] GOODWIN A. W., JENMALM P., JOHANSSON R. S.: Control of grip force when tilting objects: Effect of curvature of grasped surfaces and applied tangential torque. *The Journal of Neuroscience* 18, 24 (1998), 10724–10734.
- [GN94] GLOSSER G., NEWMAN W.: The implementation of a natural admittance controller on an industrial robot. In *Proc. of the IEEE Conference on Robotics and Automation* (1994), pp. 1209–1215.
- [GW84] G. WESTLING R. J.: Factors influencing the force control during precision grip. *Exp Brain Res* 53 (1984), 277–284.
- [HC96] HOWE R. D., CUTKOSKY M. R.: Practical force-motion models for sliding manipulation. *International Journal of Robotic Research* 15 (1996), 557–572.
- [HCLR94] HAYWARD V., CHOKSI J., LANVIN G., RAMSTEIN C.: *Advances in Robot Kinematics*. Kluwer Academics, 1994, ch. Design and multi-objective optimization of a linkage for a haptic interface, pp. 352–359.

- [JBF03] JANSSON G., BERGAMASCO M., FRISOLI A.: A new option for the visually impaired to experience 3d art at museums: Manual exploration of virtual copies. *Visual Impairment Research* 5 (2003), 1–12.
- [JGB73] JOHANNES V. I., GREEN M. A., BROCKLEY C. A.: The role of the rate of application of the tangential force in determining the static friction coefficient. *Wear* 24 (1973), 381–85.
- [JM03] JANSSON G., MONACI L.: Haptic identification of objects with different numbers of fingers. In *Touch, Blindness and Neuroscience*, Press U., (Ed.). Madrid, 2003.
- [JP98] JENMALM P. GOODWIN A.W. J. R.: Control of grasp stability when humans lift objects with different surface curvatures. *J. Neurophysiol.*, 79 (1998), 1643–1652.
- [Ka90] KLATZKY R. L., AL.: Procedures for haptics object exploration vs. manipulation. In *Vision and action: The control of grasping*. 1990, pp. 110–127.
- [KBF*97] KINOSHITA H., BÄCKSTRÖM L., FLANAGAN J. R., JOHANSSON R. S.: Tangential torque effects on the control of grip forces when holding objects with a precision grip. *J Neurophysiol* 78 (1997), 1619–1630.
- [KLCR99] KLATZKY R., LEDERMAN S., C. H., RAMSAY G.: Perceiving roughness via a rigid probe: effects of exploration speed. In *Proceedings of the International Mechanical Engineering Congress, Dynamic Systems and Control Division (Haptic Interfaces for Virtual Environments and Teleoperator Systems* (1999), vol. 67, pp. 27–33.
- [KNK*05] KURODA Y., NAKAO M., KURODA T., OYAMA H., YOSHIHARA H.: Shape perception with friction model for indirect touch. In *Proceedings of World-Haptics, First Joint EuroHaptics Conference and IEEE Symposium on Haptic Interfaces for Virtual Environments and Teleoperator Systems* (Pisa, 2005).
- [Law88] LAWRENCE D.: Impedance control stability properties in common implementations. In *Proceedings of the 1988 IEEE International Conference on Robotics and Automation* (1988), pp. 1185–1190.
- [MB86] MAPLES J., BECKER J.: Experiments in force control of robotic manipulators. In *In Proc. of the IEEE Conference on Robotics and Automation* (1986), pp. 695–702.
- [MGBS05] MORRIS D., GIROD S., BARBAGLI F., SALISBURY K.: An Interactive Simulation Environment for Craniofacial Surgical Procedures. *Proceedings of MMVR (Medicine Meets Virtual Reality) XIII, Long Beach, CA, January* (2005).
- [MH04] MELDER N., HARWIN W. S.: Extending the friction cone algorithm for arbitrary polygon based haptic objects. In *HAPTICS* (2004), pp. 234–241.
- [MIHB85] MUSSA-IVALDI F., HOGAN N., BIZZI E.: Neural, mechanical and geometric factors subserving arm posture in humans, 1985.
- [MPT99a] MCNEELY W., PUTERBAUGH K., TROY J.: Six degree-of-freedom haptic rendering using voxel sampling. In *Proc. of ACM SIGGRAPH* (1999), pp. 401–408.
- [MPT99b] MCNEELY W., PUTERBAUGH K., TROY J.: Six degree-of-freedom haptic rendering using voxel sampling. *Proceedings of the 26th annual conference on Computer graphics and interactive techniques* (1999), 401–408.
- [MS94] MASSIE T. H., SALISBURY J.: The phantom haptic interface: A device for probing virtual objects. In *Proceedings of the ASME Winter Annual Meeting, Symposium on Haptic Interfaces for Virtual Environment and Teleoperator Systems* (1994).
- [MSS*00] MCCLAUGHLIN M., SUKHATME G., SHAHABI C., HESPANHA J., ORTEGA A., MEDIONI G.: The Haptic Museum. *Proceedings of the EVA 2000 Conference on Electronic Imaging and the Visual Arts* (2000).
- [MW03] M. WAN W. A. M.: Quasi-static approximation for 6 degrees-of-freedom haptic rendering. *Proc. of IEEE Visualization* (2003), 257–262.
- [OL03] OTADUY M. A., LIN M.: Sensation preserving simplification for haptic rendering. *ACM Transactions on Graphics* 22 (2003), 543–553.
- [RHD99] ROBERT HOWE T. D., DUPONT P.: Twice the fun: Two phantoms as a high-performance telemanipulation system. In *Proceedings of the Fourth Annual PHANTOM Users Group Workshop* (1999).
- [RJ84] R.S. JOHANSSON G. W.: Roles of glabrous skin receptors and sensorimotor memory in automatic control of precision grip when lifting rougher or more slippery objects. *Experimental Brain Research* 56 (1984), 550–564.
- [RKK97] RUSPINI D. C., KOLAROV K., KHATIB O.: The haptic display of complex graphical environments. *Computer Graphics* 31, Annual Conference Series (1997), 345–352.
- [SYYM04] SATO Y., YOSHIKAWA T., YOKOKOHI Y., MURAMORI N.: Designing an encountered-type haptic display for multiple fingertip contacts based on the observation of human grasping behavior. In *Proceedings of the Symposium on haptic interfaces for virtual environment and teleoperator systems* (2004).
- [WMT99] W. MCNEELY K. P., TROY J.: Six degree-of-freedom haptic rendering using voxel sampling. In *Proceedings of ACM SIGGRAPH* (1999), p. 401–408.
- [YI03] YOSHIKAWA T., ICHINOO Y.: Impedance identification of human fingers using virtual task environment. In *Proceedings of the 2003 IEEE/RSJ Intl. Conference on Intelligent Robots and Systems* (Las Vegas, Nevada, 2003).

- [Yos90] YOSHIKAWA T.: *Foundations of Robotics - Analysis and Control*. MIT Press, Cambridge, Massachusetts, 1990.
- [YYMZ95] YOSHIKAWA T., YOKOKOHJI Y., MATSUMOTO T., ZHENG X.: Display of feel for the manipulation of dynamic virtual objects. *Transactions of the ASME Journal of Dynamic Systems, Measurement, and Control* 117, 4 (1995), 554–558.
- [ZS95a] ZILLES C., SALISBURY J.: A constraintbased god-object method for haptic display. In *Proc. IEE/RSJ International Conference on Intelligent Robots and Systems, Human Robot Interaction, and Cooperative Robots* (1995), vol. 3, pp. 146–151.
- [ZS95b] ZILLES C. B., SALISBURY J. K.: A constraint-based god-object method for haptic display. In *Proc. of IROS* (1995).

Modeling virtual worlds for RT interactive applications

Nadia Magnenat-Thalmann
Alessandro Foni
Nedjma Cadi
George Papagiannakis
MIRALab – University of Geneva

MIRALab University of Geneva www.miralab.ch Eurographics 2006

Aspendos Site (161-180 A.D.)

MIRALab University of Geneva www.miralab.ch Eurographics 2006

Sources

MIRALab University of Geneva www.miralab.ch Eurographics 2006

Geometrical Restitution of the Scene

MIRALab University of Geneva www.miralab.ch Eurographics 2006

Texture restauration

Samples from the Material Gallery assembled from the on-site taken photographic documentation (color corrected)

MIRALab University of Geneva www.miralab.ch Eurographics 2006

Textured Model

MIRALab University of Geneva www.miralab.ch Eurographics 2006

Scene Restitution with Statues and Textures

MIRALab University of Geneva www.miralab.ch Eurographics 2006

Velum Restitution

MIRALab University of Geneva www.miralab.ch Eurographics 2006

Roof Restitution

MIRALab University of Geneva www.miralab.ch Eurographics 2006

Roof Restitution Hypothesis

MIRALab University of Geneva www.miralab.ch Eurographics 2006

Chosen Interpretations

MIRALab University of Geneva www.miralab.ch Eurographics 2006

Geometrical 3D Model of the modern theatre

MIRALab University of Geneva www.miralab.ch Eurographics 2006

Modeling of the Terrain

MIRALab University of Geneva www.miralab.ch Eurographics 2006

From Procedural to Modern environment

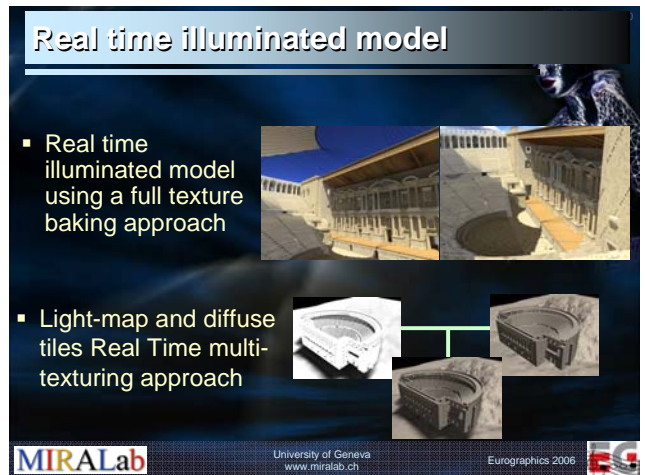
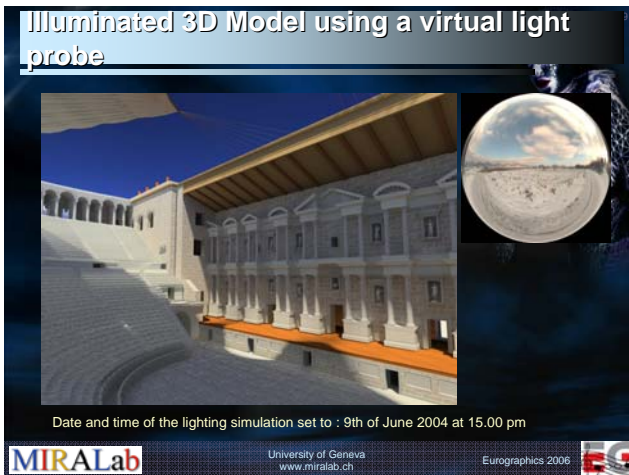
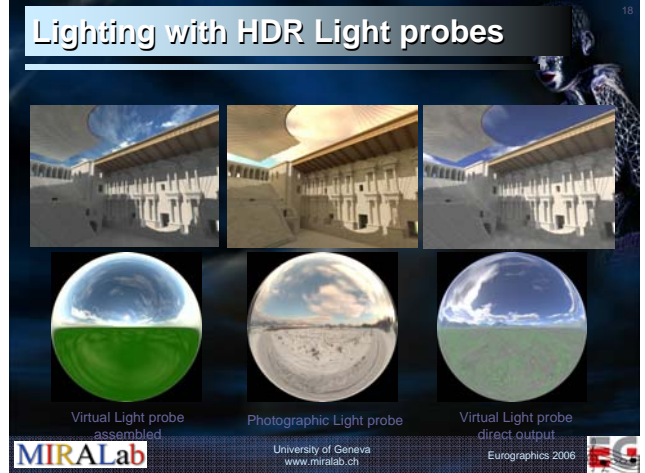
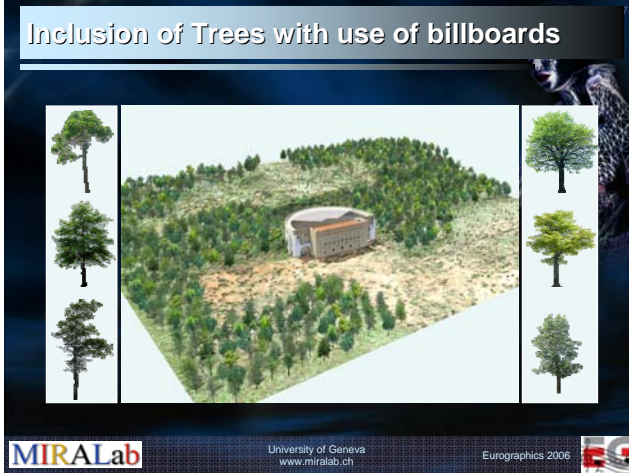
MIRALab University of Geneva www.miralab.ch Eurographics 2006

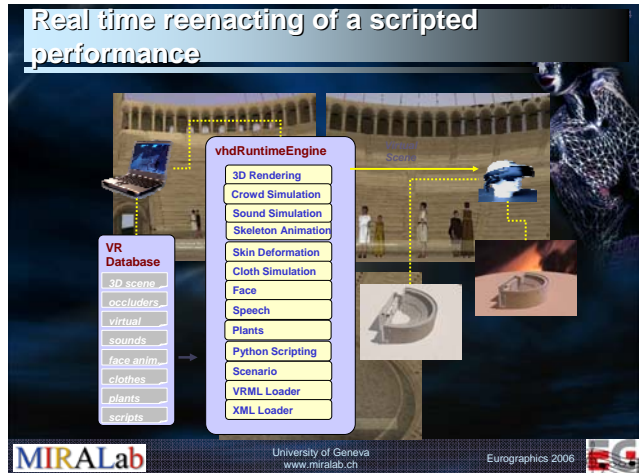
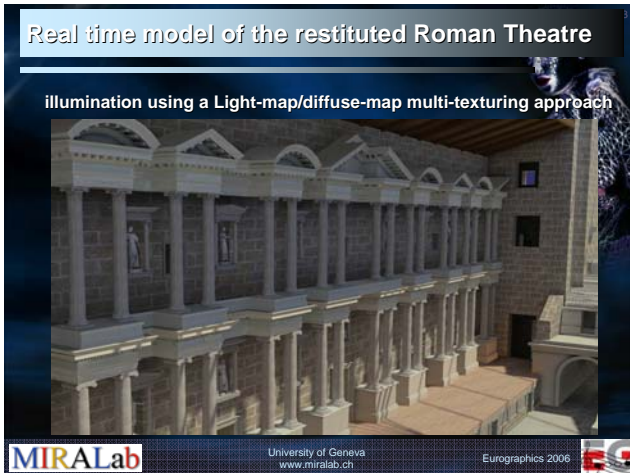
From Modern environment to Roman environment

MIRALab University of Geneva www.miralab.ch Eurographics 2006

Modern Environment vs Roman Environment

MIRALab University of Geneva www.miralab.ch Eurographics 2006







Platform Choice for Inhabited virtual worlds = framework + components

George Papagiannakis
Nadia Magnenat-Thalmann
MIRALab – University of Geneva

MIRALab University of Geneva www.miralab.ch Eurographics 2006

facing it ...

- **VR-AR Research, game industry**
 - revolution in real-time graphics
 - atomic simulation technologies affordable to nearly everyone
- **demand:**
 - Interactive, inhabited virtual worlds
 - integrate multiple features / qualities / technologies
 - under a single application roof
 - deliver always newer, always faster, always more robust algorithms
 - deliver in shorter time
- **effect:**
 - system complexity growing exponentially
- **need:**
 - methodology and tools to curb and handle dev complexity
 - continuous extensions
 - massive code and design reuse
 - big teams of developers / experts working in parallel

MIRALab University of Geneva www.miralab.ch Eurographics 2006

integrating...

experts / developers work independently producing heterogeneous technologies e.g. networking, rendering, sound, animation, vision, behaviours, AI, HCI, VR, AR ...

sure, we get it ... but "not exactly" what we wanted ...

we would like to integrate them and let them interplay under a single application hood to get a feature rich and complex simulation

MIRALab University of Geneva www.miralab.ch Eurographics 2006


... integration issues.

- **integration of heterogeneous technologies**
 - e.g. net, graphics, sound, animation, behaviours, AI, HCI, VR, AR ...
 - each one developed with different toolkits
 - different semantics and abstraction levels > no common vocabulary
 - best effort integration is not enough
 - system complexity growing exponentially
 - we need the tools / methodology to curb and handle complexity
- **numerous experts / developers**
 - need to work in parallel > to stay motivated and efficient
 - should stay within their expertise > experts too expensive to do that
 - should not be preoccupied with integration > guidelines, conventions
 - should adapt and follow some common rules
- **new projects ... new use cases ... needs**
 - extensions, adaptations > non-centralized way
 - fast prototyping

MIRALab University of Geneva www.miralab.ch Eurographics 2006

... searching for solutions ...

- frameworks**
 - massive design & code reuse
 - born for extensions
 - curbing complexity
 - exposing ready to use design
 - conventions, common vocabulary
 - domain specific fundamental services
 - ready classes and design patterns
 - ready generic engine
- concept in short**
 "partially completed application pieces of which are customized by the user to complete the application"
G. Rogers (1997)
Framework Based Software Development in C++
- component based development**
 - massive code reuse
 - can enclose any technology
 - hiding complexity
 - exposing easy to use interfaces
 - components developed in parallel
 - fast prototyping
 - robustness
- concept in short**
 composing applications out of ready made binary units of well defined and tested behaviour

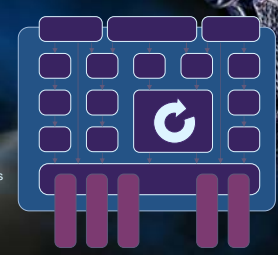


MIRALab University of Geneva www.miralab.ch Eurographics 2006

... lets try to combine both .

unifying development framework

- unifying "glue architecture" providing common class vocabulary allowing for seamless collaboration of pluggable components
- top level SDK for app development
- deep SDK to access and customize deep levels
- domain specific fundamental/common services
- comprehensive set of classes and interfaces
- ready to use and generic runtime engine
- providing concurrent "power supply" to active elements
- common conventions and guidelines



plug-in components (active services)


- encapsulate heterogeneous technologies in form of active services
- e.g. rendering, sound, animation, behaviours, AI, VR devices, interaction paradigms, etc.
- used on the simulation abstraction level
- hide complexity of their operation and state
- expose easy to use interfaces
- get "power supply" from the framework's engine

MIRALab University of Geneva www.miralab.ch Eurographics 2006

dividing, identifying, categorising ...

- investigating use cases of VR/AR applications**
 - identifying repeating architectural patterns
 - identifying repeating mechanisms, services and components
- categorising**


| | | |
|-------------------|-----|------------------------|
| time-critical | vs. | non-time-critical |
| performance heavy | vs. | light |
| control | vs. | event driven |
| synchronous | vs. | asynchronous |
| containing | vs. | processing |
| data sharing | vs. | transmitting |
| local | vs. | remote |
| compiled | vs. | interpreted |
| compile-time | vs. | run-time configuration |



MIRALab University of Geneva www.miralab.ch Eurographics 2006

VHD++ in short

- object oriented application development framework**
 - optimised for real-time speed
 - interactive audio-visual performance
 - VR/AR applications
- offering**
 - component based development
 - fast prototyping by composition of pluggable vhdServices
 - plug-in architecture
 - clear OO extension and customisation methodology
 - platform separating middleware character
 - vhdKernel SDK and generic vhdRuntimeEngine
- special focus**
 - virtual human RT simulation technologies



MIRALab University of Geneva www.miralab.ch Eurographics 2006

VHD++ overview

The VHD++ development Framework

Active plug-in service with Heterogeneous Technology

MIRALab University of Geneva www.miralab.ch Eurographics 2006

dividing, identifying, categorising ...

- investigating use cases of VR/AR applications
 - identifying repeating architectural patterns
 - identifying repeating mechanisms, services and components
- categorising

| | | |
|-------------------|-----|------------------------|
| time-critical | vs. | non-time-critical |
| performance heavy | vs. | light |
| control | vs. | event driven |
| synchronous | vs. | asynchronous |
| containing | vs. | processing |
| data sharing | vs. | transmitting |
| local | vs. | remote |
| compiled | vs. | interpreted |
| compile-time | vs. | run-time configuration |

MIRALab University of Geneva www.miralab.ch Eurographics 2006

... fundamental services ...

- embedded into the framework kernel in order to optimise real-time performance
- low abstraction level:
 - object referencing
 - garbage collection
 - containers
 - serialization mechanisms (for loading/saving/transmission purposes)
 - active object scheduling (threads, timers, schedulers)
 - time management
 - networking
- intermediate abstraction level:
 - concurrent data sharing
 - asynchronous event handling
 - asynchronous operation requests
 - remote method invocation
 - system runtime configuration
 - dynamic scripting

> Python OO scripting language

MIRALab University of Geneva www.miralab.ch Eurographics 2006

... plug-in vhdServices ...

- vhdService == component
 - encapsulate any simulation technology e.g.
 - rendering, sound, animation,
 - behaviours, AI,
 - VR devices, interaction paradigms,
 - etc. ...
 - provides easy to use service interface
 - hides internal state and operational complexity
 - provides entry points for expert users
 - implements set of plug-in methods
 - loaded dynamically on runtime based on XML config
 - developers draw from the pool of existing vhdServices
 - each new vhdService is added to the pool for future reuse
 - developers compose applications out of vhdServices
 - quick prototyping
 - robustness as composed of tested vhdServices

MIRALab University of Geneva www.miralab.ch Eurographics 2006

... vhdProperties ...

- **vhdProperty == shareable data**
 - classes encapsulating generic data e.g.
 - configuration data,
 - VRML models,
 - animation data,
 - sound samples,
 - etc. ...
 - developers may freely add their own new data types
 - each vhdProperty can have sub-properties
 - vhdProperties form treelike structures to express generic dependencies
 - e.g. a VH model may have sound sub-property or keyframe sub-property
 - e.g. a system root may have config sub-property
 - dependencies are interpreted and used by vhdServices operating / sharing vhdProperties
 - vhdProperties provide thread-safe data sharing mechanism
 - each vhdProperty may be equipped with respective vhdPropertyDecorator able interpret XML and to create vhdProperty instance
 - in this way VHD++ provides fully extendible XML configuration syntax

MIRALab University of Geneva www.miralab.ch Eurographics 2006

vhdRuntimeEngine 1/2

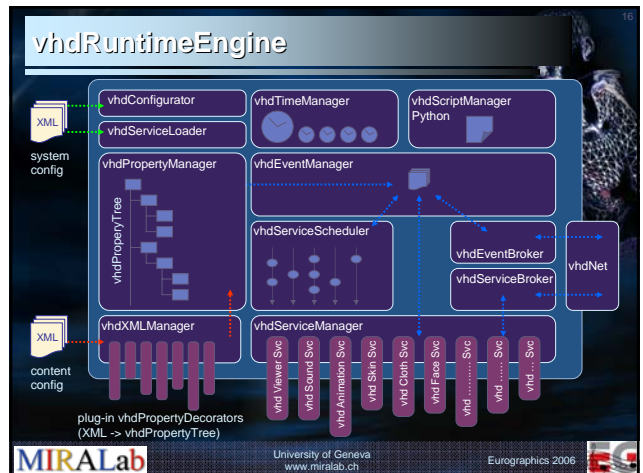
- **vhdServiceLoader**
 - loads specified vhdServices on runtime (based on XML config)
 - initialises loaded vhdServices with params read from the XML config
 - passes loaded vhdServices to vhdServiceManager
- **vhdServiceManager**
 - manages generic state of vhdServices on runtime
 - each vhdService implements init(), run(), freeze(), terminate(), update() methods that are used by vhdServiceManager
- **vhdServiceScheduler**
 - according to the XML config puts vhdServices on concurrent threads
- **vhdXMLManager**
 - user provided plug-ins used by the kernel to load vhdProperties that encapsulate simulation content e.g. configs, VRML models, VH models, sounds, semantic information, animation data, etc.
- **vhdPropertyManager**
 - provides thread safe data sharing mechanism to vhdServices operating on vhdProperties

MIRALab University of Geneva www.miralab.ch Eurographics 2006

vhdRuntimeEngine 2/2

- **vhdTimeManager**
 - maintains centralized system, simulation and time-wrap clocks that are used for synchronization of fundamental and plug-in vhdServices
- **vhdEventManager**
 - receives and forwards vhdEvents
- **vhdScriptManager** > Python scripting language
 - allows to call the API's of vhdServices from the Python level
- **vhdEventBroker / vhdServiceBroker**
 - net brokers responsible for communication with other vhdRuntimeEngines forming distributed vhdRuntimeSystem
 - exchanging vhdEvents with remote vhdRuntimeEngines
 - brokering information about existence and state of vhdServices

MIRALab University of Geneva www.miralab.ch Eurographics 2006



some pluggable vhdServices

- vhdViewerService**
 - high performance rendering
 - shutter glasses, HMD support
- vhdSoundService**
 - environmental 3D effects
 - home cinema surround sound 5.1
 - multiple sound file formats
- vhdSkeletonAnimationService**
 - mixing of motion generators
 - walking engine, keyframes,
 - real-time magnetic motion capture, etc.
- vhdSkinDeformService**
 - skin deformation
 - "fake clothes" deformation
- vhdClothAnimationService**
 - physically based cloth animation
 - skin to cloth collisions
- vhdFaceAnimationService**
 - mixing of facial expressions
- vhdVoiceService**
 - controls speech of VHs
- vhdCrowdService**
 - controls crowds of VHs
- vhdSpeechRecognitionService**
 - recognition of natural voice commands
 - generation of generic events
- vhdVRNavigationService**
 - VR navigation paradigms for
 - shutter glasses and HMD using
 - magnetic head tracking
- vhdScenarioEditorAndPlayerService**
 - authoring and execution of interactive multi-path VR scenarios
- ...
- application specific vhdServices**
 - GUIs, controls, etc.

MIRALab University of Geneva www.miralab.ch Eurographics 2006

VHD++ in numbers

- framework**
 - more than ~500 classes
 - grouped into ~35 packages including ~10 kernel packages
 - already ~14 existing vhdServices (big plug-in components)
- development effort**
 - ~40 contributing experts / researchers / developers
 - ~10 direct developers
 - ~3 kernel designers / lead programmers
 - design and development started in March 2001 (3 years)
- now in real-world application tests**
 - used in multiple EU level and national level projects
 - becomes quickly main real-time framework solution for MIRALab and VRlab research and development in VR/AR domain

MIRALab University of Geneva www.miralab.ch Eurographics 2006

growing spectrum of applications

- vhd JUST**
 immersive VR *health emergency personnel training*
- vhd STAR**
 AR *training of hardware maintenance professionals*
- vhd ERATO**
 VR *recreation of ancient theatres and plays*
- vhd CAHRISMA**
 VR *reconstruction and preservation of cultural heritage*
- vhd LIFEPLUS**
 AR *edutainment reconstruction of ancient life in Pompeii (Italy)*

MIRALab University of Geneva www.miralab.ch Eurographics 2006

vhd JUST

- immersive VR health emergency personnel training**

MIRALab University of Geneva www.miralab.ch Eurographics 2006

vhd JUST

21

- Interplaying technologies :
 - network deployment
 - simulation runtime engine networked with
 - GUI equipped simulation controller
 - immersive 3D graphics
 - stereoscopic rendering
 - shutter glasses or HMD support
 - immersive 3D sound
 - home cinema 5.1 surround sound
 - real time environmental effects
 - VR interaction
 - intuitive VE navigation paradigm
 - using head magnetic tracking
- interactive scenario
 - interactive authoring GUIs
 - interactive execution GUIs
- virtual human animation
 - skeleton animation
 - walking engine
 - keyframes
 - animation mixing
 - skin deformation
 - face animation mixing
 - face deformation
 - speech
- others
 - VRML, HANIM, XML, MPEG-4, ...

MIRALab University of Geneva www.miralab.ch Eurographics 2006

vhd CAHRISMA

22

- VR reconstruction and preservation of cultural heritage
 - 

MIRALab University of Geneva www.miralab.ch Eurographics 2006

vhd CAHRISMA

23

- Interplaying technologies :
 - high performance 3D graphics
 - huge model rendering
 - realistic lighting effects
 - immersive 3D sound
 - home cinema 5.1 surround sound
 - real time environmental effects
 - VR interaction
 - intuitive VE navigation paradigm
 - using head magnetic tracking
 - speech recognition
 - giving orders to the system
 - changing point of views
- virtual crowd
 - behavioural control
 - rules, scripts
- virtual human animation
 - skeleton animation
 - walking engine
 - keyframes
 - animation mixing
 - skin deformation
 - face animation mixing
 - face deformation
 - speech
- others
 - VRML, HANIM, XML, MPEG-4, ...

MIRALab University of Geneva www.miralab.ch Eurographics 2006

vhdLIFEPLUS

LIFEPLUS proposes an innovative 3D reconstruction of ancient frescoes-paintings through the real-time revival of their fauna and flora, featuring groups of virtual animated characters with artificial life dramaturgical behaviours, in an immersive mobile AR environment.

LIFEPLUS:
<http://www.miralab.unige.ch/subpages/lifeplus>

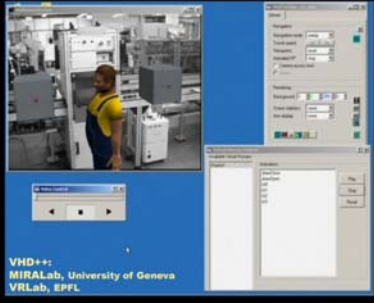


LIFEPLUS IN POMPEI MIRALab 2d3 VR

MIRALab University of Geneva www.miralab.ch Eurographics 2006

vhdSTAR

STAR: <http://www.realviz.com/STAR>



VHD++:
MIRALab, University of Geneva
VRLab, EPFL

STAR aims at mixing images of real environments, virtual objects and virtual humans to produce mixed reality simulations of an existing environment.



University of Geneva
www.miralab.ch

Eurographics 2006



Emotion, Interaction and Real-Time Animation

Nadia Magnenat-Thalmann and Arjan Egges

MIRALAB- UNIVERSITY OF GENEVA

MIRALab
Where Research Means Creativity

University of Geneva
www.miralab.ch

Eurographics 2006




Overview

- Introduction
- Background
 - Interactive Virtual Human
 - Performance Animation
- The MIRAnim Engine
- Adding emotions to animation
- Interactive Virtual Human

MIRALab
Where Research Means Creativity

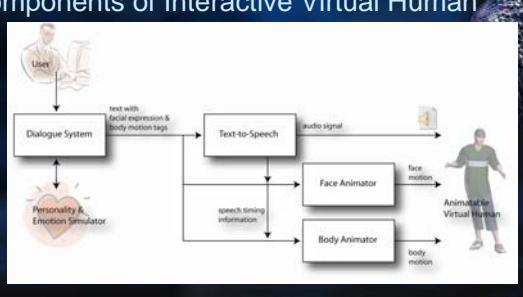
University of Geneva
www.miralab.ch

Eurographics 2006



Introduction


Components of Interactive Virtual Human



MIRALab
Where Research Means Creativity

University of Geneva
www.miralab.ch

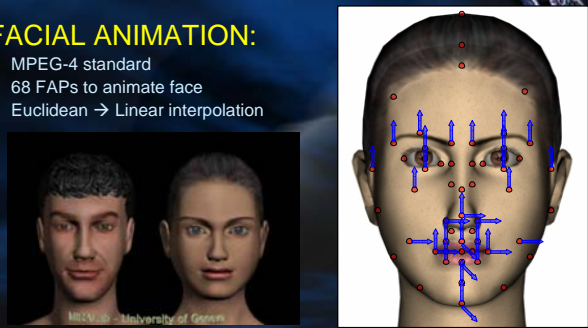
Eurographics 2006



Introduction

FACIAL ANIMATION:

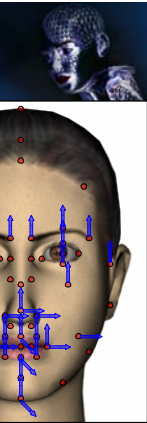
- MPEG-4 standard
- 68 FAPs to animate face
- Euclidean → Linear interpolation



MIRALab
Where Research Means Creativity

University of Geneva
www.miralab.ch

Eurographics 2006



Introduction

BODY ANIMATION:

- H-Anim joints
- 1 global translation
- 1 rotation for each joint

Problematic:

- Non-linear rotations
- Physical constraints
- Collisions



Background

Systems for automatically animating VHs

- The BEAT System [Cassell01]

Example animation schedule in BEAT:

```
<VISEME time=0.0 spec="A">
<GAZE word=1 time=0.0 spec=AWAY_FROM_HEARER>
<VISEME time=0.24 spec="E">
<VISEME time=0.314 spec="A">
<VISEME time=0.364 spec="TH">
<VISEME time=0.453 spec="E">
<GAZE word=3 time=0.517 spec=TOWARDS_HEARER>
<R_GESTURE_START word=3 time=0.517 spec=BEAT>
<EYEBROWS_START word=3 time=0.517>
```



J. Cassell, H. Vilhjalmsson, and T. Bickmore. BEAT: the Behavior Expression Animation Toolkit. In Computer Graphics Proceedings, Annual Conference Series. ACM SIGGRAPH, 2001.



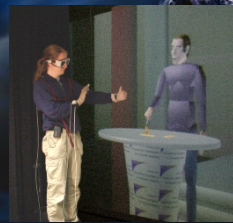
Background

Systems for automatically animating VHs

- The MAX System [Kopp04]

Example animation schedule in MAX:

```
<utterance>
<specification>
And now take <time id="t1"/> this bar. <time id="t2"/>
</specification>
<behaviorspec id="gesture_1">
<gesture>
<affiliate onset="t1" end="t2" focus="this"/>
<function name="refer_to_loc">
<param name="refloc" value="Stool-Bar_1"/>
</function>
</gesture>
</behaviorspec>
</utterance>
```



S. Kopp and J. Wachsmuth. Synthesizing multimodal utterances for conversational agents. Computer Animation and Virtual Worlds, 15(1):39–52, 2004.



Background

Systems for automatically animating VHs

- The GRETA System [Hartmann02]

Example animation schedule in GRETA:

```
GESTURECLASS adjectival STARTFRAME 0.4
GESTUREINSTANCE small FRAMETYPE stroke_end
DURATION 1.5 ARM XC YIpperF IMiddle
STARTFRAME 0.0 WRIST FPredefault Palmdefault:
FRAMETYPE stroke_start ENDFRAME
ARM XC YIpperF IMear STARTFRAME 1.0
HAND symbol_1_open FRAMETYPE hold
FINGER index bend_curved ARM XC YIpperF IMiddle
WRIST FPrep PalmInwards HAND symbol_1_open
ENDFRAME FINGER index bend_curved
WRIST FPrep PalmInwards ENDFRAME
```



B. Hartmann, M. Mancini, C. Pelachaud. Formational parameters and adaptive prototype instantiation for MPEG-4 compliant gesture synthesis. Computer Animation, Geneva, June 2002.



Background

Global limitations of these systems:

- Motions are not very realistic, because they are produced procedurally for a few joints
- No full body motions taken into account
- No emotion simulation



Background

In order to improve realism, several motion capture techniques exist.

- Motion graphs [Kovar02]



L. Kovar, M. Gleicher, and F. Pighin. Motion graphs. In Proc. SIGGRAPH 2002, 2002.



Background

Other methods for segmentation and control:

- Segmentation into textons using linear dynamic system [Li02]
- Controlling motion from music rhythm [Kim03]
- Synthesizing motion path from annotated database [Arikan03]

Y. Li, T. Wang, and H. Y. Shum. Motion texture: A two-level statistical model for character motion synthesis. In Proc. SIGGRAPH 2002, 2002.
Okan Arikan, David A. Forsyth, and James F. O'Brien. Motion synthesis from annotations. ACM Transactions on Graphics, 33(3):402–408, 2003.
T. H. Kim, S. I. Park, and S. Y. Shin. Rhythmic-motion synthesis based on motor-beat analysis. ACM Transactions on Graphics, 22(3):392–401, 2003.



Background

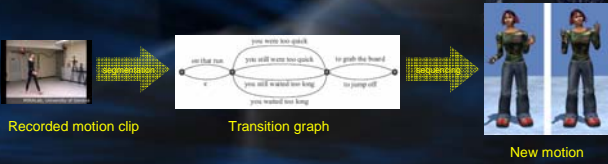
Limitations of such methods:

- Computationally expensive distance criterion
- Real-time application depends on the type of constraints
- Precise constraints required not only for target and source frames, but also for intermediate animation
- Vertices/edges have no meaning



Background

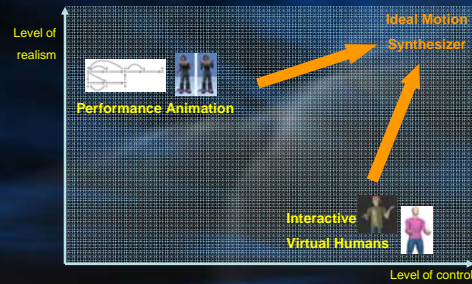
- Stone et al. [Stone04] are the first to use motion capture techniques for gestures



M. Stone, D. DeCarlo, I. Oh, C. Rodriguez, A. Stone, A. Lenta, C. Bregler. Speaking with hands: creating animated conversational characters from recordings of human performance. SIGGRAPH 2004, pages 206-213, 2004.

Background

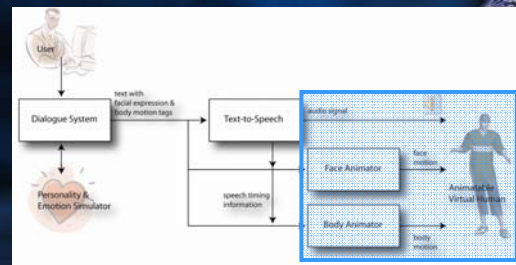
Overview:



Our contributions

- A simpler distance criterion for construction motion graphs
- Real-time motion synthesis with loose constraints
- Realistic gesture synthesis (automatic calculation of dependent joint motion)
- Animation engine independent of animation type (face, body, ...)
- High-level animation control (dialogue system, emotions)
- Implementation as a part of existing framework in MIRALab

The MIRAnim Engine



The MIRAnim Engine

In the MIRAnim animation engine, we use different representations for orientations:

Viewer

- Quaternions**
 - Widely used
 - SLERP interpolation
- Exponential Map**
 - Linear interpolation
 - Small format
- Principal Components**
 - Statistical analysis
 - Dimension reduction

MIRALab Where Research Means Creativity University of Geneva www.miralab.ch Eurographics 2006

The MIRAnim Engine

Cassell et al. [Cassell99] identify two types of communicative body motions:

Gestures

Posture shifts

BLENDING

J. Cassell, T. Bickmore, M. Billinghurst, L. Campbell, K. Chang, Vilhjalmsson, H., and H. Yan. Embodiment in conversational interfaces: Rea. In Proceedings of the CHI 99 Conference, pages 320-327. 1999.

MIRALab Where Research Means Creativity University of Geneva www.miralab.ch Eurographics 2006

The MIRAnim Engine

Creating posture shift motions (idle motions):

Recorded motion

Left postures Right postures

MIRALab Where Research Means Creativity University of Geneva www.miralab.ch Eurographics 2006

The MIRAnim Engine

- Creating idle motions from motion capture segments
- We need to add **small variations in posture** to make the motion look more realistic [Perlin95]
- We apply a noise function [Perlin85] onto a subset of **Principal Components** in stead of directly on joints

without variation

with variation

Ken Perlin. Real time responsive animation with personality. IEEE Transactions on Visualization and Computer Graphics, 1(1), 1995.

Ken Perlin. An image synthesizer. In Proceedings of the 12th Annual Conference on Computer Graphics and Interactive Techniques, pages 287-296. ACM Press, 1985.

MIRALab Where Research Means Creativity University of Geneva www.miralab.ch Eurographics 2006

The MIRAnim Engine

- Gesture motions → automatic creation of joint motions

We apply a scaling filter on each posture, to automatically generate dependent joint motions.

MIRALab
Where Research Means Creativity

University of Geneva
www.miralab.ch

Eurographics 2006

The MIRAnim Engine

MIRALab
Where Research Means Creativity

University of Geneva
www.miralab.ch

Eurographics 2006

The MIRAnim Engine

Animation blending:

MIRALab
Where Research Means Creativity

University of Geneva
www.miralab.ch

Eurographics 2006

The MIRAnim Engine

Different levels of animation control

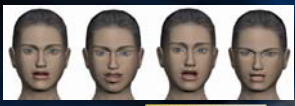


MIRALab
Where Research Means Creativity

University of Geneva
www.miralab.ch

Eurographics 2006

Emotional Animation

Different **representations** for emotions: Ekman, OCC, Plutchik, Cowie

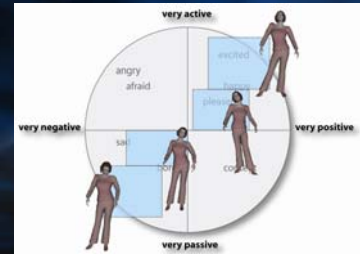




Irene Albrecht, Marc Schröder, Jörg Haber, Hans-Peter Seidel, Mixed feelings: expression of non-basic emotions in a muscle-based talking head. Virtual Reality, Volume 8, Issue 4, Sep 2005, Pages 201 – 212.

MIRALab University of Geneva Eurographics 2006
Where Research Means Creativity www.miralab.ch

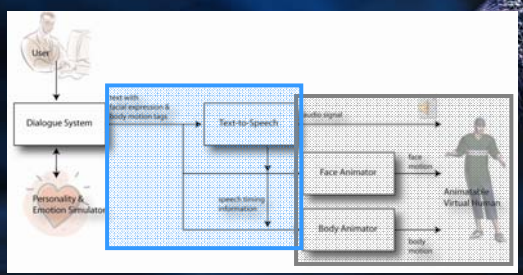
Emotional Animation

- Mapping animation segments onto intervals on the emotion disc



MIRALab University of Geneva Eurographics 2006
Where Research Means Creativity www.miralab.ch

Interactive Virtual Human



MIRALab University of Geneva Eurographics 2006
Where Research Means Creativity www.miralab.ch

Interactive Virtual Human

Creating face and body animation

```
<begin_gesture id="raise_eyebrows"/>I don't know what that means.<end_gesture id="raise_eyebrows"/> but <begin_gesture id="lower_eyebrows"/>you do.<end_gesture id="lower_eyebrows"/>
```



9 2673 3145 3860

Krienn B., Piker H., Defining the Gesticon: Language and Gesture Coordination for Interacting Embodied Agents, in Proceedings of the AISB-2004 Symposium on Language, Speech and Gesture for Expressive Characters, University of Leeds, UK, pp.107-115, 2004.
 Irene Albrecht, Marc Schröder, Jörg Haber, Hans-Peter Seidel, Mixed feelings: expression of non-basic emotions in a muscle-based talking head, Virtual Reality, Volume 8, Issue 4, Sep 2005, Pages 201 – 212

MIRALab University of Geneva Eurographics 2006
Where Research Means Creativity www.miralab.ch

Funding/Support

- FP6 HUMAINE Network of Excellence
(<http://www.emotion-research.net>)

humaine

- FP6 ENACTIVE Network of Excellence
(<http://www.enactivenetwork.org>)

ENACTIVE
Enactive Interfaces

- FP5 MUHCI RTN project
(http://poseidon.csd.auth.gr/Projects/muhci/muhci_ns.html)

muHCI

MIRALab
Where Research Means Creativity


University of Geneva
www.miralab.ch

Eurographics 2006



Real-time illumination models for interactive virtual inhabitants

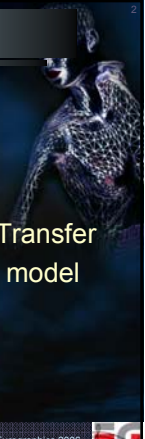
George Papagiannakis
Nadia Magnenat-Thalmann
MIRALab – University of Geneva



MIRALab University of Geneva www.miralab.ch Eurographics 2006

Summary

- Introduction
- Previous Work
- Our MR illumination model design
- Dynamic Precomputed Radiance Transfer
- All-Frequency 'key-fill' illumination model
- Results and Conclusions
- Future Work



MIRALab University of Geneva www.miralab.ch Eurographics 2006

Introduction


- Virtual Characters composited via offline Special Effects (SFX) in movie industry



MIRALab University of Geneva www.miralab.ch Eurographics 2006

Objectives

- *Physically-principled illumination model*
- *Application for simulating and compositing dynamic virtual characters*
- *Low real-time computational cost*
- *Consistent, believable MR registration*
- *Input requirements, assumptions and level of automation*



MIRALab University of Geneva www.miralab.ch Eurographics 2006

Problem Statement

- algorithms and extensions for an MR illumination model for virtual humans:
 - complex (multi-segmented, multi-material)
 - dynamic (animatable) skeleton-based deformable
 - rendered in real-time
 - consistent with the real environment area-light

MIRALab

University of Geneva
www.miralab.ch

Eurographics 2006



Previous work: Nomenclature

- *Lighting*
- *Shading*
- *Local illumination*
- Global illumination (GI)
- GI for Real-Time (RT)
- Image-Based Lighting
- high dynamic range (HDR)

MIRALab

University of Geneva
www.miralab.ch

Eurographics 2006



Previous work: Mathematical and Physical Principles

| Radiant term | Symbol | Definition | Unit |
|-----------------------|--------|---|------------------------|
| Radiant Energy | Q | basic light definition | J |
| Luminous Energy | | | talbot |
| Radiant Power (flux) | Φ | $\frac{dQ}{dt}$ | W (watt) |
| Luminous Power (flux) | | $\frac{d\Phi_v}{dt}$ | lm (lumen) |
| Radiant Intensity | I | $\frac{d\Phi}{d\Omega}$ | W/sr (watt/steradian) |
| Luminous Intensity | | $\frac{d\Phi_v}{d\Omega}$ | cd (candela) |
| Irradiance | E | $\frac{d\Phi}{dA}$ | W/m ² |
| Illuminance | | $\frac{d\Phi_v}{dA}$ | lm/m ² |
| Radiance | L | $\frac{d^2\Phi}{dA d\Omega \cos\theta}$ | W/(m ² sr) |
| Luminance | | $\frac{d^2\Phi_v}{dA d\Omega \cos\theta}$ | lm/(m ² sr) |

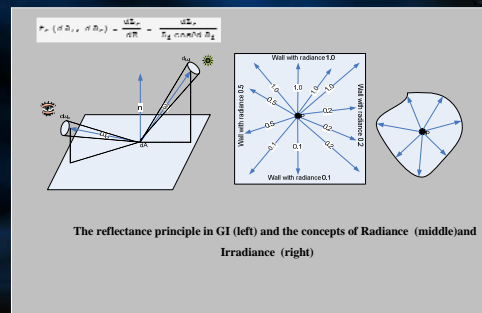
MIRALab

University of Geneva
www.miralab.ch

Eurographics 2006



Previous work: Mathematical and Physical Principles



MIRALab

University of Geneva
www.miralab.ch

Eurographics 2006



Previous work: Precomputed Radiance Transfer equations

$$L_o(\vec{x}, \vec{v}) = L_{eq}(\vec{x}, \vec{v}) + \int_{\Omega} \vec{f}_r(\vec{x}, \vec{l}', \vec{v}') L_i(\vec{x}, \vec{l}) (\vec{n}, \vec{l}) d\Omega \quad [1]$$

$$L_{eq}(\vec{x}, \vec{l}) = L_{eq}(\vec{l}) V(\vec{x}, \vec{l})$$

$$L_{eq}(\vec{x}, \vec{v}) = \int_{\Omega} \vec{f}_r(\vec{x}, \vec{l}', \vec{v}') L_{eq}(\vec{l}) V(\vec{x}, \vec{l}) (\vec{n}, \vec{l}) d\Omega \quad [2]$$

$$L_o = \int_{\Omega^2} \vec{f}_r * (\vec{\omega}) L_s(\vec{\omega}) V(\vec{\omega}) d\Omega \quad [8] \quad \mathbb{T}(\vec{\omega}) = V(\vec{\omega}) \vec{f}(\vec{\omega})$$

$$r(\vec{\omega}) = \sum_i r_i y_i(\vec{\omega}) \quad \tau(\vec{\omega}) = \sum_j \tau_j y_j(\vec{\omega}) \quad [9] \quad \sigma_{ij} = \int_{\Omega^2} y_i(\vec{\omega}) y_j(\vec{\omega}) d\Omega = \sigma_{ji}$$

$$L_o = \int_{\Omega^2} \left(\sum_i L_i y_i(\vec{\omega}) \right) \left(\sum_j \tau_j y_j(\vec{\omega}) \right) d\Omega +$$

$$L_o = \sum_i \sum_j L_i \tau_j \int_{\Omega^2} y_i(\vec{\omega}) y_j(\vec{\omega}) d\Omega +$$

$$L_o = \sum_i \sum_j L_i \tau_j \sigma_{ij} \Rightarrow L_o = \sum_i L_i \tau_i \Rightarrow$$

$$L_o = L \cdot \tau$$

MIRALab University of Geneva www.miralab.ch Eurographics 2006

Previous work: Spherical Harmonics Basis

$$Y_l^m(\theta, \phi) = \sqrt{\frac{2l+1}{4\pi} \frac{(l-m)!}{(l+m)!}} P_l^m(\cos\theta) e^{im\phi}$$

| | | | | | |
|-----|------|------|-----|-----|-----|
| | m=-2 | m=-1 | m=0 | m=1 | m=2 |
| l=0 | | | | | |
| l=1 | | | | | |
| l=2 | | | | | |

MIRALab University of Geneva www.miralab.ch Eurographics 2006

Image Based Lighting [Debevec 98]

Algorithm

- Capture High Dynamic Range image based model using light probe
- this model replaces any synthetic light sources
- scene is partitioned in three components
- An approximate material based model of the 'local scene' needed
- Render all components with GI
- Final compositing using differential rendering: $LS_{final} = LS_{back} + (LS_{obj} - LS_{noobj})$

MIRALab University of Geneva www.miralab.ch Eurographics 2006

Irradiance Maps [Ramamoorthi01]

$$B = \rho E$$

Radiosity (image intensity) ← Reflectance (albedo/texture) ← Irradiance (incoming light)

Assumptions

- Diffuse surfaces
- Distant illumination
- No shadowing, interreflection
- Hence, Irradiance is a function of surface normal


Classically, hemispherical integral for each pixel

MIRALab University of Geneva www.miralab.ch Eurographics 2006

Precomputed Radiance Transfer [Sloan02]

Previous Work

- Better light integration and transport
 - dynamic, area lights
 - self-shadowing
 - interreflections
- For diffuse and glossy surfaces
- At real-time rates



point light area light


area lighting, no shadows area lighting, shadows

MIRALab University of Geneva www.miralab.ch Eurographics 2006

Skin in the Dawn Demo [Beeson04]

Previous Work


- Ad hoc shader programs (vertex, fragment)
 - Tangent space bump mapping using pixel shaders
 - Offline Irradiance maps
 - Joint Dependant Deformation algorithm in GPU hardware
 - Fast performance, static area light, no self-shadow, interreflections, BRDF



MIRALab University of Geneva www.miralab.ch Eurographics 2006

Self-Shadowing of Dynamic Objects [Kautz04b]


Previous Work



- interactive rendering of dynamic models with self-shadows due to time-varying, low frequency lighting environments
- a hemispherical s/w rasterizer, which rapidly computes visibility
 - Rendering blocker geometry into a 2D occlusion mask with correct occluder fusion.
- response of an object to the lighting = integrating the visibility function at each of the vertices against the spherical harmonic functions
- Interactive performance (not real-time), supports only self-shadowing

MIRALab University of Geneva www.miralab.ch Eurographics 2006

Previous work: Graphical Comparison



AR Dynamic: Papagiannakis04, Pomi04, Debevec98, Drettakis97, Fournier93, Agusanto03, Haller03-04, Gibson03, our contribution

AR Static: Bunnell04

VR Dynamic: Zhou05, Tamura05, Beeson05, Kautz04b, Xu04, James03, Sloan02,05

VR Static: Tabellion04, Papagiannakis01, Ramamoorthi01

Categories: Radiosity/Ray Tracing, Image Based Lighting, Irradiance Maps, GI with Env Maps, Shadow Maps/volumes, Ambient Occlusion, PRT Methods

MIRALab University of Geneva www.miralab.ch Eurographics 2006

Dynamic Precomputed Radiance Transfer: Diffuse Shadowed Merged Transfer

- Comparisons

Phong DU DS DSM

MIRALab University of Geneva www.miralab.ch Eurographics 2006

All-Frequency 'key-fill' illumination model: Overview

- inspired from traditional cinematography
- 'key' principal light responsible for all major direct scene lighting
- 'fill' light for all indirect, ambient illumination
- registering VHs with 'natural' area lights for both VR and AR

MIRALab University of Geneva www.miralab.ch Eurographics 2006

All-Frequency 'key-fill' illumination model: Area Light Capturing Process

- Environment images combined to create a high dynamic range (HDR) image [Debevec97]
- Interactive Exposure matching with dPRT

Our capturing process of a light probe via a mirrored chrome hall at different day-light times (top) and the resulting HDR light probe (bottom)

MIRALab University of Geneva www.miralab.ch Eurographics 2006

All-Frequency 'key-fill' illumination model: Algorithm

$$L = K + F \Rightarrow$$

$$E_0(R, \vartheta) = \sum_{j=0}^n E_f(R, \mathcal{L}^j, \varphi^j) \frac{r_j}{2\pi} V(R, \mathcal{L}^j)(R, \mathcal{L}^j) + k_a E_a \Rightarrow$$

$$E_0(R, \vartheta) = \sum_{j=0}^n E_f(R, \mathcal{L}^j, \varphi^j) \frac{r_j}{2\pi} V(R, \mathcal{L}^j)(R, \mathcal{L}^j) +$$

$$\int_{\Omega} E_f(R, \mathcal{L}^j, \varphi^j) E_a(\mathcal{L}^j) V(R, \mathcal{L}^j)(R, \mathcal{L}^j) d\Omega \quad \text{for a single principal key light}$$

$$E_0(R, \vartheta) = E_f(R, \mathcal{L}^j, \varphi^j) \frac{r_j}{2\pi} V(R, \mathcal{L}^j)(R, \mathcal{L}^j) +$$

$$\int_{\Omega} E_f(\mathcal{L}^j) E_a(\mathcal{L}^j) V(\mathcal{L}^j)(R, \mathcal{L}^j) d\Omega \Rightarrow$$

$$E_0(R, \vartheta) = E_f(R, \mathcal{L}^j, \varphi^j) \frac{r_j}{2\pi} V(R, \mathcal{L}^j)(R, \mathcal{L}^j) +$$

$$\frac{r_a}{\pi} \int_{\Omega} E_a(\mathcal{L}^j) \frac{r_a}{2\pi} d\Omega \quad \text{fixed given value of } k_a, \varphi$$

$$E_0 = E_f(\mathcal{L}^j) \frac{r_j}{2\pi} V(\mathcal{L}^j)(R, \mathcal{L}^j) + E_a \cdot \frac{r_a}{2\pi} \quad [10]$$

- Unique combination of low-frequency dPRT and high-frequency direct lighting with Depth Shadow mapping
- Similar ideas in [Phong 75], [Blinn 77], [Wang05], [Kautz05]

MIRALab University of Geneva www.miralab.ch Eurographics 2006

All-Frequency 'key-fill' illumination model: Overview of our algorithm

MIRALab University of Geneva www.miralab.ch Eurographics 2006

All-Frequency 'key-fill' illumination model: Comparisons

MIRALab University of Geneva www.miralab.ch Eurographics 2006

All-Frequency 'key-fill' illumination model: Validation

- Offline(3DSMax) and our real-time model comparisons

MIRALab University of Geneva www.miralab.ch Eurographics 2006

Results and Conclusions: Architecture

Our MR-Rendering system is incorporated on the VHD++ [Ponder03], component-based framework engine

MIRALab University of Geneva www.miralab.ch Eurographics 2006

Results and Conclusions: Shader Graphs

flexibly and interchangeably apply a rendering effect anywhere in the multi-segmented character node hierarchy

University of Geneva
www.miralab.ch

Eurographics 2006

Results and Conclusions: LIFEPLUS

- Marker-less, feature based camera tracking system for geometrical illumination
- AR simulation in ancient Pompeii [movie]

University of Geneva
www.miralab.ch

Eurographics 2006

Results and Conclusions: ARToolkit

- Marker-based camera tracking system for geometrical illumination

University of Geneva
www.miralab.ch

Eurographics 2006

Results and Conclusions: ERATO

- VR cultural heritage simulation in ancient Aspendos [movie]

University of Geneva
www.miralab.ch

Eurographics 2006

Results and Conclusions: Statistical analysis on VR/AR Measurements

| VH | Number of Polygons | Preprocessing Time (mins) | dPRT (fps) | | All frequency Key-fill (fps) | | OpenGL Phong (fps) | |
|--------------------|--------------------|---------------------------|------------|------|------------------------------|-----|--------------------|------|
| | | | VR | AR | VR | AR | VR | AR |
| Antigone | 17458 | 53 | 19 | 11 | 10 | 7.5 | 25 | 15 |
| Creon | 20430 | 65 | 16 | 10.1 | 8.1 | 6.2 | 23 | 12.4 |
| Combined 3VH scene | 53799 | 170 | 10.1 | 8.2 | 6.2 | 3.5 | 15.2 | 10.6 |

Contribution I

- A new DSM Transfer for multi-segmented, skeleton-based deformable VHs [Chapter 4]
- Rotation of SH light coefficients [Ivanic98] from global to local for articulated structures:
 - a series of transformations applied each frame,
 - estimate the local to world joint transformation matrix for each vertex
 - for every frame we rotate the light according to each skinned mesh joint world space matrix
- Occluder, Receiver Posture Dependent, Posture Independent mesh identification

Contribution II

- Uniform Grid acceleration structure, [Amanatides86] voxel traversal, with [Moller97] fast ray-triangle intersection
- All frequency illumination model for articulated characters including:
 - low frequency (dPRT)
 - high frequency (Point-Light, Shadow Map) shading/shadowing [Chapter 5]
- AR Illumination Registration for fully simulated VHs via various geometrical registration methods [Chapter 6]

Limitation and Future work I

- challenge for a truly dynamic self-shadowing occlusion
- Challenge for the kind of lighting (indoor-outdoor)
- other basis functions (frequencies of evaluation and projection) more fitted for the VH topology
 - e.g. Bessel basis functions

Limitation and Future work II

- Where do we need to reduce complexity for VH rendering:
 - In the Lighting environment
 - In the Transfer vector
 - In the basis function scheme (storage, access, compression)
- employ our illumination registration with natural light algorithms to 3D scanned virtual humans

MIRALab

University of Geneva
www.miralab.ch

Eurographics 2006



MIRALab

University of Geneva
www.miralab.ch

Eurographics 2006



Emotion, Interaction and Real-Time Animation

Nadia Magnenat-Thalmann and Arjan Egges

MIRALAB- UNIVERSITY OF GENEVA

MIRALab
Where Research Means Creativity

University of Geneva
www.miralab.ch

Eurographics 2006




Overview

- Introduction
- Background
 - Interactive Virtual Human
 - Performance Animation
- The MIRAnim Engine
- Adding emotions to animation
- Interactive Virtual Human

MIRALab
Where Research Means Creativity

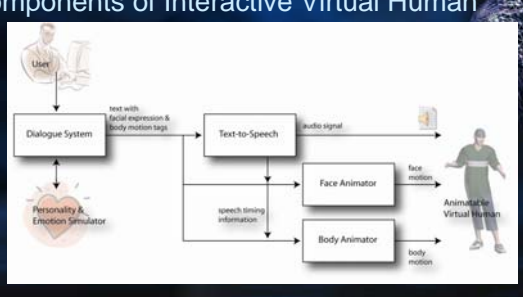
University of Geneva
www.miralab.ch

Eurographics 2006



Introduction


Components of Interactive Virtual Human



MIRALab
Where Research Means Creativity

University of Geneva
www.miralab.ch

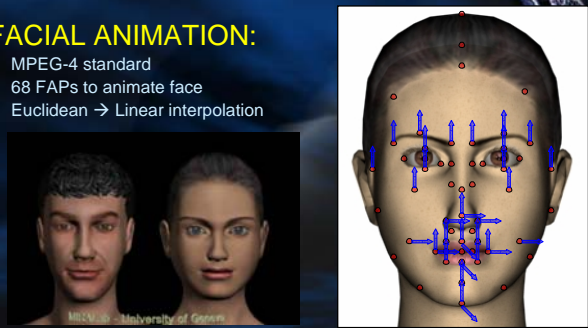
Eurographics 2006



Introduction

FACIAL ANIMATION:

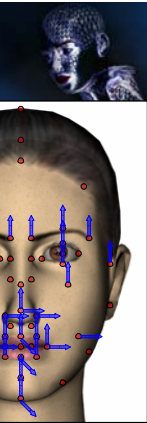
- MPEG-4 standard
- 68 FAPs to animate face
- Euclidean \rightarrow Linear interpolation



MIRALab
Where Research Means Creativity

University of Geneva
www.miralab.ch

Eurographics 2006



Introduction

BODY ANIMATION:

- H-Anim joints
- 1 global translation
- 1 rotation for each joint

Problematic:

- Non-linear rotations
- Physical constraints
- Collisions



Background

Systems for automatically animating VHs

- The BEAT System [Cassell01]

Example animation schedule in BEAT:

```
<VISEME time=0.0 spec="A">
<GAZE word=1 time=0.0 spec=AWAY_FROM_HEARER>
<VISEME time=0.24 spec="E">
<VISEME time=0.314 spec="A">
<VISEME time=0.364 spec="TH">
<VISEME time=0.453 spec="E">
<GAZE word=3 time=0.517 spec=TOWARDS_HEARER>
<R_GESTURE_START word=3 time=0.517 spec=BEAT>
<EYEBROWS_START word=3 time=0.517>
```



J. Cassell, H. Vilhjálmsson, and T. Bickmore. BEAT: the Behavior Expression Animation Toolkit. In Computer Graphics Proceedings, Annual Conference Series. ACM SIGGRAPH, 2001.



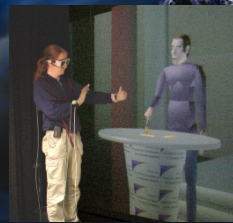
Background

Systems for automatically animating VHs

- The MAX System [Kopp04]

Example animation schedule in MAX:

```
<utterance>
<specification>
And now take <time id="t1"/> this bar. <time id="t2"/>
</specification>
<behaviorspec id="gesture_1">
<gesture>
<affiliate onset="t1" end="t2" focus="this"/>
<function name="refer_to_loc">
<param name="refloc" value="Stool-Bar_1"/>
</function>
</gesture>
</behaviorspec>
</utterance>
```



S. Kopp and J. Wachsmuth. Synthesizing multimodal utterances for conversational agents. Computer Animation and Virtual Worlds, 15(1):39–52, 2004.



Background

Systems for automatically animating VHs

- The GRETA System [Hartmann02]

Example animation schedule in GRETA:

```
GESTURECLASS adjectival STARTFRAME 0.4
GESTUREINSTANCE small FRAMETYPE stroke_end
DURATION 1.5 ARM XC Ylpperf ZMiddle
STARTFRAME 0.0 WRIST FDefault Palmdefault;
FRAMETYPE stroke_start ENDFRAME
ARM XC Ylpperf ZNear STARTFRAME 1.0
HAND symbol_1_open FRAMETYPE hold
FINGER index bend_curved ARM XC Ylpperf ZMiddle
WRIST FFlp PalmInwards HAND symbol_1_open
ENDFRAME FINGER index bend_curved
WRIST FFlp PalmInwards ENDFRAME
```



B. Hartmann, M. Mancini, C. Pelachaud. Formational parameters and adaptive prototype instantiation for MPEG-4 compliant gesture synthesis. Computer Animation, Geneva, June 2002.



Background

Global limitations of these systems:

- Motions are not very realistic, because they are produced procedurally for a few joints
- No full body motions taken into account
- No emotion simulation



Background

In order to improve realism, several motion capture techniques exist.

- Motion graphs [Kovar02]



L. Kovar, M. Gleicher, and F. Pighin. Motion graphs. In Proc. SIGGRAPH 2002, 2002.



Background

Other methods for segmentation and control:

- Segmentation into textons using linear dynamic system [Li02]
- Controlling motion from music rhythm [Kim03]
- Synthesizing motion path from annotated database [Arikan03]

Y. Li, T. Wang, and H. Y. Shum. Motion texture: A two-level statistical model for character motion synthesis. In Proc. SIGGRAPH 2002, 2002.
Okan Arikan, David A. Forsyth, and James F. O'Brien. Motion synthesis from annotations. ACM Transactions on Graphics, 33(3):402–408, 2003.
T. H. Kim, S. I. Park, and S. Y. Shin. Rhythmic-motion synthesis based on motor-beat analysis. ACM Transactions on Graphics, 22(3):392–401, 2003.



Background

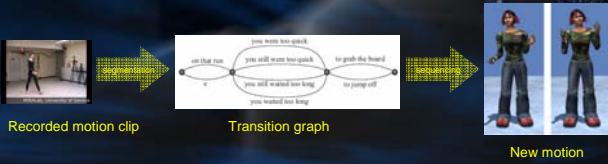
Limitations of such methods:

- Computationally expensive distance criterion
- Real-time application depends on the type of constraints
- Precise constraints required not only for target and source frames, but also for intermediate animation
- Vertices/edges have no meaning



Background

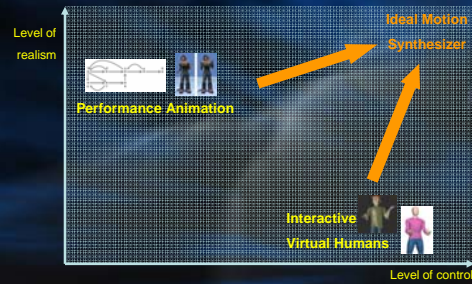
- Stone et al. [Stone04] are the first to use motion capture techniques for gestures



M. Stone, D. DeCarlo, I. Oh, C. Rodriguez, A. Stone, A. Lenta, C. Bregler, Speaking with hands: creating animated conversational characters from recordings of human performance, SIGGRAPH 2004, pages 206-213, 2004.

Background

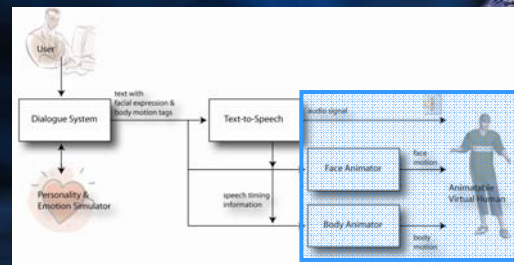
Overview:



Our contributions

- A simpler distance criterion for construction motion graphs
- Real-time motion synthesis with loose constraints
- Realistic gesture synthesis (automatic calculation of dependent joint motion)
- Animation engine independent of animation type (face, body, ...)
- High-level animation control (dialogue system, emotions)
- Implementation as a part of existing framework in MIRALab

The MIRAnim Engine



Body Animation and retargeting

Nadia Magnenat-Thalmann and Etienne Lyard

MIRALab – University of Geneva

MIRALab
Where Research Means Creativity

University of Geneva
www.miralab.ch

Eurographics 2006



Virtual Characters

- Several models layers for a complete character



MIRALab
Where Research Means Creativity

University of Geneva
www.miralab.ch

Eurographics2006

Skin deformation

- Skeletal Subspace Deformation (SSD)[1][2]
The skeleton animation is used for deforming the skin layer
- Example based methods [3]
A deformation model is tuned so that it reproduces a given set of example poses
- Physics based approaches
The skin is physically deformed according to the skeleton motion: finite elements

[1] N. Magnenat-Thalmann, R. Laperriere, and D. Thalmann, *Joint-dependent Local Deformation for Hand Animation and Object Grasping*. In Proc of Graphics Interface 1988.
[2] P.G. Kry, D.L. James, D.K. Pai, *EigenSkin: real time large deformation character skinning in hardware*, SCA2002.
[3] B. Allen, B. Curless, Z. Popovic, *Articulated body deformation from range scan data*. SIGGRAPH 2002.

MIRALab
Where Research Means Creativity

University of Geneva
www.miralab.ch

Eurographics2006

Skeletal Subspace Deformation

- Most widely used approach
- Simplest method
- Easy to implement
- Deformations must be designed semi-automatically using production software
- Drawbacks: artifacts appear when the deformation becomes large

MIRALab
Where Research Means Creativity

University of Geneva
www.miralab.ch

Eurographics2006

Skeletal Subspace Deformation


- The skin vertices are deformed using nearby joints of the skeleton
- Several approaches were proposed in order to get rid of the deformation artifacts
- Can be implemented in graphics hardware for performances gain

Skeleton Animation

- Various means of creation
 - Traditional animation [4]
 - Key-framing
 - Motion capture[5,6]
 - Physics and AI based simulations[7]
- One animation does only match one particular skeleton
- Need for motion adaptation when applying a motion clip to a skeleton

[4] J. Lasseter, *Principles of traditional animation applied to 3D computer animation*, SIGGRAPH 1987.
[5] ViconPeak corp, www.vicon.com
[6] Motion Analysis corps, www.motion-analysis.com
[7] J. K. Hodgins, *Three-Dimensional human Running*, IEEE Conference on Robotics and Automation.

Motion Retargeting

- Process of adapting a given motion clip to the particular features of a target character
- No 2 different virtual character have the same dimensions:

- Thus there is a need to adapt the motion to the particular character it will animate.

Motion Retargeting

- Adapt a given motion clip so that it satisfies criterions imposed by the user
- The constraints can be character oriented
 - Foot skating
 - Self penetration
 - Gait
- Or environment related
 - Grasp a particular object
 - Follow a given path
 - Adapt to a different terrain
- Philosophy: preserve the fine details of the motion while changing its macroscopic behavior

Motion Retargeting Strategies

- Direct parameters tweak [8]
- Spacetime optimization [9,10]
- Inverse Kinematics [11,15]
- Hybrid systems [12]
- Dedicated methods for footskate cleanup [13,14]

[8] Z. Popovic, A. Witkin. Motion warping. SIGGRAPH1995.

[9] M. Gleicher. Retargeting motion to new characters. SIGGRAPH 1998.

[10] J. Lee, S. Shin. A hierarchical approach to interactive motion editing for human-like figures. SIGGRAPH 1999.

[11] K. Choi, H. Ko. Online motion retargeting. Journal of Visualization and computer animation 11, 5, 223-235, 2000.

[12] H. Shin, J. Lee, S. Shin, M. Gleicher. Computer puppetry: an importance-based approach. ACM Transactions on Graphics 20, 2, 67-94, 2001.

[13] L. Kovar, J. Schreiner, M. Gleicher. Foot-skate cleanup for motion capture editing. SCA 2002.

[14] P. Glerdon, R. Boulic, D. Thalmann. Robust on-line adaptive footplant detection and enforcement. The Visual Computer, 22(3): 194-209, 2006.

[15] D. Tolani, A. Goswami, N.I. Badler. Real-time inverse kinematics techniques for anthropomorphic limbs. Graphical models, 62:353-388, 2000.

MIRALab

Where Research Means Creativity

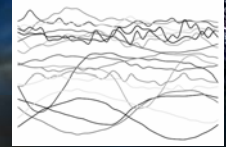
University of Geneva

www.miralab.ch

Eurographics2006

Motion warping

- Directly modify the parameter curves of the motion
- Easy to implement
- Not really retargeting – rather motion editing
- No guarantee regarding the quality of the results



MIRALab

Where Research Means Creativity

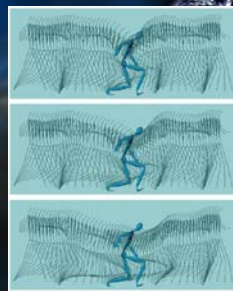
University of Geneva

www.miralab.ch

Eurographics2006

Spacetime optimization

- Constrained optimization formulation
- Take into account the motion as a whole
- Tricky to code
- High quality results which can comply with any kind of requirement from the user



MIRALab

Where Research Means Creativity

University of Geneva

www.miralab.ch

Eurographics2006

Inverse Kinematics

- 2 classes:
 - Numerical – close from spacetime
 - Analytical – uses the specificities of the human body in order to use an analytical formulation of the problem
- Numerical methods can assign a strict number of priority among the constraints
- Analytical methods are super fast

MIRALab

Where Research Means Creativity

University of Geneva

www.miralab.ch

Eurographics2006

Hybrid systems


- Combines the best of optimization and analytical inverse kinematics
- Architecture of the code tailored to the application
- Used for computer puppetry



Footskate cleanup methods

- Applications targeted for removing this very unpleasant artifact
- Ad-hoc methods have proven to work well [13]
- More complex approaches can also estimate the foot planting automatically [14]





State of the art for hair

Prof. Nadia Magnenat-Thalmann

MIRALab – University of Geneva

Thalmann@miralab.unige.ch


MIRALab University of Geneva
Where Research means Creativity
www.miralab.ch
Eurographics 2006



Hair Simulation Tasks - Styling

- Hair shape is a result of complex physical interaction between hair-hair and hair-body
- Hairstyling – a constant human passion curlers, clips, knots, braids and up-dos
- Hair dynamics at interactive speed is impossible. Heuristic approach is needed for hair shape modeling
- Thus, hair shape modeling is an exclusive task in computer graphics

MIRALab University of Geneva
Where Research means Creativity
www.miralab.ch
Eurographics 2006



Hair Simulation Tasks - Dynamics

- Highly anisotropic physical behavior
- Solid-liquid duality
- Light weight of hair as compared to its acceleration, stiffness, friction and air drag
- Constant collisions / frictional interactions with the body
- 100,000 to 150,000 hair strands on scalp
- Hair-hair interaction, one of the unsolved problems of Computer Graphics

MIRALab University of Geneva
Where Research means Creativity
www.miralab.ch
Eurographics 2006



Hair Simulation Tasks - Rendering

- Intricate geometry of individual hair
- Large number of hair strands
- Complex interaction with light and shadows multiple scattering, luster, self-shadowing
- Anisotropy in shading
- Small thickness of the hair – anti-aliasing
- How artists paint hair?

MIRALab University of Geneva
Where Research means Creativity
www.miralab.ch
Eurographics 2006

Open Problems in Hair Simulation

- Hair Shape Modeling
 - Many recent attempts, however not yet matured
- Hair Dynamics
 - Stiffness dynamics of individual hair was grossly approximated considering current computing power (1GHz, 1GB RAM)
 - Hair-hair interaction not attempted (until recently)

MIRALab University of Geneva
Where Research means Creativity www.miralab.ch Eurographics 2006

Open Problems in Hair Simulation

- Hair Rendering
 - Fairly matured and is available through commercial systems. However, global-illumination for hair with detailed shading models is not yet attempted.
- Real-time hair animation and rendering
 - With possible compromise on the realism
- Hair interaction with a user (hairdresser for example)

MIRALab University of Geneva
Where Research means Creativity www.miralab.ch Eurographics 2006

Our Approach in Non Real-Time

- Hair Shape Modeling*
 - Hair shape as streamlines of fluid flow
- Hair Rendering
 - Single iteration hair rendering including volumetric shadows using graphics hardware

*Sunil Hadap and Nadia Magnenat-Thalmann. "Interactive Hair Styler based on Fluid Flow", Eurographics Workshop on Computer Animation and Simulation/2000, Interlaken 2000

MIRALab University of Geneva
Where Research means Creativity www.miralab.ch Eurographics 2006

Making of...

Placement of smoothed particles to realize hair-fluid

MIRALab University of Geneva
Where Research means Creativity www.miralab.ch Eurographics 2006

Our Approach (2)

- Hair Dynamics**
 - Stiffness dynamics of non-straight hair strand
 - Elaborate inertial dynamics using reduced coordinate formulation
 - Hair-hair, hair-body and hair-air interaction dynamics



--Sunil Hadap, Nadia Magnenat-Thalmann, "Modeling Dynamic Hair as a Continuum", Computer Graphics Forum, Volume 20, Issue 3, Eurographics 2001 Proceedings, Manchester, United Kingdom, September 2001



Individual Hair Dynamics



Without stiffness



Body forces



Collision as fluid boundary

With stiffness



Results – Computer Animations



Bunch of hair




Results – Computer Animations



Hair fall



Results – Computer Animations



Blown by wind

MIRALab University of Geneva
Where Research means Creativity
www.miralab.ch

Eurographics 2006

Experiments with real hair

A typical experiment on bunch of hair



Low stiffness High stiffness


As stiffness increases the "swing" reduces

MIRALab University of Geneva
Where Research means Creativity
www.miralab.ch

Eurographics 2006

Virtual Experimental Setup

- Switch length – 24cm
- Number of hair strands – 1000
- Hair segment length 0.9cm
- Amplitude – 4cm
- Frequency – 1Hz
- Number of cycles - 2




MIRALab University of Geneva

MIRALab University of Geneva
Where Research means Creativity
www.miralab.ch

Eurographics 2006

Variations in Strand Stiffness

- Increase in stiffness gives considerable phase difference.
- In Reality, it is the change in hair thickness which varies the bending stiffness.
- However, it is hard to model various hair thickness
- We may simulate the process by changing the stiffness coefficient E
- Observe the tip movement with respect to the movement of the base




$E=250$ $E=500$ $E=750$

MIRALab University of Geneva
Where Research means Creativity
www.miralab.ch

Eurographics 2006

Simulation - Adjusting the air drag



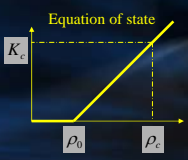
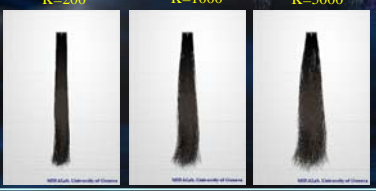
Normal hair makes 5-6 oscillations before coming to rest.

When hair is treated with styling products, air drag increases to reduce number of oscillations to merely 1-2

MIRALab University of Geneva
Where Research means Creativity
www.miralab.ch
Eurographics 2006

Variations in Hair-hair Interaction

- The spread in the bunch of hair is a result of hair-hair interaction
 - One can vary the constant K_c to change this interaction
- An immediate effect is on the spread of the tip
 - One can also observe how the tip makes a "bouncy" movement as K_c increases.

MIRALab University of Geneva
Where Research means Creativity
www.miralab.ch
Eurographics 2006

Variations in Internal Damping

- The internal damping is associated to energy loss as elastic material undergoes deformation
- Though the large change in internal damping has minute effect on the hair movement, it is important to increase stability of the simulation ID



MIRALab University of Geneva
Where Research means Creativity
www.miralab.ch
Eurographics 2006

Full head of hair


- By means of varying hair-hair interaction (the coefficient K_c) one can achieve different quality of hair movements
- When K_c is low, hair appears to be straight and oily. Increase in K_c gives much "volume" to the hair and it then appears more dry and airy.



MIRALab University of Geneva
Where Research means Creativity
www.miralab.ch
Eurographics 2006

Result – Perturbations to Few Individual Hair


- Few individual hair strands break away from the flow and follow the perturbations



MIRALab University of Geneva
Where Research means Creativity www.miralab.ch Eurographics 2006

Result - Shaping Hairstyle Using Fluid Elements


- Vortices as curlers



MIRALab University of Geneva
Where Research means Creativity www.miralab.ch Eurographics 2006

Result – Applying Clumps and Waves

- Under adhesive forces, in reality, hair strands form clumps.




clump radius
min clump length
max clump length
clump radius * clump radius = clump area
clump area

MIRALab University of Geneva
Where Research means Creativity www.miralab.ch Eurographics 2006

Real-Time Animation of Hairstyles

- Managing Complexity of Hair Simulation
 - More than 100 000 hair strands
 - Mechanical behavior of individual strands
 - Collisions and friction on the skull
 - Collisions and friction between strands
 - Physical state (wetness, styling products)
 - Aerodynamics
- No chances to simulate an explicit mechanical model in real-time.



MIRALab University of Geneva
Where Research means Creativity www.miralab.ch Eurographics 2006

Real-Time Animation of Hairstyles

- Ideas for Speeding Up Hair Simulation
 - Simplification of the mechanical model
 - Reduction of the degrees of freedom
 - Macroscopic approximations
 - Interpolation
- Techniques
 - Whisp or Cluster models
 - Particle systems of variable topology
 - Volume hair models
 - Free-Form Deformations

MIRALab University of Geneva
Where Research means Creativity www.miralab.ch Eurographics 2006

1. Real-Time FFD Hair Animation

- The main idea: Deforming the complete hairstyle using a mechanically-animated Free-Form Deformation lattice.



MIRALab University of Geneva
Where Research means Creativity www.miralab.ch Eurographics 2006

1. Real-Time FFD Hair Animation

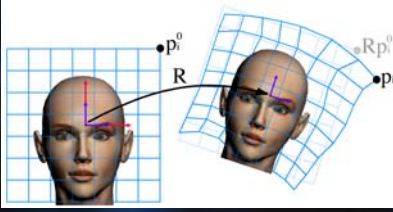
- Main advantages:
 - Drastic and controllable reduction of the number of degrees of freedom of the mechanical model
 - => Real-time mechanical simulation
 - Simple and fast interpolation scheme for computing the deformed hairstyle
 - => Real-time motion of any feature of the hairstyle
 - Any hairstyle can be animated
 - => Versatility and design simplicity



MIRALab University of Geneva
Where Research means Creativity www.miralab.ch Eurographics 2006

2. FFD Hairstyle Deformation

- Building the lattice around the hairstyle
 - The lattice is attached to the rigid-body motion R of the skull
 - The lattice is then deformed by mechanical simulation



MIRALab University of Geneva
Where Research means Creativity www.miralab.ch Eurographics 2006

2. FFD Hairstyle Deformation

- Attaching Strand Roots on the Skull
 - Attachment of the hair strands on the skull should be ensured whatever the deformation
 - Strand roots should be defined by the rigid motion of the skull only
 - Continuous transition between rigid motion ($\delta = 0$) and deformed lattice ($\delta = 1$) along the hair

$$\mathbf{p} = \sum_i w_i (\delta \mathbf{p}_i + (1 - \delta) \mathbf{R} \mathbf{p}_i^0)$$



3. Animating the FFD Lattice

- Mechanical Properties to be Simulated
 - Mechanical behavior of hair:
 - Density, Elasticity
 - Interactions between strands
 - External forces exerted on hair:
 - Gravity
 - Aerodynamic effects
 - Collisions between hairs and other objects:
 - Body parts: Skull, shoulders...
 - Other objects



3. Animating the FFD Lattice

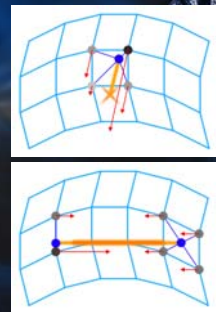
- Building Blocks: Lattice Stiffners
 - Mechanical interaction between lattice nodes
 - Weighted contributions of lattice nodes
 - Viscoelastic behavior law $\sigma(\epsilon, \epsilon')$
 - Relating lattice forces \mathbf{f}_i to positions \mathbf{p}_j and speeds \mathbf{p}'_j

$$\mathbf{f}_i = \mathbf{w}_i \boldsymbol{\sigma} \quad \text{with} \quad \boldsymbol{\epsilon} = \sum_j \mathbf{w}_j \mathbf{p}_j \quad \text{and} \quad \boldsymbol{\epsilon}' = \sum_j \mathbf{w}_j \mathbf{p}'_j$$




3. Animating the FFD Lattice

- Particular Lattice Stiffners
 - Lattice Attachment
 - Relates one location of the lattice to a given point in space
 - Weights: Linear interpolation coefficients of the location in the lattice
 - Lattice Spring
 - Relates two locations of the lattice
 - Weights: Linear interpolation coefficients, positive and negative



3. Animating the FFD Lattice

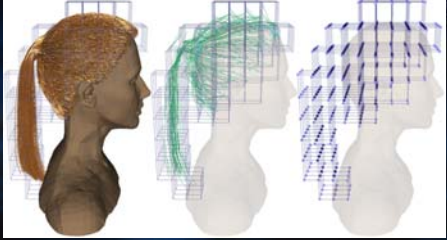
- Hair Strand Discretization
 - Creating lattice springs between grid edges ($>45^\circ$)
 - Creating lattice attachment on root



MIRALab University of Geneva
Where Research means Creativity www.miralab.ch Eurographics 2006

3. Animating the FFD Lattice

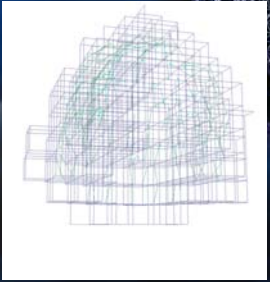
- Hair Strand Discretization
 - Mass of each strand distributed on the lattice nodes using weights of linear interpolation of strand segment extremities



MIRALab University of Geneva
Where Research means Creativity www.miralab.ch Eurographics 2006

3. Animating the FFD Lattice

- Decimation of the Model
 - Number of lattice stiffners reduced at will
 - Similar stiffners are consolidated
 - Parallelism and projections in the space of lattice node weights
 - Optimal accuracy - speed tradeoff
 - Initial strands
 - Initial model: 12100 strands, 3500 attachments
 - Low decimation: 800 strands, 200 attachments
 - High decimation: 200 strands, 50 attachments




MIRALab University of Geneva
Where Research means Creativity www.miralab.ch Eurographics 2006

3. Animating the FFD Lattice

The Ether Model


- Nodes surrounded by lattices empty of any hair may exhibit erratic behaviour.
- To limit this, the whole lattice is considered as an ether medium with its own stable behaviour.
- Additional weak viscoelastic forces are attached to the lattice nodes to rest position (rigid motion of the head)
 - Stabilize and damp the motion of the hairs
 - Improve the robustness
 - Additional custom parameters for simulating hair stiffness (short hair, styling gel...)
 - May include additional physical effects (aerodynamics)



MIRALab University of Geneva
Where Research means Creativity www.miralab.ch Eurographics 2006

3. Animating the FFD Lattice

- Collision Effects
 - Between the hair and the body
 - Head
 - Shoulders
 - Metaball-based model of body parts
 - Approximate modeling with a low number of primitives
 - Easy animation of body deformations
 - Attached to the rigid head motion (skull) or the body skeleton (shoulders)

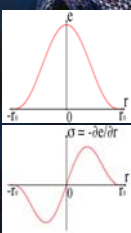


MIRALab University of Geneva
Where Research means Creativity www.miralab.ch Eurographics 2006

3. Animating the FFD Lattice

- Collisions with Metaballs
 - 6th-order polynomial metaballs (n=3) modeled as lattice attachments


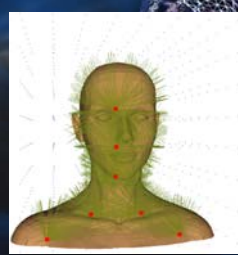
- Potential:
$$e = \begin{cases} \frac{e_0}{r_0^{2n}} s^n & \text{if } s \geq 0 \\ 0 & \text{elsewhere} \end{cases} \quad \text{with } s = r_0^2 - |\mathbf{e} - \mathbf{e}_0|^2$$
- Force:
$$\boldsymbol{\sigma} = -\frac{\partial e}{\partial \mathbf{e}} = \begin{cases} \frac{e_0}{r_0^{2n}} (2n) s^{n-1} (\mathbf{e} - \mathbf{e}_0) & \text{if } s \geq 0 \\ 0 & \text{elsewhere} \end{cases}$$



MIRALab University of Geneva
Where Research means Creativity www.miralab.ch Eurographics 2006

3. Animating the FFD Lattice

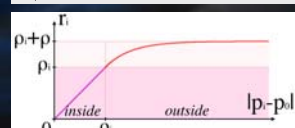
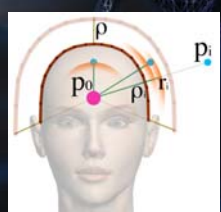
- Customizing Metaballs on Lattice Nodes
 - Low number of metaballs
 - Their center are attached to the skeleton
 - Their radius is customized to each lattice node according to its position

MIRALab University of Geneva
Where Research means Creativity www.miralab.ch Eurographics 2006

3. Animating the FFD Lattice

- Customizing Metaballs on Lattice Nodes
 - The metaball radius is chosen so as to:
 - Keep nodes outside the skull to a given distance from the surface
 - Prevent nodes inside the skull from moving deeper

$$r_i = \begin{cases} \rho_i + \rho \left(1 - \exp\left(-\frac{\rho_i - |p_i - p_d|}{\rho}\right) \right) & \text{if } |p_i - p_d| \geq \rho_i \\ |p_i - p_d| & \text{elsewhere} \end{cases}$$



MIRALab University of Geneva
Where Research means Creativity www.miralab.ch Eurographics 2006

3. Animating the FFD Lattice

- Customizing Metaballs on Lattice Nodes
 - Normalizing the strength of the metaballs
 - The base potential of the metaball should be chosen so as to give same repulsion (acceleration) whatever:
 - The mass of the lattice node
 - The radius of the metaball

$$e_i = r_i^2 m_i \gamma$$



3. Animating the FFD Lattice

- Metaball-Based Collision Handling
 - Approximate collision response
 - Low computational overhead
 - Suited for animation



3. Animating the FFD Lattice

- Numerical Integration
 - Particle system integrated by using the implicit Inverse Euler method
 - Using the Conjugate Gradient as linear system solver
 - On-the-fly matrix assembly for capturing all the nonlinearities of the mechanical system
 - Good robustness with any mechanical system when using constant time steps



4. Scalability and Level-of-Detail

- Options for Adjusting the Accuracy Tradeoff
 - Number of lattice attachments
 - The more attachments, the more accurate the mechanical behavior of the hairs
 - Size of the free-form deformation grid
 - The finer the grid, the richer and diverse the deformation patterns of the hair
 - Number of metaballs
 - The more metaballs, the more accurate the collisions between the hair and the body



4. Scalability and Level-of-Detail

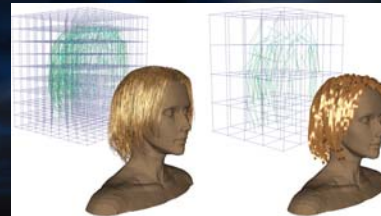
- Performance and Level-of-Detail
 - Computation times for a 1/25 s frame on a 3GHz Pentium4 PC computer

| Mech.Mod | 0 Att. | 0 Att. | 50 Att. | 100 Att. | 200 Att. |
|----------|---------|---------|----------|----------|----------|
| ----- | 0 Spr. | 0 Spr. | 200 Spr. | 400 Spr. | 800 Spr. |
| Lat.Size | 0 Meta. | 7 Meta. | 7 Meta. | 7 Meta. | 7 Meta. |
| 10x10x10 | 1.1 ms | 5.2 ms | 10.1 ms | 13.8 ms | 21.4 ms |
| 5x5x5 | 0.1 ms | 0.2 ms | 2.1 ms | 3.8 ms | 7.6 ms |



4. Scalability and Level-of-Detail

- Performance and Level-of-Detail
 - Level-of-Detail schemes have to be combined with adequate multiresolution rendering techniques



4. Scalability and Level-of-Detail

- Benefits of the FFD Model
 - Scalability, for efficient LOD implementations
 - Compatible with any hair rendering method
 - Weak reliance on the strand nature of hairs
 - Total freedom of hairstyle design using any standard design tool



P. Volino, N. Magnenat-Thalmann "Real-time Animation of Complex hairstyles",
IEEE Transactions of Visualization and Computer Graphics, vol.12, no 2, pp131-142, March-April 2006



The MIRAnim Engine

In the MIRAnim animation engine, we use different representations for orientations:

Viewer

- Quaternions**
 - Widely used
 - SLERP interpolation
- Exponential Map**
 - Linear interpolation
 - Small format
- Principal Components**
 - Statistical analysis
 - Dimension reduction

MIRALab University of Geneva Eurographics 2006
Where Research Means Creativity www.miralab.ch

The MIRAnim Engine

Cassell et al. [Cassell99] identify two types of communicative body motions:

Gestures

Posture shifts

BLENDING

J. Cassell, T. Bickmore, M. Billinghurst, L. Campbell, K. Chang, Vilhjalmsson, H., and H. Yan. Embodiment in conversational interfaces: Rea. In Proceedings of the CHI 99 Conference, pages 320-327. 1999.

MIRALab University of Geneva Eurographics 2006
Where Research Means Creativity www.miralab.ch

The MIRAnim Engine

Creating posture shift motions (idle motions):

Recorded motion

MIRALab University of Geneva Eurographics 2006
Where Research Means Creativity www.miralab.ch

The MIRAnim Engine

- Creating idle motions from motion capture segments
- We need to add **small variations in posture** to make the motion look more realistic [Perlin95]
- We apply a noise function [Perlin85] onto a subset of **Principal Components** in stead of directly on joints

without variation

with variation

Ken Perlin. Real time responsive animation with personality. IEEE Transactions on Visualization and Computer Graphics, 1(1), 1995.
Ken Perlin. An image synthesizer. In Proceedings of the 12th Annual Conference on Computer Graphics and Interactive Techniques, pages 287-296. ACM Press, 1985.

MIRALab University of Geneva Eurographics 2006
Where Research Means Creativity www.miralab.ch

The MIRAnim Engine

- Gesture motions → automatic creation of joint motions

We apply a scaling filter on each posture, to automatically generate dependent joint motions.

MIRALab
Where Research Means Creativity

University of Geneva
www.miralab.ch

Eurographics 2006

The MIRAnim Engine

MIRALab
Where Research Means Creativity

University of Geneva
www.miralab.ch

Eurographics 2006

The MIRAnim Engine

Animation blending:

MIRALab
Where Research Means Creativity

University of Geneva
www.miralab.ch

Eurographics 2006

The MIRAnim Engine

Different levels of animation control

MIRALab
Where Research Means Creativity

University of Geneva
www.miralab.ch

Eurographics 2006

Funding/Support

- FP6 HUMAINE Network of Excellence
(<http://www.emotion-research.net>)

humaine

- FP6 ENACTIVE Network of Excellence
(<http://www.enactivenetwork.org>)

ENACTIVE
Enactive Interfaces

- FP5 MUHCI RTN project
(http://poseidon.csd.auth.gr/Projects/muhci/muhci_ns.html)

muHCI

MIRALab
Where Research Means Creativity

University of Geneva
www.miralab.ch

Eurographics 2006



Case study: simulating life in Pompeii

Nadia
MAGNENAT-THALMANN

MIRALab
University of Geneva
Switzerland

MIRALab
University of Geneva
Where Research means Creativity
www.miralab.ch

Nadia Magnenat-Thalmann

The making of clothes with our MIRALab Fashionizer platform

2D patterns

3D garments from 2D patterns

DEMO

MIRALab
University of Geneva
Where Research means Creativity
www.miralab.ch

Nadia Magnenat-Thalmann

MIRALab
University of Geneva
Where Research means Creativity
www.miralab.ch

Nadia Magnenat-Thalmann

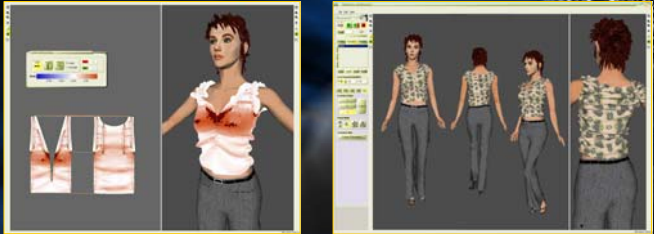
« Prêt-à-porter » Collection

MIRALab
University of Geneva
Where Research means Creativity
www.miralab.ch

Nadia Magnenat-Thalmann

Garment Creation Tools

Interactive tools for creating, draping, animating and prototyping garments on animated virtual characters [1]



[1] P. Volino, N. Magnenat-Thalmann, Accurate Garment Prototyping and Simulation, Computer-Aided Design and Applications journal, CAD Solutions, 2(5), pp 645-654, 2005.

MIRALab
University of Geneva

Where Research means Creativity
www.miralab.ch

Nadia Magnenat-Thalmann

Research collaboration with Adidas



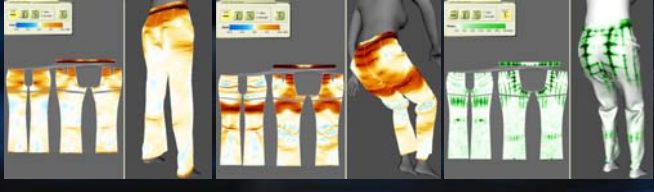
MIRALab
University of Geneva

Where Research means Creativity
www.miralab.ch

Nadia Magnenat-Thalmann

Garment Prototyping

- Accurate Simulation of Parameters
 - Evaluation of strain, stress and
 - contact pressure all over all over the cloth surface

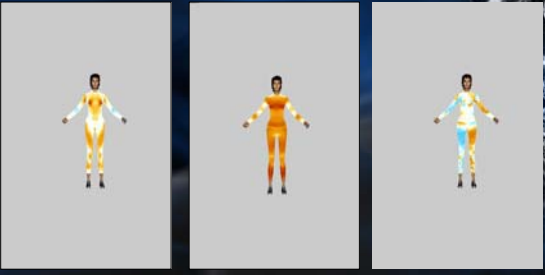


MIRALab
University of Geneva

Where Research means Creativity
www.miralab.ch

Nadia Magnenat-Thalmann

Color coded visualizations of deformation parameters

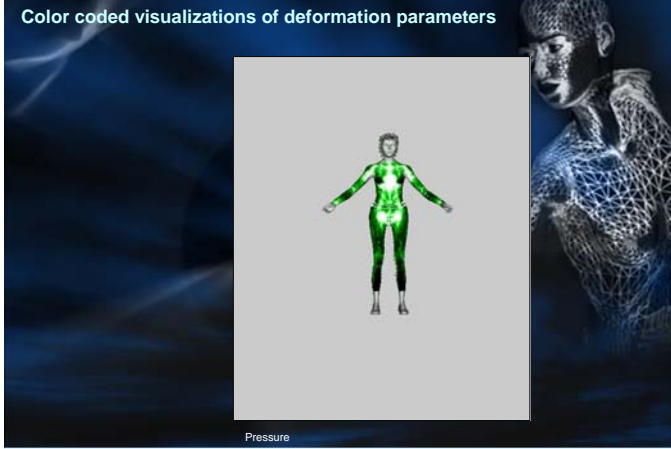


Deformation in Warp direction Deformation in Welt direction Deformation in Shear direction

MIRALab
University of Geneva

Where Research means Creativity
www.miralab.ch

Nadia Magnenat-Thalmann



MIRALab
University of Geneva

Where Research means Creativity
www.miralab.ch

Nadia Magnenat-Thalmann

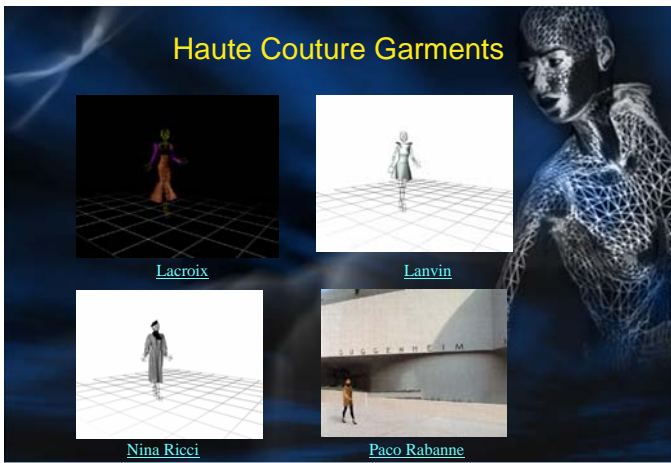


Mode, Passion et Collection - Le regard d'une femme" Musée d'Art et d'histoire, Genève

MIRALab
University of Geneva

Where Research means Creativity
www.miralab.ch

Nadia Magnenat-Thalmann



MIRALab
University of Geneva

Where Research means Creativity
www.miralab.ch

Nadia Magnenat-Thalmann



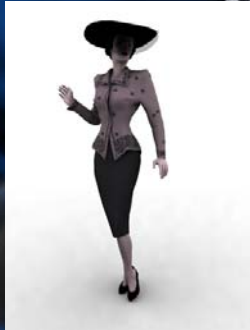
MIRALab
University of Geneva

Where Research means Creativity
www.miralab.ch

Nadia Magnenat-Thalmann



Exhibition Robert Piguet/Yverdon



Modèle designed by Bohan

MIRALab
University of Geneva

Where Research means Creativity
www.miralab.ch

Nadia Magnenat-Thalmann



Exhibition Robert Piguet/Yverdon



Modèle designed by Givenchy

MIRALab
University of Geneva

Where Research means Creativity
www.miralab.ch

Nadia Magnenat-Thalmann



Exhibition Robert Piguet/Yverdon



Modèle designed by Givenchy

MIRALab
University of Geneva

Where Research means Creativity
www.miralab.ch

Nadia Magnenat-Thalmann



CULTUREAL HERITAGE: European Research Project Lifeplus: augmented life in Pompeii

- LIFEPLUS proposes new Augmented Reality narrative spaces for the innovative revival of life in ancient frescos-paintings in Pompeii



MIRALab
University of Geneva

Where Research means Creativity
www.miralab.ch

Nadia Magnenat-Thalmann



Scenario 3,
e.g. La Villa
dei Misteri

Scenario 1,
e.g. Thermopoglio
di Vetuzio Placido

Scenario 2,
e.g. La Casa dei
Vettii

MIRALab
University of Geneva

Where Research means Creativity
www.miralab.ch

Nadia Magnenat-Thalmann

Research in CLOTHES AND FACIAL ANIMATION

- *Real-time Cloth and hair simulation*
 - Hybrid deformation
- *Real-time Facial emotion expression and Speech animation*

MIRALab
University of Geneva

Where Research means Creativity
www.miralab.ch

Nadia Magnenat-Thalmann

MIRALab
University of Geneva

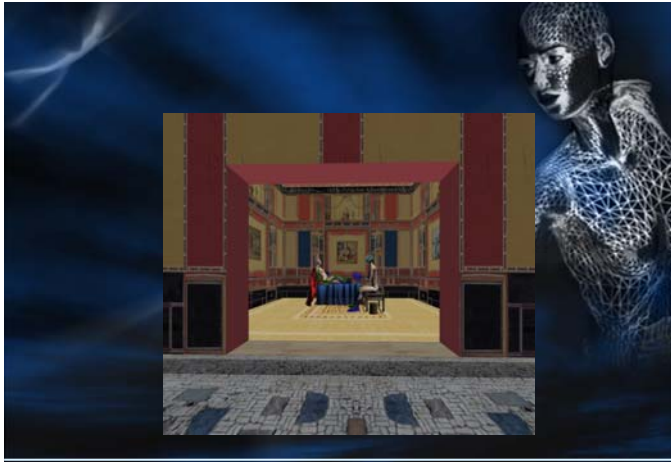
Where Research means Creativity
www.miralab.ch

Nadia Magnenat-Thalmann

MIRALab
University of Geneva

Where Research means Creativity
www.miralab.ch

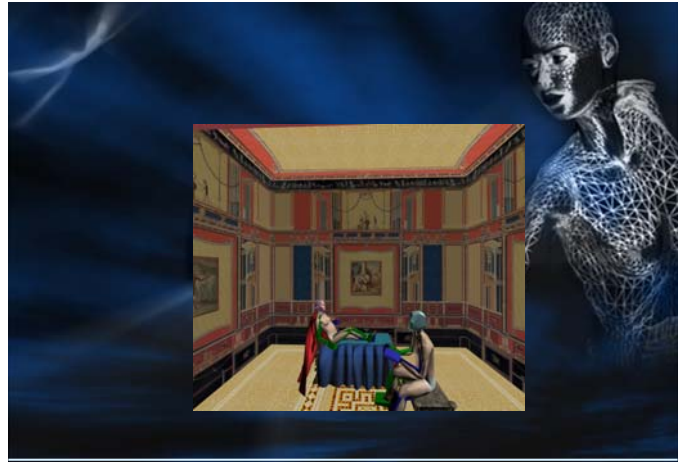
Nadia Magnenat-Thalmann



MIRALab
University of Geneva

Where Research means Creativity
www.miralab.ch

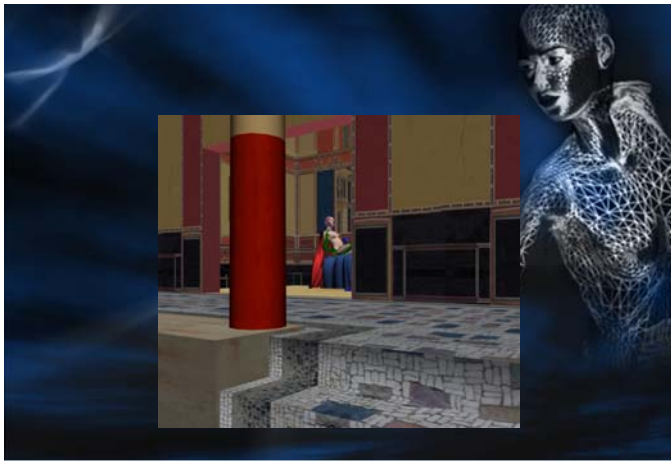
Nadia Magnenat-Thalmann



MIRALab
University of Geneva

Where Research means Creativity
www.miralab.ch

Nadia Magnenat-Thalmann



MIRALab
University of Geneva

Where Research means Creativity
www.miralab.ch

Nadia Magnenat-Thalmann



MIRALab
University of Geneva

Where Research means Creativity
www.miralab.ch

Nadia Magnenat-Thalmann





MIRALab
University of Geneva

Where Research means Creativity
www.miralab.ch

Nadia Magnenat-Thalmann



MIRALab
University of Geneva

Where Research means Creativity
www.miralab.ch

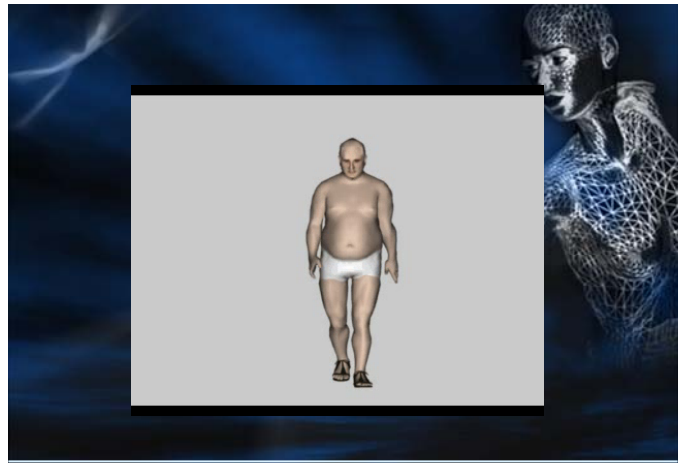
Nadia Magnenat-Thalmann



MIRALab
University of Geneva

Where Research means Creativity
www.miralab.ch

Nadia Magnenat-Thalmann



MIRALab
University of Geneva

Where Research means Creativity
www.miralab.ch

Nadia Magnenat-Thalmann



Research in HUMANS Simulation

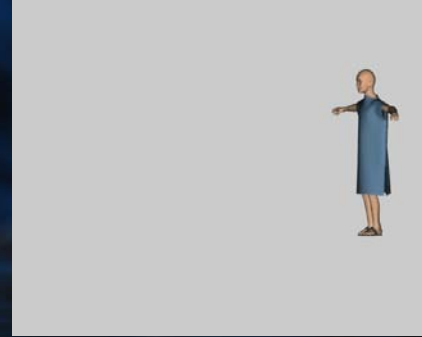
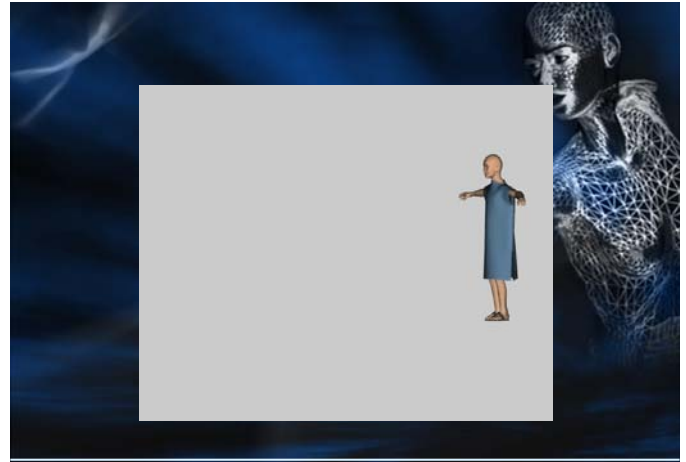
- Real-time realistic skin rendering and interactive programmable shading module
- Artificial life methods for behavioural animation of virtual characters



MIRALab
University of Geneva

Where Research means Creativity
www.miralab.ch

Nadia Magnenat-Thalmann



MIRALab
University of Geneva

Where Research means Creativity
www.miralab.ch

Nadia Magnenat-Thalmann



Early Mixed Realities simulations in ancient Pompeii (offline AR)



movie

MIRALab
University of Geneva

Where Research means Creativity
www.miralab.ch

Nadia Magnenat-Thalmann



AR Life: User Experience

- **User arrives at the AR Life "hot spot"**
 - inform about AR Life Simulation option
 - start theater-like immersive AR simulation
- **User participation and interaction**
 - using HMD + head mounted camera
 - watching AR revival of the ancient life
 - dramatic scenario featuring high quality Virtual Humans
 - blended into the real scenery
 - moving around the scene, changing point of view

MIRALab
University of Geneva

Where Research means Creativity
www.miralab.ch

Nadia Magnenat-Thalmann



AR Life: Functional Elements

33

- **main functional elements**

- real-time camera tracking: **marker-less**
- real-time VR simulation: **advanced Virtual Humans**
- blending

track camera



generate VR



blend
Camera and VR

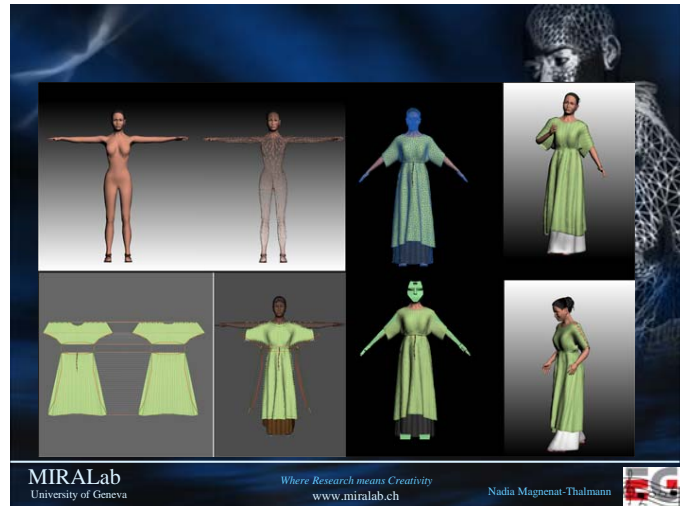


result

MIRALab
University of Geneva

Where Research means Creativity
www.miralab.ch

Nadia Magnenat-Thalmann



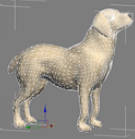
MIRALab
University of Geneva

Where Research means Creativity
www.miralab.ch

Nadia Magnenat-Thalmann



Attaching the skeleton & adding a motion



Hanim skeleton

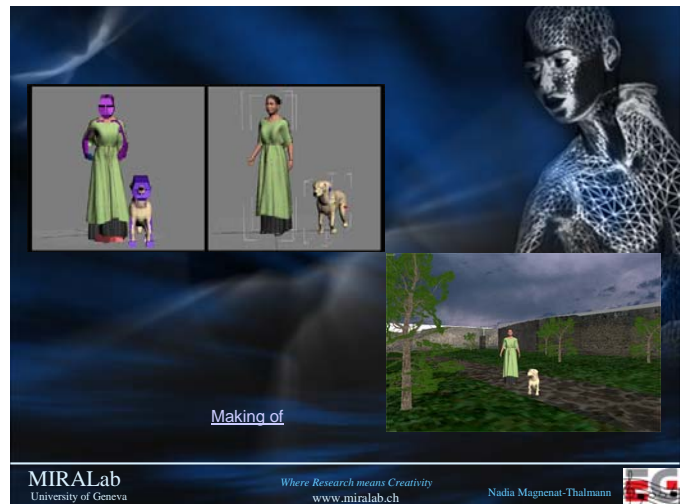
The segmented model



MIRALab
University of Geneva

Where Research means Creativity
www.miralab.ch

Nadia Magnenat-Thalmann



MIRALab
University of Geneva

Where Research means Creativity
www.miralab.ch

Nadia Magnenat-Thalmann



Simulating Interactive virtual plays in ancient theatres

Nadia Magnenat-Thalmann
George Papagiannakis
MIRALab – University of Geneva

MIRALab University of Geneva www.miralab.ch Eurographics 2006

Aspendos Site (161-180 A.D.)

MIRALab University of Geneva www.miralab.ch Eurographics 2006

Objectives

- Interactive Real time Visualization
- Inclusion of Virtual Humans
- Reenacting of a Roman Play
- Simulation of physically correct illumination
- Restitution of the original appearance of the site

MIRALab University of Geneva www.miralab.ch Eurographics 2006

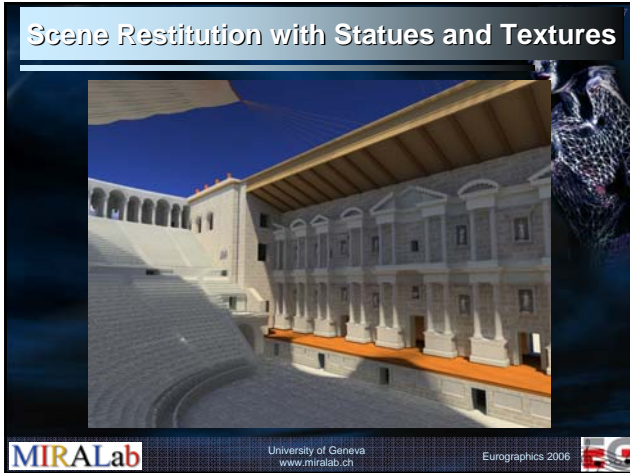
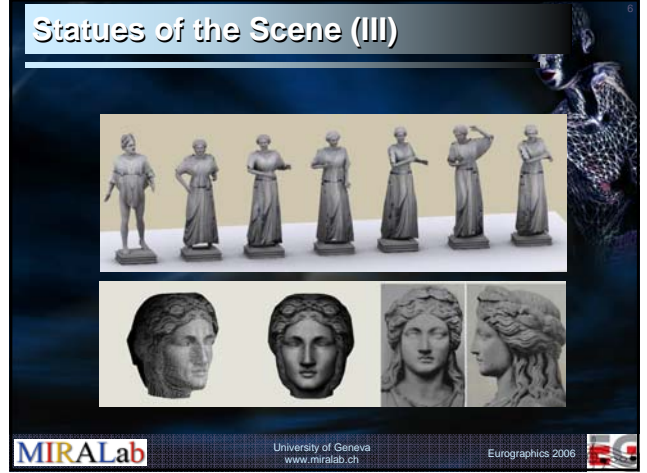
Statues of the Scene (I)

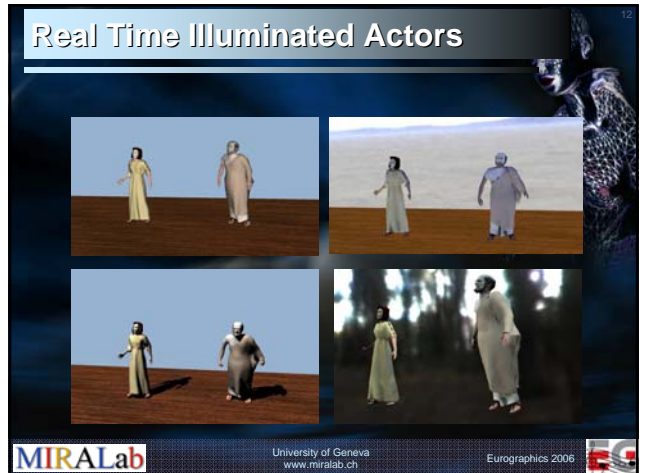
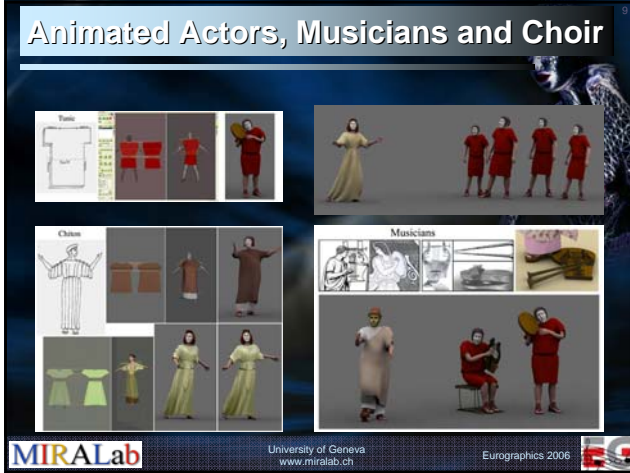
▪ Sources

The Gods

Imperial family

MIRALab University of Geneva www.miralab.ch Eurographics 2006





Real time reenacting of a scripted performance

VR Database

- 3D scene
- occluders
- virtual
- sounds
- face anim
- clothes
- plants
- scripts

vhdRuntimeEngine

- 3D Rendering
- Crowd Simulation
- Sound Simulation
- Skeleton Animation
- Skin Deformation
- Cloth Simulation
- Face
- Speech
- Plants
- Python Scripting
- Scenario
- VRML Loader
- XML Loader

University of Geneva
www.miralab.ch

Eurographics 2006

All-Frequency MR Illumination model for deformable virtual characters

- 'key-fill' illumination setup approach consisting of:
 - High-Frequency Shadow Mapping (key)
 - Low-Frequency Dynamic Precomputed Radiance Transfer (fill)
- Dynamic Precomputed Radiance Transfer
 - New Diffuse Shadow Merged Transfer
 - Multi-mesh, multi-material, articulated hierarchies
 - Real-time low order Spherical Harmonics basis for Global Illumination effects

University of Geneva
www.miralab.ch

Eurographics 2006

All-Frequency MR Real Time Illumination model: Results

University of Geneva
www.miralab.ch

Eurographics 2006

Final Prototype Real Time Application (I)


- Based on the VHD++ MR framework for virtual characters (soon to be released as open-source project)
- Real-time simulated virtual actors with body, cloth, skin, speech simulation
- All-frequency illumination model

University of Geneva
www.miralab.ch

Eurographics 2006

Final Prototype Real Time Application (I)

- Complex scene of ~300.000 triangles
- Virtual Aspendos Theatre
- Surrounding Flora simulation
- Sophocles: Antigone play excerpt



MIRALab University of Geneva www.miralab.ch Eurographics 2006

QUESTIONS





MIRALab University of Geneva www.miralab.ch Eurographics 2006




**Introduction to the XVR technology:
the basic framework**

Franco Tecchia, Emanuele Ruffaldi, Antonio Frisoli, Massimo Bergamasco

PERCRO, Scuola Superiore Sant'Anna

General concepts

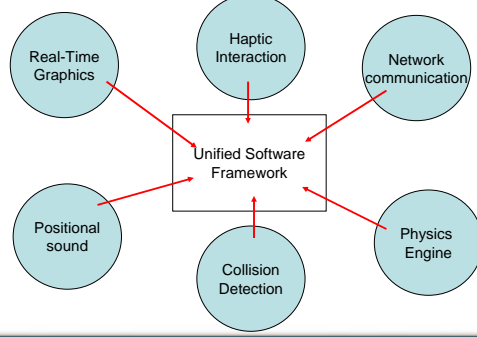
5/29/2006 Interacting in virtual worlds with haptic devices 2

XVR: An IDE for VR applications



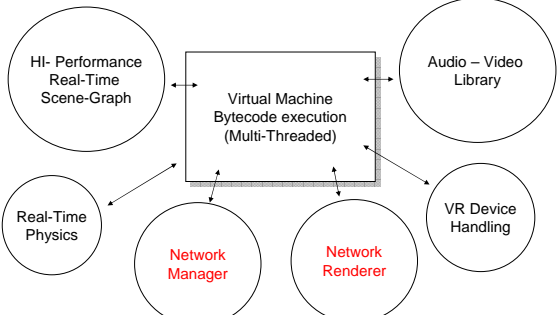
5/29/2006 Interacting in virtual worlds with haptic devices 3

The importance of technology integration



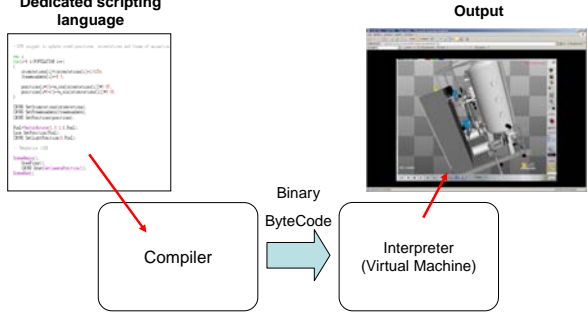
5/29/2006 Interacting in virtual worlds with haptic devices 4

XVR Architecture



5/29/2006 Interacting in virtual worlds with haptic devices 5

XVR Workflow



5/29/2006 Interacting in virtual worlds with haptic devices 6

PERCRO EG XVR

What does XVR provide

- A complete and very fast 3D Scene Graph Manager
- Low level OpenGL wrapping for added flexibility
- Vertex and pixel-shaders (OpenGL2.0 GLSL)
- Basic GDI and 2D GUI functions (menus, text)
- Sound management: MIDI, MP3, 3D Positional Sound
- Collision detection & Real-time Physics
- Haptic devices control
- Network data management
- Basic streaming support
- Support for advanced devices: Trackers, Stereo projection, HMDs, Haptic Interfaces, CAVE

5/29/2006 Interacting in virtual worlds with haptic devices 7

PERCRO EG XVR

Why: from demos to complex applications

- Demos as single-minded applications
- Very limited interaction
- Problems can be ignored or postponed
- Most of the work to pass from concept demo to application stage
- We learn from our work and our students

Features VS. Complexity

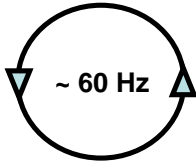
Linear increase → Exponential grow

5/29/2006 Interacting in virtual worlds with haptic devices 8

PERCRO EG XVR

The simplest architecture: the single loop

One loop to manage everything:



- Graphic Rendering
- User Input
- Animation
- Collision detection
- Physical simulation

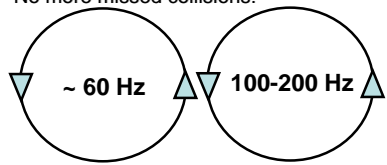
Refresh rate is usually the upper bound
Collision and physics can give troubles

5/29/2006 Interacting in virtual worlds with haptic devices 9

PERCRO EG XVR

Second option: separate rendering from the rest

- Animation independent from frame rate
- No more missed collisions!



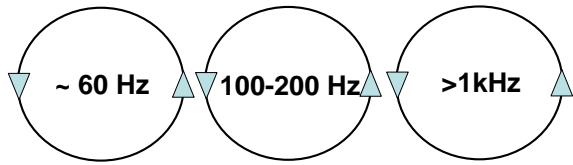
- Variables need to be shared between processes
- Atomicity should be carefully addresses
- Two threads, one rendering context?

5/29/2006 Interacting in virtual worlds with haptic devices 10

PERCRO EG XVR

Third step: Haptic Devices get into the picture

- The Haptic Loop is *very* fast
- More representations for the same objects



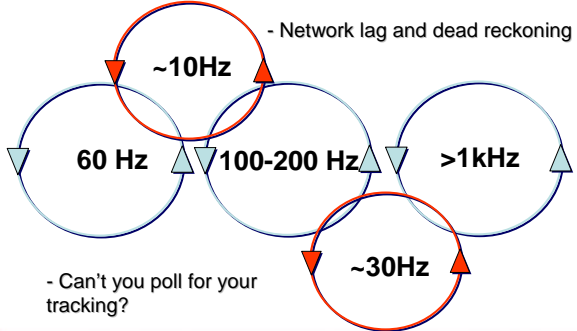
- Problem: How does Haptics influence Physics?

5/29/2006 Interacting in virtual worlds with haptic devices 11

PERCRO EG XVR

Going further: loops are everywhere

- Network lag and dead reckoning




- Can't you poll for your tracking?

5/29/2006 Interacting in virtual worlds with haptic devices 12

PERCRO EG XVR

Preprocessor commands

- #DEFINE
- #IFDEF
- #ENDIF
- #ELSE
- #INCLUDE
- #PRAGMA



Preprocessor directives, such as #define and #ifdef, are typically used to make source programs easy to change and easy to compile in different execution environments. Directives in the source file tell the preprocessor to perform specific actions. For example, the preprocessor can replace tokens in the text, insert the contents of other files into the source file, or suppress compilation of part of the file by removing sections of text. Preprocessor lines are recognized and carried out before macro expansion.

5/29/2006 Interacting in virtual worlds with haptic devices 19

PERCRO EG XVR

Functions

- Same as usual
- Parameter type is not specified
- Type of the return value is not specified

```
function MoveCameraTo(dest)
{
    var temp;
    var speed=0.90;
    temp=GetCameraPosition();
    temp=speed*temp+(1.0-speed)*dest;
    mySetCameraPosition(temp);
    return (temp);
}
```

5/29/2006 Interacting in virtual worlds with haptic devices 20

PERCRO EG XVR

S3D Variables

- Variable type is not explicitly declared
- The same variable can assume different types as the program evolve
- The construct "reset" can be useful!

```
VAR i;
VAR j,k;
VAR x = 2;
VAR y = 3.1;
VAR s = "Don't panic !!!"
k = 4.3;
i = 8;
i = 9.2; VAR v = [0.0, 1.0, 0.0];

static var a = 10;
...
a = 7;
...
reset a; // a = 10
```

5/29/2006 Interacting in virtual worlds with haptic devices 21

PERCRO EG XVR

S3D Types

INT, FLOAT, BOOLEAN, STRING

VECTOR: (of floats - monodimensional)

```
Var1 = [ 0.2 , 2 , 3.33 , 4 ];
Var2 = Vector(16); // create a 16-elements vector
Var3 = Var1[0]; // Var3 equals 0.2
```

MATRICES:

Although not directly supported, often XVR functions return, or accept as input, 16-dim vectors representing MATRICES. In this case the matrix is stored in column-major order, like in OpenGL.

5/29/2006 Interacting in virtual worlds with haptic devices 22

PERCRO EG XVR

ARRAY

An **Array** is a set of elements which can be accessed through an index. The elements of a S3D array can be of different type. The array size can be changed at run-time. To specify the index in order to access the desired element, the operator [] is used.

```
Var1 = { 1, true, { 12, 3 } }; // Array made of different types
Var2 = Array(12); // Create an array of 12 elements
Var3 = Var1[0]; // Var3 equals 1
Var4 = Var1[2][0]; // Var4 equals 12
Var1[1] = false; // Now Var1[1] equals "false"
```

5/29/2006 Interacting in virtual worlds with haptic devices 23

PERCRO EG XVR

Classes

- S3D is heavily object-oriented
- Built-in objects
- Script-based classes
- Imported objects (DLLs)

5/29/2006 Interacting in virtual worlds with haptic devices 24

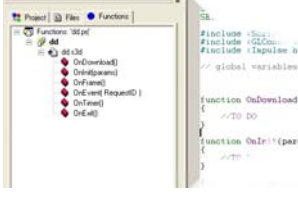
PERCRO EG XVR

Programming with XVR

5/29/2006 Interacting in virtual worlds with haptic devices 25

PERCRO EG XVR

How is an application organised?

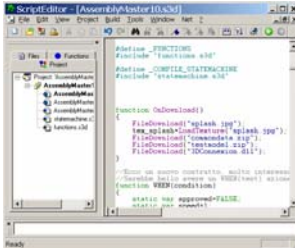


- Any XVR application is based on 6 fundamental function (built in all the scripts)
- Currently there are 2 threads calling these functions. There could be more in the future.
- Atomicity of the operations is guaranteed. Global variables are properly shared between threads

5/29/2006 Interacting in virtual worlds with haptic devices 26

PERCRO EG XVR

OnDownload()

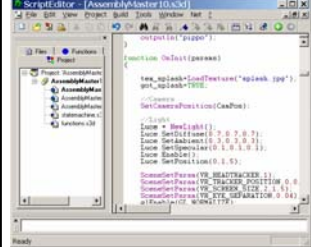


- Every time an XVR script is executed it creates a temporary working directory (inside the user temp)
- OnDownload is used to move files from their original location to the working directory
- Zip Files are automatically exploded
- Generic code can be executed inside OnDownload

5/29/2006 Interacting in virtual worlds with haptic devices 27

PERCRO EG XVR

OnInit()

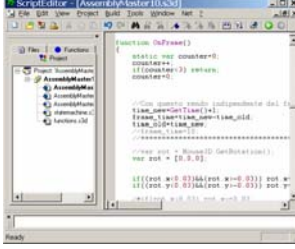


- Once the download is complete, this is the right place for initialization code
- Please note that OnInit accept a "params" value. This is the "UserParam" string reported in the HTML code
- There is an implicit OpenGL "SwapBuffer" when OnInit ends

5/29/2006 Interacting in virtual worlds with haptic devices 28

PERCRO EG XVR

OnFrame()

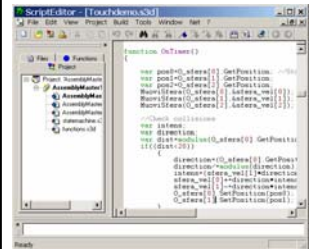


- Function dedicated to rendering. By default it gets called after each screen refresh (60 Hz).
- Desired framerate can be changed using SetFramerate(Value)
- It's the ONLY function that has access to the OpenGL frame buffer
- All the rendering code must be inside this function (or inside functions called by OnFrame)
- The maximum Frame Rate allowed is 100 Hz

5/29/2006 Interacting in virtual worlds with haptic devices 29

PERCRO EG XVR


OnTimer()





- Function normally dedicated to manage an high speed loop. By default it gets called at 100Hz
- Desired time-step can be changed using SetTimestep(Value)
- Minimum time-step = 1ms
- Independent from framerate (unless the system is overloaded)
- Excellent place for updating objects positions, sound, real time physics, haptic interfaces and network programming.
- It has no access to the framebuffer

5/29/2006 Interacting in virtual worlds with haptic devices 30




HapticWeb
Haptic rendering and interaction with XVR



PERCRO  XVR 

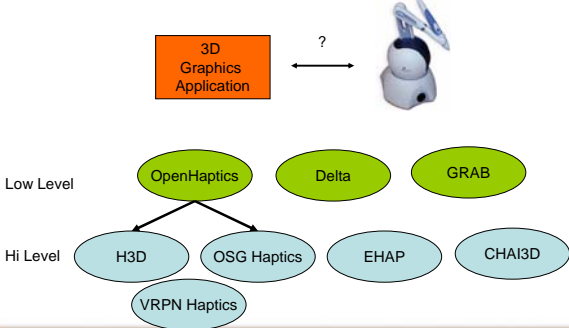
Overview




- **Introducing Haptics for XVR**
- **Programming Model**
- **Features**
 - Devices
 - Mesh Objects
 - Effects
 - Capture
 - Integration with Physics
 - High Level Example
- **Future Directions**

PERCRO  EG  XVR 

5/29/2006 Interacting in virtual worlds with haptic devices 38

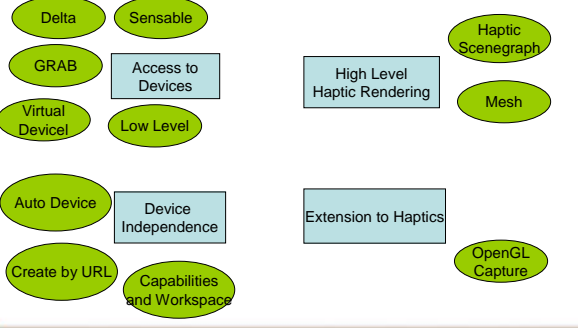
Haptics for Virtual Reality






PERCRO  EG  XVR 

5/29/2006 Interacting in virtual worlds with haptic devices 39

HapticWeb - Haptics for XVR



PERCRO  EG  XVR 

5/29/2006 Interacting in virtual worlds with haptic devices 40

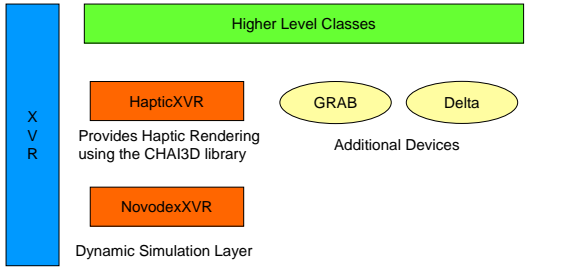
HapticWeb Examples






PERCRO  EG  XVR 

5/29/2006 Interacting in virtual worlds with haptic devices 41

HapticWeb structure



PERCRO  EG  XVR 

5/29/2006 Interacting in virtual worlds with haptic devices 42

PERCRO EG XVR

Programming Model

- **Haptic Rendering**
 - Low level force command to the device
 - Haptic Scene Graph with Geometry and Effects
- **Haptic Loop**
 - External Thread Haptic Loop
 - OnTimer based

5/29/2006 Interacting in virtual worlds with haptic devices 43

PERCRO EG XVR

Haptic Scene Graph

- Based on the CHAI3D scene graph
- Simplifies the Haptic Rendering
- Hierarchy parallel to the Graphics one

5/29/2006 Interacting in virtual worlds with haptic devices 44

PERCRO EG XVR

Haptic Loop

Three different models of computation of managing the Haptic Loop using HapticWeb

- Separate
- OnTimer
- Local Model

5/29/2006 Interacting in virtual worlds with haptic devices 45

PERCRO EG XVR

Application Setup

```
#include "hapticweb.h.s3d"

var h_world;

function OnInit()
{
    HLoadModule ();
    h_world = HWorld();

    ...

    h_world.run();
}
```

5/29/2006 Interacting in virtual worlds with haptic devices 46

PERCRO EG XVR

HapticWeb Deployment

- Which files are needed by HapticWeb?
- Use provided hapticxvr.zip
- **Core Haptics**
 - hapticxvr.dll – the extension module
 - PhantomDriver.dll and PhantomXXX.dll
 - Sphere.aam – for the graphics
- **Additional Devices**
 - dlportio.dll – for Delta
 - GrabExtDll.dll – for the PERCRO's GRAB
- **Physics**
 - Novodexvr.dll
 - NxFoundation.dll and NxPhysics.dll

5/29/2006 Interacting in virtual worlds with haptic devices 47



PERCRO EG XVR

Loading Modules during Development

- The HapticWeb module can be loaded using `LoadModule("hapticxvr.dll");`
- But the additional files for drivers are provided by the HapticXVR.zip
- During the local development it is possible to reduce the unpacking time by using the AutoLocal approach:
 1. The `AutoLocal` function returns `true` if we are running on local instead of Web
 2. Use the `GetScriptPath` function to get the script directory
 3. Change directory using `SetCurrentDir`

```
if(AutoLocal(forceLocalMode))
    SetCurrentDir(GetScriptPath());
```



5/29/2006 Interacting in virtual worlds with haptic devices 48

PERCRO  

HObject

- The basic haptic class that corresponds to the cGenericObject of CHAI3D
- HObject provides:
 - Hierarchy (add/removeChild, getChild)
 - Bounding Box
 - Transformation (rotate, translate, rotation, position)
 - Rendering (for debugging)
 - Additional XVR data: tag



5/29/2006 Interacting in virtual worlds with haptic devices 49

PERCRO  

Haptic Devices

- HapticWeb** supports all the CHAI3D devices and PERCRO devices
- The Haptic Interface is represented by a 3/6DOF Haptic Point of Contact of class **HTool**
- The device can be specified by using an URL or automatically detected
- If nothing is found the CHAI3D Virtual Device is activated (if dhdVirtual.exe is present)



5/29/2006 Interacting in virtual worlds with haptic devices 50

PERCRO  

Haptic Devices URL

- We use an URL for using a specific device or automatically selecting the attached device
- Currently supported URLs:
 - null**: - useful for debugging and custom virtual device
 - ehap://grab/left** and **ehap://grab/right** for the left and right arm of the GRAB
 - virtual**: - standard CHAI3D virtual device
- The URL will be used to specify remote devices or additional device parameters



5/29/2006 Interacting in virtual worlds with haptic devices 51

PERCRO  

HTool class

- Manages a 6DOF point of contact and a proxy
- Device:
 - forceEnabled : bool
 - devicePosition : vector in device coordinates
 - deviceOrientation : vector as 4x4 matrix
 - deviceLocalPosition : vector in tool coordinates
 - force : vector of force in N
 - torque : vector of torque in N mm
 - buttonPressed : bool
 - buttonCount : int
 - deviceURI : string (useful for testing initialization and device)
 - initialize() start() stop()



5/29/2006 Interacting in virtual worlds with haptic devices 52

PERCRO  

Virtual Device

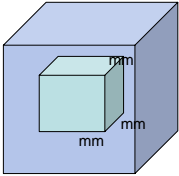
- The standard CHAI3D virtual device based on an external application (dhdvirtual.exe) connected by Shared Memory
- The contact point is controlled by the Mouse
- Useful for debugging or when the device is not available
- The Shared Memory can be used for interfacing other devices (e.g. using Simulink)
- The Virtual Device could be implemented in XVR inside the application using the **null**: device
 - Just set **devicePosition** before **updatePose**

5/29/2006 Interacting in virtual worlds with haptic devices 53

PERCRO  

HTool Workspace

- Workspace and scaling are fundamental aspects of Haptic interfaces
- By default the **devicePosition** is in mm
- The property **workspace** returns the current workspace of the device. By default is mm. For PHANTOMS it is a Cube
- The workspace can be changed setting the **workspaceScale** factor of the tool
- IMPORTANT: stiffness should be expressed in N/mm and divided by **workspaceScale** before assigning it to meshes
 - virtualStiffness = stiffness / workspaceScale



5/29/2006 Interacting in virtual worlds with haptic devices 54

PERCRO EG XVR

HTool Proxy

- The classic God-Object proxy algorithm for Haptic Rendering
- Extended with Friction
- Properties:
 - contactObject : HMesh
 - hasContact : bool
 - lastNormal : vector if hasContact
 - proxyPosition : vector
- In OnTimer mode is updated by computeForces

5/29/2006 Interacting in virtual worlds with haptic devices 55

PERCRO EG XVR

The Haptic Loop

- When using the External thread model HapticWeb manages the haptic rendering loop
 - Simply call **h_world.run()** in the OnInit

- tool.computeForces() – computes forces using the proxy and the Haptic Effects
- tool.applyForces() – sends the forces to the device. It allows to modify the generated force

5/29/2006 Interacting in virtual worlds with haptic devices 56

PERCRO EG XVR

Example of Sphere rendering

```

#include <Script3d.h>
#include "hapticweb.h.s3d"

var h_world;
var h_tool;
var sphereCenter = [0,2,10];
var sphereRadius = 5.0;
var sphereStiffness = 2500; // N/mm

function OnDownload()
{
  FileDownload("hapticvr.zip");
}

function OnInit()
{
  HLoadModule ();
  h_world = HWorld();
  h_tool = HToolGL(h_world);
  h_tool.tool.start();
  h_world.run(false);
}

function OnTimer()
{
  var tool = h_tool.tool;
  tool.updatePose();

  var delta = tool.devicePosition - sphereCenter;
  var d = modulus(delta);
  if(d > sphereRadius || d == 0)
    tool.force = [0,0,0];
  else
    tool.force =
    sphereStiffness*(sphereRadius-d)*(delta/d);
  tool.applyForces();
}

```

DEMO

5/29/2006 Interacting in virtual worlds with haptic devices 57

PERCRO EG XVR

Adding a mesh

- An **HMesh** object is a triangular mesh that can be haptically touched using the standard proxy algorithm
- Geometry
 - Created from AAM/3DS/OBJ files
 - Created from CvmMesh/CvmNewMesh/CvmObj (with all children)
 - Created explicitly using newVertex/newTriangle
 - Created from OpenGL capture using begin/endCapture
- Surface Properties
 - friction – set using **setFriction(ms, md)**
 - stiffness – should be scaled by workspaceScale

5/29/2006 Interacting in virtual worlds with haptic devices 58

PERCRO EG XVR

Adding a mesh

From a CvmObj or CvmNewMesh

```

var h_mesh= HMesh(h_world);
h_mesh.loadFromMesh(mymesh);
h_mesh.createAABBCollisionDetector();
h_world.addChild(h_mesh);
h_mesh.stiffness = 10;

```

From a file

```

var h_mesh= HMesh(h_world);
h_mesh.loadFromFile("x.aam");
h_mesh.createAABBCollisionDetector();
h_world.addChild(h_mesh);
h_mesh.stiffness = 10;

```

5/29/2006 Interacting in virtual worlds with haptic devices 59

PERCRO EG XVR

Creating a Mesh

```

var h_mesh= HMesh(h_world);
h_mesh.newVertex(0,0,0,0,0);
h_mesh.newVertex(size.x,0,0,0,0);
h_mesh.newVertex(size.x,this.size.y,0,0,0);
h_mesh.newVertex(0,this.size.y,0,0,0);
h_mesh.newTriangle(0,1,2);
h_mesh.newTriangle(0,2,3);
h_mesh.computeBoundingBox();
h_mesh.computeAllNormals();

```

5/29/2006 Interacting in virtual worlds with haptic devices 60

PERCRO EG XVR

Capturing a Mesh

- It is possible to use the OpenGL Feedback mode to construct a HMesh from a block of OpenGL primitives

```

var h_mesh= HMesh(h_world);
h_mesh.beginCapture();
glBegin(GL_TRIANGLES);
...
glEnd();
h_mesh.endCapture();

```

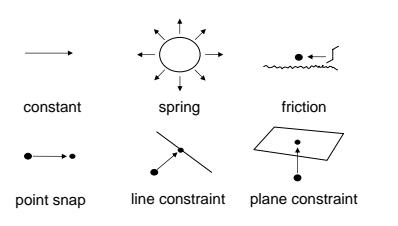
- The primitives are mapped from the world frame into the mesh local frame, but only if visible in the viewport

5/29/2006 Interacting in virtual worlds with haptic devices 61

PERCRO EG XVR

Haptic Effects

- Programmable Haptic effects imposed over the Haptic Rendering**

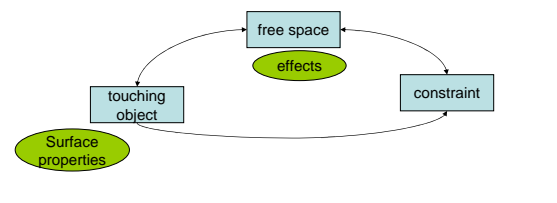


constant spring friction
point snap line constraint plane constraint

5/29/2006 Interacting in virtual worlds with haptic devices 62

PERCRO EG XVR

The Haptic Rendering Pipeline



Surface properties touching object constraint free space effects

5/29/2006 Interacting in virtual worlds with haptic devices 63

PERCRO EG XVR

Haptic Effects

- HEffect class**
- Add to the HWorld by addChild**
- Common Members**
 - type
 - enable
- Constant: direction,magnitude**
- Spring: gain**
- Viscous: gain**
- Friction: gain**
- Plane: direction,gain**

- Explicitly enabling by **enabled**
- Time based behavior for triggered effects:
 - Set duration in seconds using **duration**
 - Trigger the effect using **trigger**

5/29/2006 Interacting in virtual worlds with haptic devices 64

PERCRO EG XVR

Constrained Haptic Effect

- HEffect** allows to define force constraints that are applied to a point of contact
- Constraints can be:
 - point
 - line
 - Plane
- A constraint is active if the distance to that is inferior to the **snapDistance** value.
- The constraints are created by using the OpenGL commands between begin/endCapture

5/29/2006 Interacting in virtual worlds with haptic devices 65

PERCRO EG XVR

Integration with Physics

- Depends on the Interaction Model**
- In general we have three representations**

NBody

CVmObj

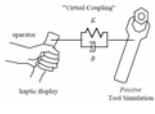
HMesh

- Touch and push model:**
 - After Simulation Step → Synchronization of Position and Rotation
 - Before Simulation Step → Send forces accumulated during the Haptic Loop by the touching. Use *threshold* for allowing surface exploration

5/29/2006 Interacting in virtual worlds with haptic devices 66

PERCRO EG XVR

Virtual Coupling



(Colgate 1998)

- Useful for simulating the grabbing of a Body
- Allows to perceive the collisions and the forces applied to the attached Body
- It is based on a damped spring that connects the Haptic Contact Point with a Body
- Two state interaction
 - Selection phase in which objects can be touched
 - Grabbing phase in which the Haptic Tool drags a body
- The force feedback is just the stiffness of the string by the string extension. It can be done both in thread mode and in the OnTimer
- The dynamic simulation can be done manually using the applyForce or better using a Spherical Joint with a Spring


5/29/2006 Interacting in virtual worlds with haptic devices 67

PERCRO EG XVR

HVirtualObject

- A XVR class that provides VirtualCoupling
 - Haptic: using a H_SPRING effect
 - Physics: compute the spring force manually
- Usage:
 - Create using NSim and HWorld
 - Attach to a physics object
 - Call it before and after the Simulation

DEMO



5/29/2006 Interacting in virtual worlds with haptic devices 68

PERCRO EG XVR

Virtual Coupling Example

```

var h_world, p_sim;
var h_tool, p_tool, h_virtual;
var p_obj;

function OnInit()
{
  HLoadModule();
  NLoadModule();
  h_world = HWorld();
  p_sim = NSim();
  h_tool = HToolGL(h_world);
  h_virtual = HVirtualObject(h_world,
    p_sim, h_tool);
  h_virtual.stiffness = 5;
  p_obj = p_sim.createBody(
    N_GEO_SPHERE, 5);
  p_obj.mass = 0.5;
  h_virtual.attach(p_obj);
  h_world.run();
  ...
}

function OnFrame()
{
  h_virtual.preStep();
  p_sim.step();
  h_virtual.postStep();
  ...
  h_virtual.render();
}

```

5/29/2006 Interacting in virtual worlds with haptic devices 69

PERCRO EG XVR

Entertainment Application: Tennis Table



S. Marcheschi

PERCRO EG XVR

PERCRO EG XVR

Introduction



Experimental set-up of virtual tennis table game

5/29/2006 Interacting in virtual worlds with haptic devices 71

PERCRO EG XVR

General architecture

| | |
|--|--|
| OnDownload() > Load Haptic Interface (HI) lib | OnInit() > Load mesh > Initialize data structures > Initialize HI lib > Set time step to 1ms |
| OnTimer() > Evaluate integration timestep > Get position data from HI > Update dynamic loop > Send force data to HI | OnFrame() > Move camera with mouse > Draw table, pad and ball > Get keyboard input > Display data |

5/29/2006 Interacting in virtual worlds with haptic devices 72

PERCRO EG XVR

Data structures

| Object dynamic parameters | Dynamic data | Visualization data |
|---|---|---|
| <pre>class ObjData { var Mass; var Inertia; var Stiffness; var AirViscosity; ... };</pre> | <pre>class ObjDin { var Force; var Torque; var Position; var Velocity; var Acceleration; ... };</pre> | <pre>class ObjView { var ScaleMesh; var ScaleGlo; var RotMatrixNotScaled; var Obj; };</pre> |
| ↓ | | |
| Objects | | |
| <pre>class Ball { var Data; var View; var Din; var Radius; };</pre> | <pre>class Pad { var Data; var View; var Din; var Radius; };</pre> | <pre>Class Table { var Data; var Din; var Lx, Ly; var VerX; var VerY; };</pre> |

5/29/2006 Interacting in virtual worlds with haptic devices 73

PERCRO EG XVR

Integration Timestep: Differential Integration Step

```
T = GetPerformanceTimer();
ΔT = Tn - Tn-1
```

- PRO: Real time simulation
- CONTRA: Integration step discontinuities

5/29/2006 Interacting in virtual worlds with haptic devices 74

PERCRO EG XVR

Integration Time step: Fixed Integration Step

```
T = GetPerformanceTimer();
ΔT = lms
```

- PRO: Continuous integration step
- CONTRA: Non real time (delayed) simulation

5/29/2006 Interacting in virtual worlds with haptic devices 75

PERCRO EG XVR

Integration time step: Variable Integration Step

```
Trender=0.0;
Tcurr = GetPerformanceTimer()/1000.0;
if ( (Tcurr - Trender) < DTmax )
  Trender = Tcurr;
else
  Trender = Trender + DTmax;
```

- PRO: Quasi-continuous integration step
- CONTRA: Quasi-real time simulation

5/29/2006 Interacting in virtual worlds with haptic devices 76

PERCRO EG XVR

Dynamic loop - Ball

Force

$$F = F_T + F_R + F_V + F_G$$

$$T = T_T + T_R$$

$F_T, T_T =$ Collision with table
 $F_R, T_R =$ Collision with pad
 $F_G =$ Gravity
 $F_V =$ Air viscosity

F, T

Direct dynamic

$$\dot{X}_n = \dot{X}_{n-1} + \frac{F}{M} \cdot \Delta T$$

$$X_n = X_{n-1} + \dot{X}_n \cdot \Delta T$$

$$\omega_n = \omega_{n-1} + \frac{T}{J} \cdot \Delta T$$

$$q_n = q_{n-1} + \omega_n \cdot \Delta T$$

X_n, q_n

5/29/2006 Interacting in virtual worlds with haptic devices 77

PERCRO EG XVR

Dynamic loop - Pad

Force

$$F = F_B + F_G$$

$F_B =$ Collision with ball
 $F_G =$ Gravity

$H^I F$

$H^I X$

5/29/2006 Interacting in virtual worlds with haptic devices 78

PERCRO  EG  XVR 




Simultaneous Presence, Telepresence and Virtual Presence

Tennis Table



Play: 0:00:00 (0:00:00)
 Deleted: 0:00:00 (0:00:00)
 File: 0:00:00 (0:00:00)

5/29/2006 Interacting in virtual worlds with haptic devices 79




PERCRO  EG  XVR 

Simultaneous Presence, Telepresence and Virtual Presence

Future Directions

- Freezing the API
- Clearer Device Instantiation
- More support for multi point
- Networked Device
- Support for PERCRO EHAP haptics library using the same XVR interface

5/29/2006 Interacting in virtual worlds with haptic devices 80

PERCRO  EG  XVR 

Simultaneous Presence, Telepresence and Virtual Presence

Exploring more

HapticWeb <http://www.hapticweb.org>

Thanks to the CHAI3D's team

5/29/2006 Interacting in virtual worlds with haptic devices 81